The Greenland-Ice-Sheet evolution over the last 24,000 years: insights from model simulations evaluated against ice-extent markers

Tancrède P.M. Leger[1,2], Jeremy C. Ely[1], Christopher D. Clark[1], Sarah L. Bradley[1], Rosie E. Archer[3], Jiang Zhu[4]

[1] School of Geography and Planning, University of Sheffield, Sheffield, S10 2TN, UK
[2] Institute of Earth Surface Dynamics, University of Lausanne, Lausanne, Switzerland
[3] Department of Geography and Environmental Sciences, Northumbria University, Newcastle, UK
[4] Climate and Global Dynamics Laboratory, NSF National Center for Atmospheric Research, Boulder, CO, USA

Correspondence: Tancrède P. M. Leger (tancrede.leger@unil.ch): personal address: tankleger@gmail.com

Abstract. Continental ice sheets ~~possess~~retain a long-term memory ~~that is~~ stored ~~within both the~~in their geometry and thermal properties ~~of ice~~. In Greenland, this ~~causes~~creates a disequilibrium ~~between~~with the present ~~day ice sheet and current~~ climate, as the ice sheet is still adjusting to past changes that occurred over millennial timescales. Data-consistent modelling of ~~the~~ paleo Greenland-Ice-Sheet evolution is ~~thus~~therefore important for improving model initialisation ~~procedures used~~ in future ~~ice sheet~~ projection experiments. ~~Additionally, open~~Open questions also remain regarding the ice sheet's former volume, extent, flux, internal flow dynamics, thermal conditions, and how such properties varied in space since the last glaciation. Here, we conduct a modelling experiment that aims to produce simulations in agreement with empirical data on ~~the~~ Greenland's ice-margin extent and timing ~~of the ice sheet's margin positions~~ over the last 24,000 years. ~~Due to~~Given large uncertainties in ~~ice sheet~~ model parameters and boundary conditions, we apply a perturbed ~~-~~parameter ensemble ~~approach and run~~of 100 ice-sheet-wide simulations at 5 x 5 km ~~horizontal~~ resolution using the Parallel Ice Sheet Model~~. Our simulations are~~, forced by paleo-climate and ocean simulations ~~of~~from the isotope-enabled Community Earth System Model. Using quantitative model-data comparison and ~~the newly developed~~a new Greenland-wide reconstruction of former ice margin retreat (PaleoGrIS 1.0), we ~~scored~~score each simulation's fit ~~across Greenland~~ from 24,000 years ago ~~until~~to 1850 AD. The resulting ensemble and best-scoring simulations provide insights ~~related to~~into the dynamics, ~~causes~~drivers, and spatial heterogeneities of the local LGM, Late-glacial, and Holocene evolution of the Greenland Ice Sheet. ~~We for~~For instance, we find that between 16 and 14 thousand years ago, the ice sheet lost most ~~of its~~ ice grounded on the continental shelf. This marine-sector ~~demise~~retreat, associated with mass loss rates up to seven times greater ~~mass loss rates~~ than ~~observed today~~today's, was ~~predominantly caused~~likely mainly driven by ocean warming, while air temperatures ~~possibly~~likely remained too cold to generate surface melt. We ~~specifically~~also detail ~~and showcase~~ results from our model ~~-~~data comparison ~~procedures~~, including regional heterogeneities in ~~model-data~~ fit and the sensitivity of ~~model-data~~ agreement scores to certain parameter configurations, ~~that will likely~~ which should prove useful for ~~others working~~

Formatted: Font: +Body (Calibri), 11 pt

Formatted: Font: +Body (Calibri), 11 pt

onfuture paleo-ice-sheet modelling experimentsstudies. Finally, we report on the remaining model-data misfits in ice extent, here found to be largest in northern, northeastern, and central-eastern Greenland, and discuss possible causes for suchthis spatial heterogeneity in model-data agreement.

Formatted: Font: 11 pt, Not Bold

Formatted: Left

1 Introduction

Due to anthropogenic climate change, the Greenland Ice Sheet (GrIS) is losing mass at an increasing rate and is now a major contributor to global mean sea level rise (Meredith et al., 2019). Its future contribution remains uncertain, however, andwith projections show importantshowing large discrepancies between models/studies, with , most estimations ranging between ~70 and ~190 mm of sea level rise contribution by the yearby 2100 under the RCP 8.5 / SSP5-85 emission scenarios (Aschwanden et al., 2019; The IMBIE Team., 2019; Goelzer et al., 2020; Edwards et al., 2021). Reducing uncertainties in GrIS projections is crucial not only crucial for estimating future sea level rise and Greenland-wide environmental changes, but also for anticipating future globalbroader climate change, in partimpacts, partly due to the ice- sheet's impactinfluence on ocean circulation and the potential slowdown of the Atlantic Meridional Overturning Circulation (AMOC) following increasingfrom increased freshwater releasesrelease (Yu et al., 2016; Martin et al., 2022; Sinet et al., 2023). A major source of uncertainty in future ice sheet projections relates to the model initialisation procedures , i.e. the 'spinup' required to obtainset an appropriate initial state, *i.e.* the model 'spinup' (Rogozhina et al., 2011; Seroussi et al., 2019). This is a challenge mainlychallenging because ice sheets are not in equilibrium with the contemporary climate but are instead still affected by past climate changes that occurred over thousands of years (Oerlemans et al., 1998; Yan et al., 2013; Calov et al., 2015; Yang et al., 2022). While paleo spinups are more appropriate to capture this ice-sheet memory, they generally fail at representing the present-day ice sheet conditions as accurately as inversiondata-assimilation schemes used inand equilibrium spinups (Goelzer et al., 2017), partly due in part to the greater uncertainties in paleo forcings, model parameterisations, and boundary conditions in the paleo realm (Aschwanden et al., 2013). Hence, there is a need to reduce such uncertainties by producing ensembles of higher-resolution paleo model simulations that are quantitatively scored against empirical reconstructions of past GrIS evolution. Although rare, such investigations may help obtain more appropriate initialisation procedures that better capture the ice-sheet's long-term memory while accurately modelling its present-day state (Pittard et al., 2022).

Formatted: Font: +Body (Calibri), 11 pt

Numerous open research questions remain regarding the past behaviour of the GrIS between the global Last Glacial Maximum (LGM), which occurred ~25 - 21 thousand years before present (kyr BP), and the present-day. For instance, the maximum GrIS volume during the last glaciation remains debated and differs, differing by a factor of up to 2.5 between modelling studies (*e.g.* Lecavalier et al., 2014; Bradley et al., 2018; Quiquet et al., 2021; Yang et al., 2022). The maximum GrIS extent, while though empirically constrained empirically

Formatted: French (Switzerland)

Formatted: French (Switzerland)

Formatted: French (Switzerland)

Formatted: French (Switzerland)

Formatted: French (Switzerland)

Formatted: French (Switzerland)

in ~~certain~~some regions (*e.g.*, Ó Cofaigh et al., 2013~~)~~), remains~~, is still~~ unknown in ~~numerous locations~~many areas due to the difficulty of ~~accessing and obtaining~~collecting offshore geomorphological and geochronological constraints on ice retreat, ~~making existing~~leaving data ~~of this nature somewhat~~ sparse (Funder et al., 2011; Sinclair et al., 2016; Leger et al., 2024). The timing, magnitude and rates of ice margin retreat and mass loss ~~experienced~~ during the last deglaciation, while essential to contextualise present-day ~~mass loss~~losses, are also poorly ~~known and challenging to determine empirically. The~~constrained. Similarly, the magnitude of ice margin retreat behind ~~its~~ present-day margins in response to the Holocene Thermal Maximum (HTM: ~10-5 kyr BP), a warmer period often used as an analogue for expected future warming ~~in the coming decades, also,~~ remains undetermined (Briner et al., 2021). A ~~final~~further rationale for 3D modelling of the former GrIS is that ~~numerous~~many characteristics of the past ice sheet, impacting former climate, ocean conditions, landscape evolution, biodiversity, and human history~~,~~ are ~~highly challenging (~~difficult, if not impossible~~),~~ to ~~constrain with~~reconstruct from field data alone. This ~~is for instance the case for paleo~~includes past changes in ice-sheet discharge, velocity, ice temperature, calving fluxes, mass balance, basal conditions, and their spatio-temporal ~~variations~~variability.

Addressing ~~some of the above~~ these knowledge gaps, ~~and~~while providing a present-day GrIS state that ~~contains~~retains the ~~appropriate~~ long-term memory of past climate changes, requires: i) ~~to force~~forcing a three-dimensional ~~and~~ thermo-mechanical ice-sheet model with a paleoclimate reconstruction, and ii) ~~to produce~~producing paleo ~~GrIS model~~ simulations that agree (within error) with ~~the~~ available empirical data on former ice-sheet geometry and behaviour, while ~~keeping the model~~remaining physically~~-~~ consistent and ~~respecting~~fully mass ~~conservation.~~ conserving. Combining these requirements is a major challenge and has yet to be achieved. ~~To this day, few~~Few studies modelling ~~the~~ GrIS evolution since the LGM have applied a quantitative model~~-~~–data comparison scheme to constrain ~~a set of~~ simulations ~~using~~with geological ~~field~~ observations (*e.g.* Huybrechts, 2002; Lecavalier et al., 2014; Born & Robinson, 2021). ~~Of those~~Those that did~~, the empirical datasets used were~~ mainly used relative sea~~-~~–level indicators, ice-core~~-~~–derived thinning curves (Vinther et al., 2009), and englacial stratigraphic isochrones (Born & Robinson, 2021; Rieckh et al., 2024). The paleo sea-level community, in particular, ~~has~~ pioneered the production of Greenland-wide datasets (*e.g.* Gowan, 2023) reconstructing the magnitude and rate of relative sea level drop during the Late-glacial and early-to-mid Holocene, when deglacial retreat caused the Greenland peripheral lithosphere to rebound. Such records have been used to assess GrIS-wide simulations by comparing modelled ~~versus~~against empirical uplift rates and relative sea level change (*e.g.* Simpson et al., 2009). However, relative sea~~-~~–level indicators ~~and other previously used datasets~~ are indirect proxies of former ice-sheet geometry, and do not provide a robust constraint on ~~the~~ grounded ice margin position and shape ~~of the former grounded GrIS margin retreat~~ through time. ~~With relative-sea-level-based comparisons, moreover~~Using such records, the quality of model-data fit is also heavily dependent on parameterisations of the Earth and glacial isostatic adjustment (GIA) models. ~~On the other hand~~In contrast, moraine ridges, ~~glacial~~ erratic boulders, trimlines, till units, and other ice-contact landforms/deposits are directly deposited and/or exposed at the ice-sheet

Formatted: Font: Italic

Formatted: Font color: Black

Formatted: Font color: Black

Formatted: Font color: Black

Formatted: Font color: Black

Formatted: Font color: Black

Formatted: Font color: Black

~~terminal or lateral~~ margins. When dated, ~~such records~~they provide a more direct ~~mean~~evidence of ~~reconstructing~~ former ice-sheet extent and thickness through time. The recent ~~production and~~ release of the PaleoGrIS 1.0 database and ice-extent isochrone reconstruction provides, for the first time, such a dataset at the GrIS-wide scale (Leger et al., 2024). Thus, despite ~~remaining~~ uncertainties ~~due to~~from the spatially and temporally heterogeneous nature of field observations, we now have the opportunity to compare numerical ~~model outputs~~simulations against a ~~different, arguably~~ more detailed and direct reconstruction of former grounded ice extent~~,~~ and ~~thus of former ice sheet~~ geometry.

We present a perturbed parameter ensemble of 100 simulations using the Parallel Ice Sheet model (PISM: Winkelmann et al., 2011) forced by transient paleoclimate and ocean simulations ~~of~~from the isotope-enabled Community Earth System Model (iCESM: Brady et al., 2019). ~~The ice sheet~~ Our simulations model the entire GrIS ~~between~~from 24 kyr BP ~~and~~to 1850 AD at ~~a~~5 x 5 km horizontal resolution ~~of 5 x 5 km~~ which, for such ~~long~~ timescales and ~~large~~ simulation numbers, is unprecedented. Each ~~ensemble~~ simulation is quantitatively scored against i) empirical data on the maximum ice-sheet size and extent ~~of the ice sheet (local LGM~~(lLGM extent), ii) the PaleoGrIS 1.0 reconstruction of ice-margin retreat during the last deglaciation (Leger et al., 2024), and iii) the present-day GrIS extent. Unlike ~~several~~previous paleo GrIS ~~modelling~~ experiments of similar design (*e.g.* Simpson et al., 2009; Lecavalier et al., 2014), empirical data is ~~here~~ not used to force the model or as a constraint during simulations. Instead, model-data fit is ~~quantified~~assessed after ~~the simulation is complete~~completion to ensure ~~simulations remain consistent~~consistency with ice-flow physics (within model approximations) and mass conservation (e.g. Ely et al., 2024). ~~The results of our~~Our ensemble~~, as well as~~ results, including best-fit simulations, ~~provide numerous~~offer new insights into the LGM-to-present evolution of the ice sheet and ~~present interesting~~highlight heterogeneities in model-data fit. We ~~report and discuss~~ present these findings ~~along with~~and our experiment methodology below.

2 Methods

2.1 The ice-sheet model setup

To model the last 24 kyrs of GrIS evolution, we use PISM version 2.0.5, an open-source, three-dimensional and thermo-mechanical model used widely to simulate ice-sheet systems (Winkelmann et al., 2011; Aschwanden et al., 2016; Albrecht et al., 2020; Clark et al., 2022; Ely et al., 2024; Khroulev & The PISM authors, 2020). Our overall approach is to run an ensemble of 100 PISM simulations over the entire Greenland Ice Sheet (GrIS) at 5 x 5 km horizontal resolution (Fig. 1), from 24 kyr BP to the Pre-Industrial era (PI: 1850 AD). Within the ensemble, we vary 10 key model parameters (Table 1). Each ensemble

simulation is scored against empirical data on the timing of ice extent using PaleoGrIS 1.0 (Leger et al., 2024) and model-data comparison procedures (e.g. ATAT 1.1; Ely et al., 2019), enabling us to isolate best-fit simulations. Together with the full ensemble, these are analysed further to provide quantitative results presented and discussed in sections 3 and 4 (Fig. 2). In the Methods sections below, we describe our model setup and input data used as forcings to the spin-up and transient simulations. For a full description of PISM and its capabilities, the reader is referred to the complete manual (https://www.pism.io/docs/; Khroulev & The PISM authors, 2020).

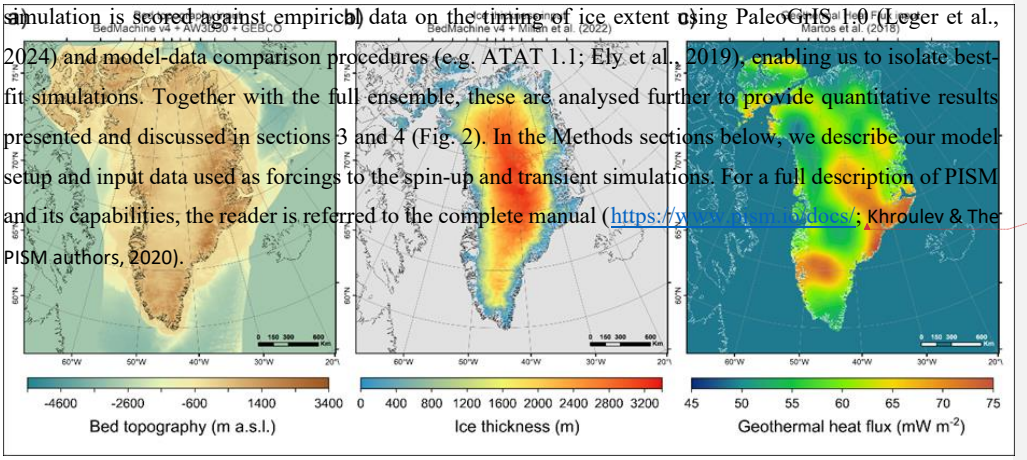

Figure 1. Time-independent and two-dimensional forcing fields used as inputs for present-day bed elevation (panel a), ice thickness (panel b; Morlighem et al., 2017; Millan et al., 2022), and geothermal heat flux (panel c; Martos et al., 2018). Bed elevation (panel a) is estimated by merging several products. Topography under the contemporary GrIS is from BedMachine v4 (Morlighem et al., 2017; spatial resolution: 150 m). For terrestrial

Formatted: Font: 11 pt

Formatted: Font: Bold

Formatted: Font: Bold

Formatted: Font: Bold

Formatted: Font: Bold

regions with no GrIS cover, we use the ALOS World 3D 30 m Digital Elevation Model (DEM; Tadono et al., 2014). Present-day periphery ice is removed using thickness estimates from Millan et al. (2022). For other regions (ice-free ocean and other landmasses), we use the 15 arc-second resolution General Bathymetric Chart of the Oceans (GEBCO Bathymetric Compilation Group 2022, 2022). These datasets are resampled (to 5 x 5 km) using cubic convolution (Keys, 1981).

Formatted: Font: Bold

Formatted: Font: Bold

Formatted: Font: Bold

Formatted: Font: Bold

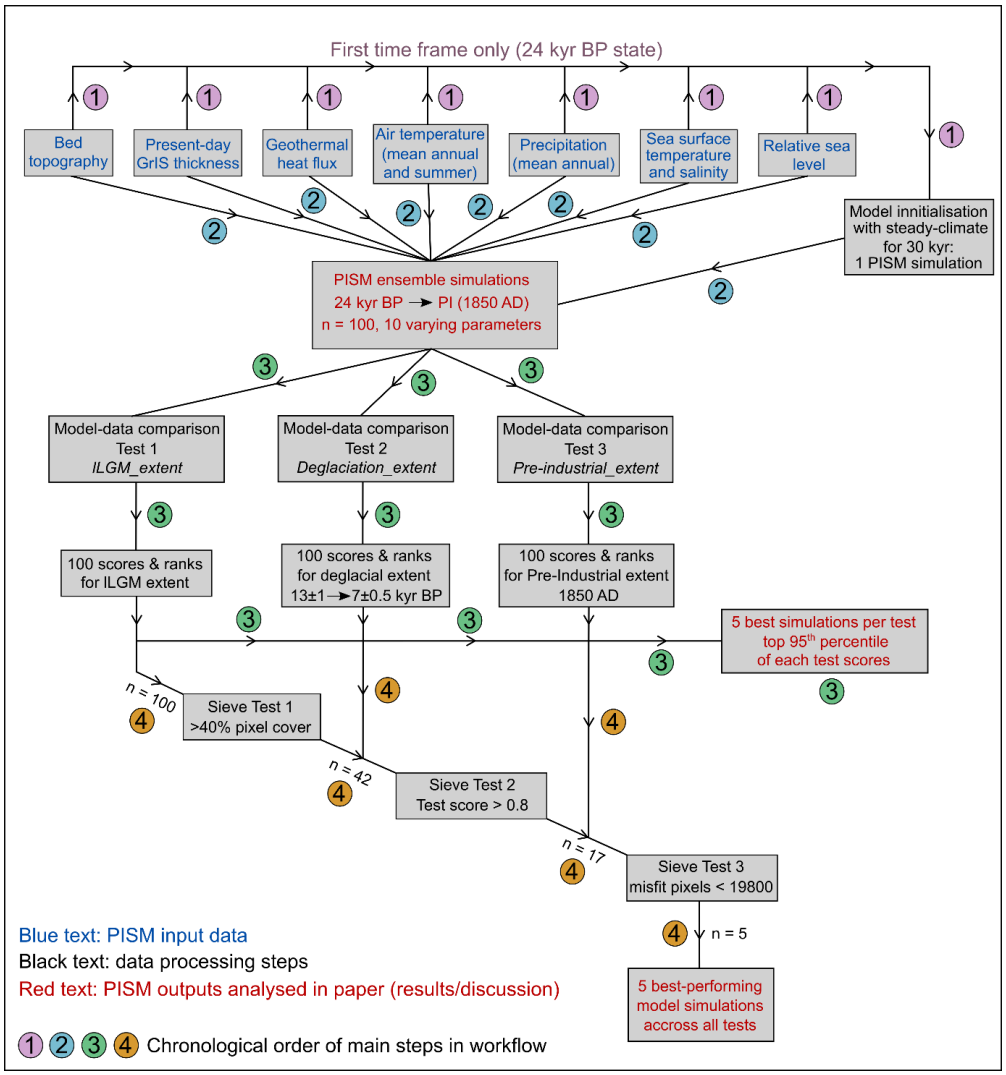
First time frame only (24 kyr BP state)
Bed topography
Present-day GrIS thickness
Geothermal heat flux
Air temperature (mean annual and summer)
Precipitation (mean annual)
Sea surface temperature and salinity
Relative sea level
Model initialisation with steady-climate for 30 kyr: 1 PISM simulation
PISM ensemble simulations 24 kyr BP → PI (1850 AD) n = 100, 10 varying parameters
Model-data comparison Test 1 ILGM_extent
Model-data comparison Test 2 Deglaciation_extent
Model-data comparison Test 3 Pre-industrial_extent
100 scores & ranks for lLGM extent
100 scores & ranks for deglacial extent 13±1→7±0.5 kyr BP
100 scores & ranks for Pre-Industrial extent 1850 AD
5 best simulations per test top 95th percentile of each test scores
n = 100
Sieve Test 1 >40% pixel cover
n = 42
Sieve Test 2 Test score > 0.8
n = 17
Sieve Test 3 misfit pixels < 19800
n = 5
5 best-performing model simulations accross all tests
Blue text: PISM input data
Black text: data processing steps
Red text: PISM outputs analysed in paper (results/discussion)
1 2 3 4 Chronological order of main steps in workflow

Figure 2. Flowchart diagram illustrating the methodological workflow followed in this study's modelling experiment including input datasets (step 1), model initialisation (step 1), transient ensemble simulations modelling (step 2) and post-processing steps including model-data comparison (3) and ensemble sieving (4). The reader is referred to the methods section for more details.

Formatted: Space After: 0 pt, Don't add space between paragraphs of the same style, Line spacing: 1,5 lines

2.1.1 Ice flow

To model ice flow, PISM uses a hybrid stress balance scheme that combines the Shallow Ice Approximation (SIA) and the Shallow Shelf Approximation (SSA) (Bueler and Brown, 2009). PISM also features an enthalpy-based and three-dimensional formulation of thermodynamics enabling to model polythermal ice and basal melt (Aschwanden et al., 2012). For ice rheology ($\dot{\epsilon}$), we use the default Glen-Paterson-Budd-Lliboutry-Duval flow law,

$$\dot{\epsilon}_{i,j} = E \cdot A(T,\omega)\, \tau_e^{n-1}\, \tau_{i,j}\ , \tag{1}$$

where n is the flow-law exponent, E a flow enhancement factor, A the Arrhenius factor (ice softness) determined by the liquid water content, ω, and ice temperature, T, while τ and τ_e represent the deviatoric and effective stresses, respectively (Aschwanden et al., 2012). In our ensemble, we vary E uniformly for both the SIA and SSA (see section 2.3) and keep $n = 3$ as default.

2.1.2 Boundary conditions

The ice-bed interface

We use the slip law of Zoet and Iverson (2020), which considers both mechanisms of glacier sliding over rigid beds and subglacial till deformation with minimal parameterisation and no required knowledge of the bed type. In PISM, this law is formulated as

$$\boldsymbol{\tau}_b = -\tau_c \frac{\boldsymbol{u}}{(|\boldsymbol{u}|+u_t)^q |\boldsymbol{u}|^{1-q}}\ , \tag{2}$$

where $\boldsymbol{\tau}_b$ is the basal shear stress, τ_c the basal yield stress, $\boldsymbol{u}$ the slip velocity and u_t the threshold velocity at which shear stress equals the Coulomb shear strength of the till. In our simulations, u_t is kept constant at 50 m yr^{-1} (Khroulev and The PISM authors, 2020; Zoet and Iverson, 2020) while q varies between simulations (see section 2.3). We account for space- and time-dependent basal yield stress, τ_c, controlled by~~:~~ ~~1)~~, firstly, a simple hydrology model (Tulaczyk et al., 2000) which determines the effective pressure, N_{till}, from the till-pore water content obtained by storing basal melt locally up to a threshold (here set to 2 m~~); and 2)~~). With this simplified parameterisation, water is not conserved as water reaching above the threshold is lost permanently. The basal water thickness in the till layer, W_{till}, is computed from the basal melt rate, m_b, obtained from the enthalpy, as follows:

$$\frac{\partial W_{till}}{\partial t} = \frac{m_b}{\rho_w} - C_{dr}, \quad (3)$$

where C_{dr} is a simple decay rate parameter and ρ_w is the density of fresh water. Secondly, τ_c is also controlled by the till friction angle, ϕ, *i.e.* the frictional strength of basal till materials (Cuffey and Paterson, 2010)

Formatted: Font color: Auto

$$\tau_c = \tan(\phi)\, N_{till}\,. \quad (34)$$

By assuming basal materials in valley troughs are generally weaker than towards mountain tops, we parameterise ϕ as a piece-wise linear function of bed elevation, b, (after Aschwanden et al., 2013; 2016; Huybrechts and de Wolde, 1999)

$$\phi(x,y) = \begin{cases} \phi_{min}, & b(x,y) \le b_{min}, \\ \phi_{min} + (b(x,y) - b_{min})M, & b_{min} < b(x,y) < b_{max}, \\ \phi_{max}, & b_{max} \le b(x,y), \end{cases} \quad (45)$$

where $M = (\phi_{max} - \phi_{min}) / (b_{max} - b_{min})$. We set ~~upper and lower~~ elevation thresholds (b_{min}, b_{max}) to -400 and 500 m a.s.l., respectively, while ϕ thresholds (ϕ_{min}, ϕ_{max}) are simulation-dependent (Table 1, see section 2.3). This PISM parameterisation was shown to produce flow velocities consistent with observations for major GrIS glaciers (Aschwanden et al., 2016).

Bed elevation is ~~estimated~~obtained by merging ~~several products including~~topographies from BedMachine v4 (Morlighem et al., 2017), the ALOS World 3D 30 m Digital Elevation Model (DEM; Tadono et al., 2014), and the General Bathymetric Chart of the Oceans (GEBCO Bathymetric Compilation Group 2022, 2022). The reader is referred to Figure 1 for more details ~~regarding these data.~~. To avoid modelling large non-Greenlandic ice bodies, Iceland and Baffin Island are ~~manually~~ removed (Fig. 1). ~~Modelling~~ We however include the Innuitian Ice Sheet (IIS) ~~together~~ as it coalesced with the GrIS ~~is important as the two ice sheets coalesced~~ (Jennings et al., 2011) and ~~thus~~ the two ice sheets dynamically ~~interacted~~impacted each other (Bradley et al., 2018). ~~We thus include~~ Modern icecaps on Ellesmere Island ~~in our domain, with local modern icecaps~~ are removed using ~~present day~~ ice thickness estimates from Millan et al. (2022). Finally, we use a two-dimensional and time-independent geothermal heat flux data from Martos et al. (2018) (Fig. 1). This dataset ranges from 0.049 to 0.073 W m^{-2}, and is consistent with a plume track (the Iceland hotspot) that crossed Greenland from NW to SE. We run PISM at the horizontal resolution of 5 x 5 km (grid size: 620 x 620), with 101 vertical ice layers using quadratic concentration ~~towards~~at the base.

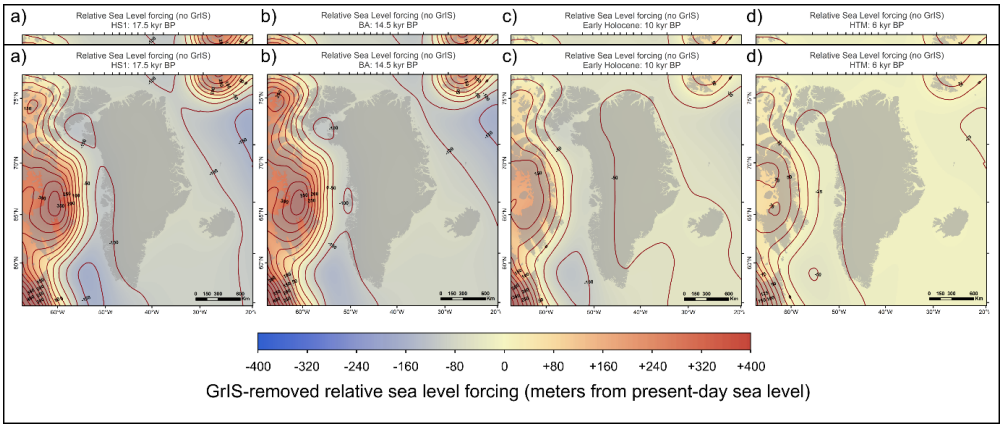

Figure 3. GrIS-removed (non-local components) relative sea-level forcing data for four different time slices and given as input to our transient ensemble simulations. These snapshots show the relative sea-level prior to adding the GrIS-specific contribution to GIA-induced relative sea-level change during our transient ensemble simulations (see methods section). Positive offset values (red) indicate isostatic bed depression relative to present and thus higher relative sea-levels than today, while negative offset values (blue) indicate isostatic bed uplift relative to present (*e.g.* on a peripheral bulge) and thus lower relative sea-levels than today. Snapshots are shown for the the HS 1 cooling event (panel a), the BA warming event (panel b; 14.5 kyr BP), the early Holocene (panel c; 10 kyr BP), and the HTM warming event (panel d; 6 kyr BP). All model input data fields are re-projected to EPSG:3413 and resampled to a 5 x 5 km resolution using cubic convolution.

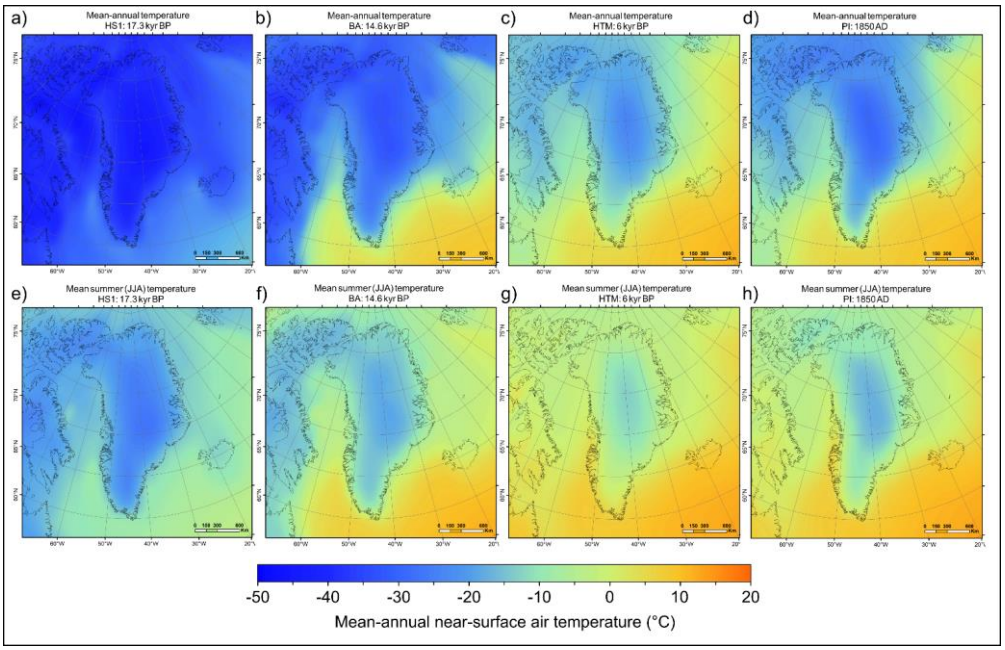
a)
Mean-annual temperature
HS1: 17.3 kyr BP
b)
Mean-annual temperature
BA: 14.6 kyr BP
c)
Mean-annual temperature
HTM: 6 kyr BP
d)
Mean-annual temperature
PI: 1850 AD
e)
Mean summer (JJA) temperature
HS1: 17.3 kyr BP
f)
Mean summer (JJA) temperature
BA: 14.6 kyr BP
g)
Mean summer (JJA) temperature
HTM: 6 kyr BP
h)
Mean summer (JJA) temperature
PI: 1850 AD
-50 -40 -30 -20 -10 0 10 20
Mean-annual near-surface air temperature (°C)

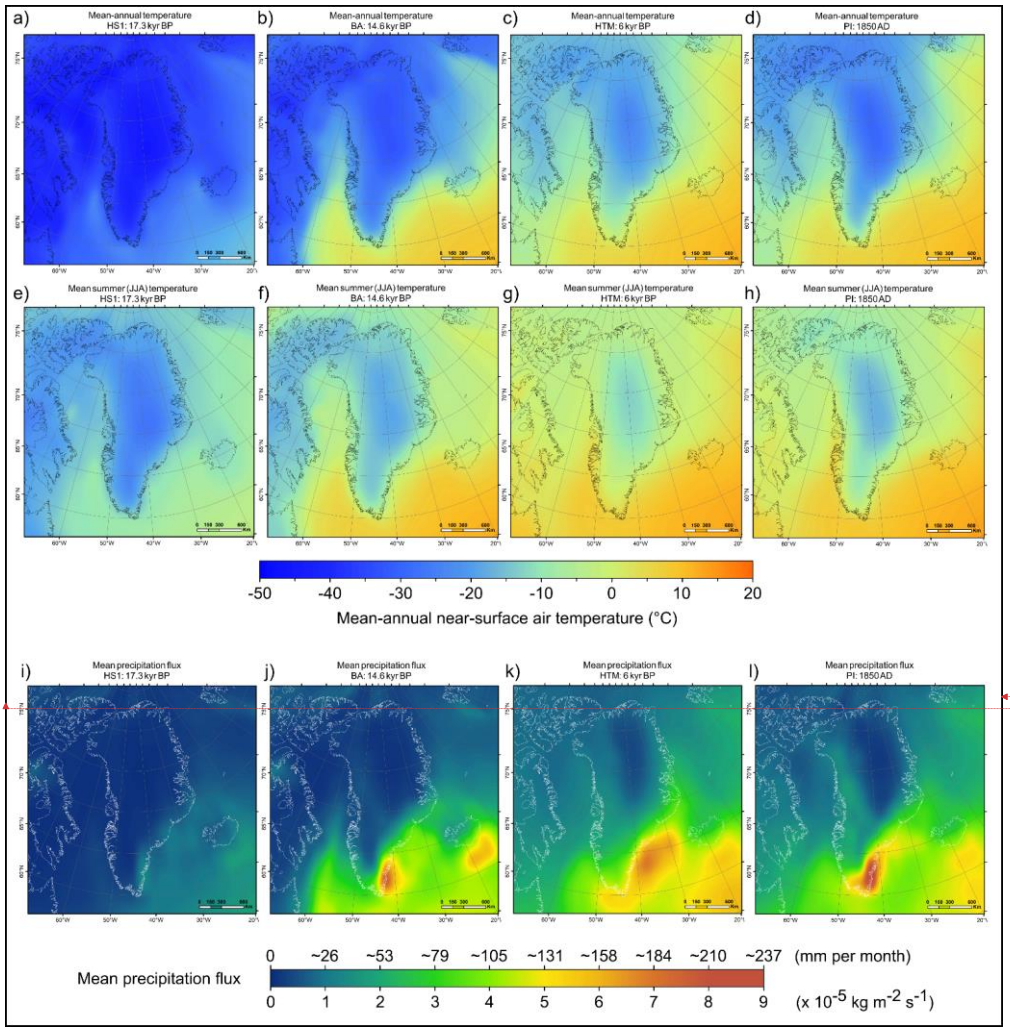

Figure 4. Two-dimensional fields of ~~reference height~~ mean-annual surface air temperature (panels a-d~~) and~~), mean-summer surface air temperature (JJA mean; panels e-h~~) temperature~~), and mean annual precipitation flux (panels i-l) data used as input in our modelling experiment, derived from iCESM transient and equilibrium time slice simulations (see methods section), and shown as snapshots for the HS 1 cooling event (panels a, e, i), the BA warming event (panels b, f, j), the HTM warming event (panels c, g, k), and the PI (1850 AD; panels d, h, l). All climate input data fields are re-projected to EPSG:3413 and resampled to a 5 x 5 km resolution using cubic convolution.

Formatted: Font: +Headings CS (Times New Roman), 11 pt, Bold, Not Italic

Formatted: Space After: 8 pt, Add space between paragraphs of the same style, Line spacing: Multiple 1,15 li

The ice-atmosphere interface

To compute Surface Mass Balance (SMB) from ~~two-dimensional fields of~~ time-dependent ~~reference height~~surface air temperature and precipitation (see section 2.1.3), we use PISM's ~~default~~ Positive-Degree-Day (PDD) model (Calov and Greve, 2005; Ritz, 1997). Precipitation when temperature is above 2 °C and under 0 °C is interpreted as rain and snow, respectively, with a linear transition between. Temperature and precipitation fields used to force the SMB are further described in section 2.1.3. The fraction of surface melt that refreezes is set to 60% (EISMINT-Greenland value; Ritz, 1997). Spatio-temporal variations in the standard deviation, σ, of daily temperature variability influences SMB (Arnold and MacKay, 1964). We parameterise σ to be a linear function of ~~reference height~~surface air temperature T (and indirectly, of ice surface elevation)

$$\sigma = aT + b. \quad (~~5~~6)$$

We assign b a value of 1.66 (after Seguinot and Rogozhina, 2014) and vary a as part of our ensemble (see section 2.3).

The ice-ocean interface

For floating sectors of the modelled GrIS, sub-shelf melt is obtained by computing basal melt rate and temperature from thermodynamics in a boundary layer at the ice shelf base (Hellmer et al., 1998; Holland and Jenkins, 1999). This model, which does not consider sub-shelf circulation, uses three equations describing: 1) the energy flux balance, 2) the salt flux balance, and 3) the pressure- and salinity-dependent freezing point in the boundary layer. This sub-shelf melt parameterisation thus requires time-dependent ~~two-dimensional~~ fields of potential temperature and practical salinity (see section 2.1.3.). More details can be found in Hellmer et al. (1998) and Holland and Jenkins (1999). Calving was ~~likely~~ a predominant ablation mechanism during the ~~local LGM~~lLGM (~21-15 kyr BP) and throughout the Late-Glacial, when the GrIS

Formatted: Font color: Black

was mostly marine-terminating (Funder et al., 2011a). Although physical calving processes remain poorly understood, we here model it following similar PISM parameterisations as Albrecht et al. (2020) and Pittard et al. (2022). Firstly, floating ice at the calving front thinner than a given threshold is ~~automatically~~ calved (see section 2.3). Secondly, we use the strain-rate-based eigen calving law (Albrecht and Levermann, 2014; Levermann et al., 2012) to determine the average calving rate, c, based on the horizontal strain rate, $\dot{\epsilon}_{\pm}$, derived from SSA-velocities, and a constant, K, integrating ice material properties at the calving front

$$c = K\,\dot{\epsilon}_{+}\,\dot{\epsilon}_{-}\,, \quad \dot{\epsilon}_{\pm} > 0. \qquad (\text{~~6~~}7)$$

We assign K a value of 5 x 10^{17} m s^{-1} (after Albrecht et al., 2020; Pittard et al., 2022). While a von Mises stress - type calving law may be more appropriate for fjord-terminating glaciers (*e.g.* Aschwanden et al., 2019), the GrIS expanded over continental shelves and was entirely marine-terminating during the ~~local LGM~~lLGM, thus forming wide ice shelves comparable to Antarctica today (Jennings et al., 2017). As the ice sheet was in this configuration for more than half our simulated timeframe, we rely on the eigen calving law throughout our simulations. Following Albrecht et al. (2020), we further restrict ice-shelf extent by calving ice when bathymetry exceeds 2 km, with the exception of Baffin Bay.

The grounding line location is determined by computing a floatation criterion (Khroulev and The PISM authors, 2020). This criterion depends on water depth, defined as the vertical distance between the geoid and the solid earth surface (Mitrovica and Milne, 2003). Around Greenland, and for ~~the~~our timeframe ~~of interest~~ (24-0 kyr BP), spatio-temporal variations in water depth result from changes in the global mean sea level and GIA-induced deformation of the solid earth (Rovere et al., 2016). The latter can result from variations in GrIS mass (local sources), and the influence of the neighbouring Laurentide Ice Sheet (LIS) and IIS, responsible for spatially and temporally variable sea level around Greenland (non-local sources)(Bradley et al., 2018). During and following glaciations, non-local contributions can be significant, as Greenland is located on the eastern peripheral forebulge generated by the LIS (Simpson et al., 2009; Lecavalier et al., 2014) (Fig. 3). ~~Here, we account for this interplay and~~We thus combine at each time step the non-local relative sea level signal calculated from an offline GIA model with the local GrIS-driven signal, enabling to compute the final water depth and resulting floatation criterion (Fig. 3).

For the local GrIS signal, we use PISM's Lingle-Clark-type viscoelastic deformation model (Lingle and Clark, 1985; Bueler et al., 2007). We use default lithosphere flexural rigidity and mantle density values of 5 x 10^{24} N m^{-1} and 3300 kg m^{-3}, respectively. For mantle (half-space) viscosity, we use a value of 5 x 10^{20} Pa s^{-1}, consistent with Lambeck et al. (2017). To calculate ~~the~~ non-local sea level ~~change~~changes across ~~the region of interest~~our domain, we run an offline GIA model. This model was run at a resolution of 512° and solves the generalized sea level equation (Mitrovica & Milne, 2003; Kendall et al., 2005) accounting for sea

level change in regions of retreating marine-based ice, perturbations to the Earth's rotation vector, and time-varying shoreline migration. For the input ice sheet reconstruction, we use a hybrid reconstruction (Lambeck et al., 2014; 2017), where the GrIS is removed from the North American ice sheet reconstruction. We use a 1D viscoelastic earth model with a lithosphere thickness of 96 km and upper and lower mantle viscosities of 5 x 10^{20} Pa s^{-1} and 1 x 10^{22} Pa s^{-1}, respectively. This offline model is used to produce two-dimensional input sea level offsets from the present-day sea level between 24 kyr BP and the PI, at 500 yr temporal resolution. PISM uses these offsets to compute the final relative sea level after computing local GIA deformation.

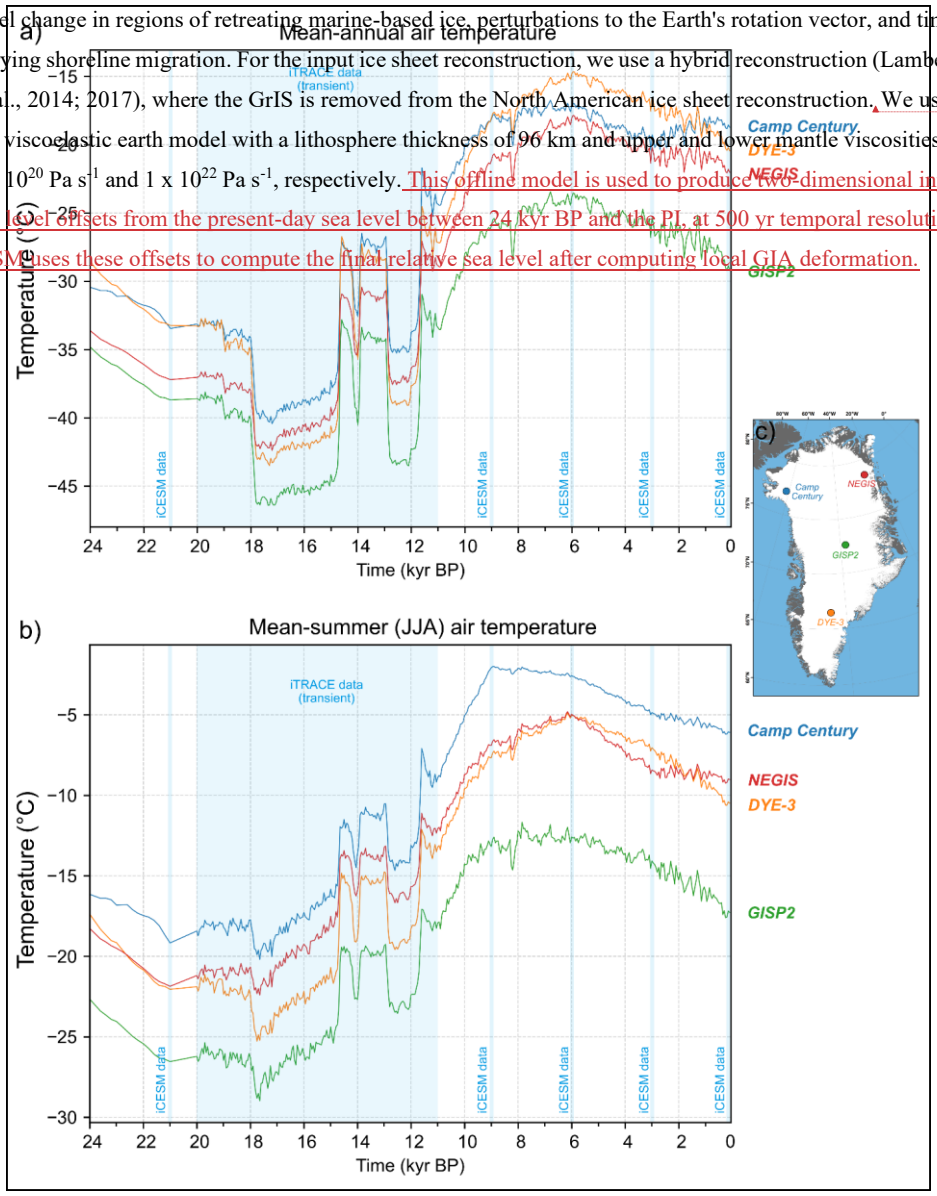

Formatted: Font: Times New Roman

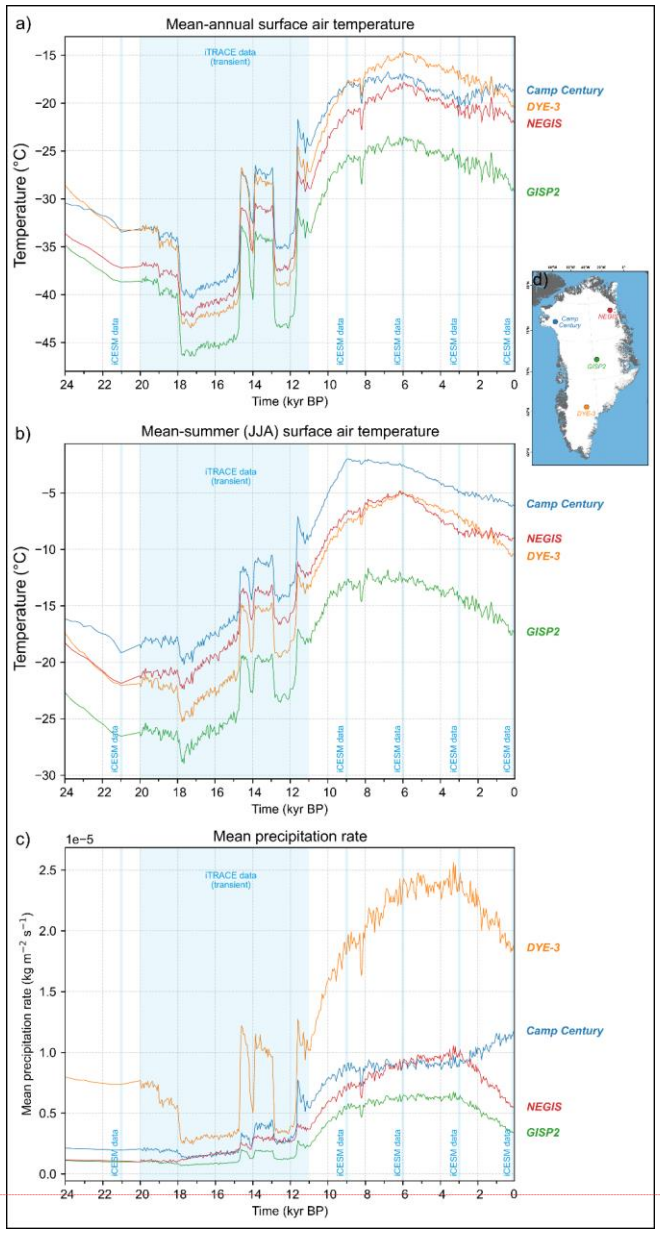

Figure 5. Time series of ~~reference height~~ mean-annual (panel a) and mean-summer (JJA-mean; panel b) surface air temperature data used as forcing in our ensemble simulations, at 4 different locations of the ice sheet (shown on inset: panel ~~e~~d). Transparent blue bands highlight time windows covered by iCESM climate data. In between these data points, forcing fields are approximated using a spatially-variable glacial index scheme (see methods section).

Formatted: Font: +Headings CS (Times New Roman), 11 pt, Bold

Formatted: Space After: 8 pt, Add space between paragraphs of the same style, Line spacing: single

Formatted: Justified, Line spacing: Multiple 1,15 li

2.1.3 Atmospheric and oceanic forcings

Air temperature and precipitation

SMB is forced with ~~two-dimensional and~~ time-dependent fields of ~~reference height~~surface air temperature and total precipitation (Figs. 4-~~8~~7). We use pre-existing simulations from iCESM (Brady et al., 2019) ~~versions 1.2 and 1.3,~~ run globally at a horizontal resolution of 1.9~~° in~~ x 2.5° (latitude ~~and 2.5° in~~x longitude) for the atmosphere and a nominal 1° for ~~the~~ oceans. We use ~~simulations ran with~~ full forcing simulations, *i.e.* including ice sheet (from ICE-6G: Peltier et al., 2015), orbital (Berger, 1978), greenhouse gases (Lüthi et al., 2008) and meltwater forcings. Between 20 and 11 kyr BP, we use ~~data~~monthly-resolution output from the iTRACE experiment, ran with iCESM 1.3 (He et al., 2021a, b). Thanks to an improved climate model, higher resolution, and the addition of water isotopes, iTRACE simulates a climate over Greenland that is more data-consistent (He et al., 2021a) than the former CESM simulation of the last deglaciation TRACE-21 (Liu et al., 2009). Additionally, we use output from five equilibrium time-slice simulations ran at 21 kyr BP ~~and PI (1850 AD)~~ (iCESM 1.3), ~~and~~ at 9, 6, and 3 kyr BP (iCESM 1.2~~).~~), and at the PI (1850 AD, iCESM 1.3) (Fig. 4).

To create continuous forcing over remaining data gaps in time, we ~~use~~apply a glacial index approach (Niu et al., 2019; Clark et al., 2022) and linearly scale our climate fields proportionally to variations in independent climate reconstructions ~~(Fig. 5).~~ in a space-dependent manner i.e. building a glacial index for each individual grid cell (Fig. 5). Between 24 and 21 kyr BP, we use surface air temperature and $\delta^{18}O$ reconstructions of Osman et al. (2021) to scale variations in temperature and precipitation fields, respectively. For data gaps between 21 kyr BP and the PI (*e.g.* 11 - 9 kyr BP), we use the seasonally-resolved Greenland-wide temperature and precipitation reconstruction of Buizert et al. (2018) as glacial index. ~~Between 24 and 21 kyr BP, we use surface air temperature and $\delta^{18}O$ reconstructions of Osman et al. (2021) to scale variations in temperature and precipitation fields, respectively. The results are time-dependent, two-dimensional fields of mean annual and mean summer (JJA) reference height air temperature and mean precipitation rate, continuous between 24 kyr BP and PI (Fig. 4-8). From mean annual and mean summer temperatures, our SMB scheme reads a cosine yearly cycle generating an idealised seasonality signal.~~

As a result, we produce time-dependent, two-dimensional fields of mean annual and mean summer (JJA) surface air temperature and precipitation rate, continuous between 24 kyr BP and PI (Fig. 4-7). From mean annual and summer temperatures, our SMB model reads a cosine yearly cycle to generate a seasonality signal.

Formatted: Font: +Headings CS (Times New Roman), 11 pt, Bold

Formatted: Justified, Space After: 8 pt, Add space between paragraphs of the same style, Line spacing: Multiple 1,15 li

Ocean temperature and salinity

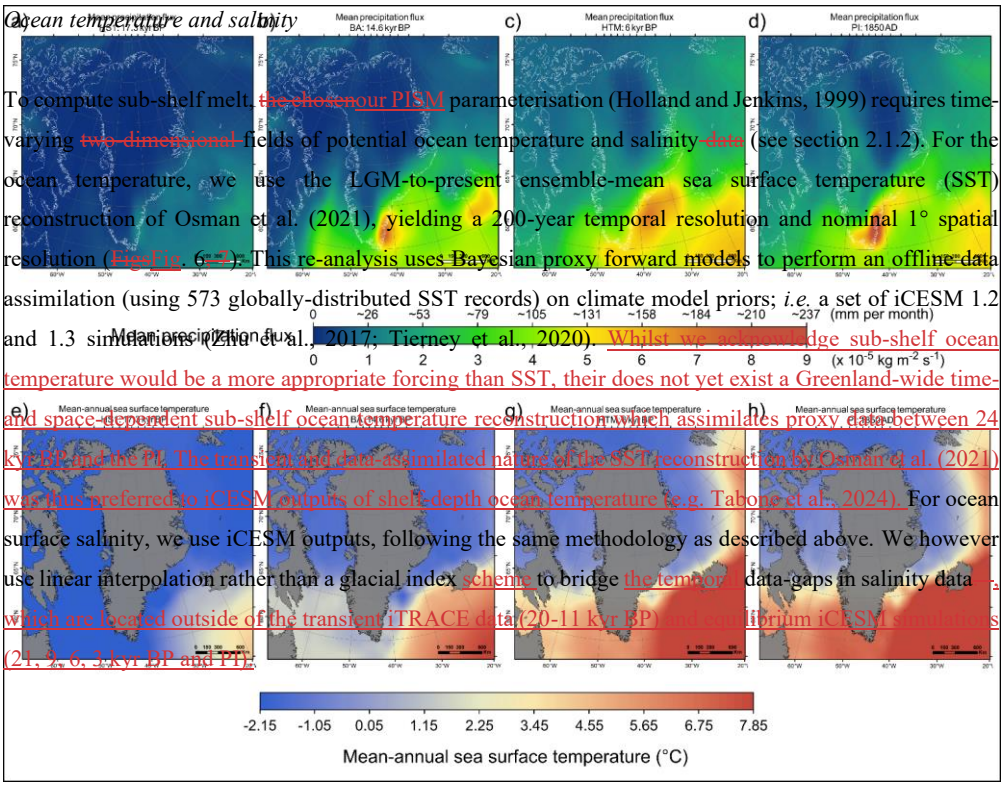

To compute sub-shelf melt, ~~the chosen~~our PISM parameterisation (Holland and Jenkins, 1999) requires time-varying ~~two-dimensional~~ fields of potential ocean temperature and salinity ~~data~~ (see section 2.1.2). For the ocean temperature, we use the LGM-to-present ensemble-mean sea surface temperature (SST) reconstruction of Osman et al. (2021), yielding a 200-year temporal resolution and nominal 1° spatial resolution (~~Figs~~Fig. 6a–d). This re-analysis uses Bayesian proxy forward models to perform an offline data assimilation (using 573 globally-distributed SST records) on climate model priors; *i.e.* a set of iCESM 1.2 and 1.3 simulations (Zhu et al., 2017; Tierney et al., 2020). Whilst we acknowledge sub-shelf ocean temperature would be a more appropriate forcing than SST, their does not yet exist a Greenland-wide time- and space-dependent sub-shelf ocean temperature reconstruction which assimilates proxy data between 24 kyr BP and the PI. The transient and data-assimilated nature of the SST reconstruction by Osman et al. (2021) was thus preferred to iCESM outputs of shelf-depth ocean temperature (e.g. Tabone et al., 2024). For ocean surface salinity, we use iCESM outputs, following the same methodology as described above. We however use linear interpolation rather than a glacial index scheme to bridge the temporal data-gaps in salinity data, which are located outside of the transient iTRACE data (20-11 kyr BP) and equilibrium iCESM simulations (21, 9, 6, 3 kyr BP and PI).

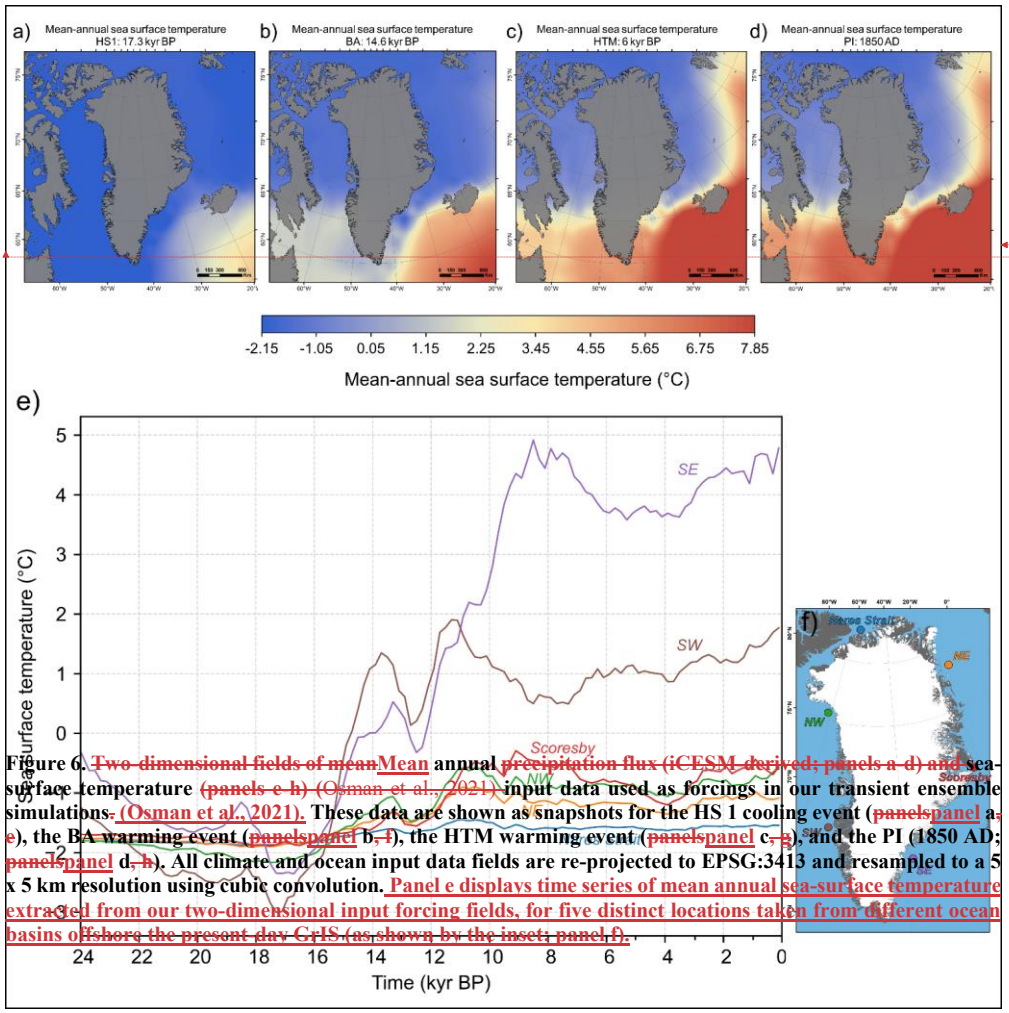

Figure 6. ~~Two-dimensional fields of mean~~**Mean annual** ~~precipitation flux (iCESM-derived; panels a–d) and~~ **sea-surface temperature** ~~(panels e–h) (Osman et al., 2021)~~ **input data used as forcings in our transient ensemble simulations.** ~~(Osman et al., 2021).~~ **These data are shown as snapshots for the HS 1 cooling event (**~~panels~~**panel a**~~,~~ ~~e~~**), the BA warming event (**~~panels~~**panel b**~~, f~~**), the HTM warming event (**~~panels~~**panel c**~~, g~~**), and the PI (1850 AD;** ~~panels~~**panel d**~~, h~~**). All climate and ocean input data fields are re-projected to EPSG:3413 and resampled to a 5 x 5 km resolution using cubic convolution.** ~~Panel e displays time series of mean annual sea-surface temperature extracted from our two-dimensional input forcing fields, for five distinct locations taken from different ocean basins offshore the present-day GrIS (as shown by the inset; panel f).~~

Formatted: Font: +Headings CS (Times New Roman), 11 pt

Formatted: Justified, Space After: 8 pt, Add space between paragraphs of the same style, Line spacing: single

2.2 Model initialisation ~~procedure~~

For model initialisation, we simulate a GrIS in balance with boundary conditions at 24 kyr BP, ~~*i.e.*~~ the starting year of our transient simulations, chosen to be significantly earlier ~~(up to~~ (~9 kyr) than the ~~local LGM~~lLGM (17.5-15 kyr BP; Lecavalier et al., 2014). ~~To do so, we~~We use present-day GrIS thickness (~~see section 2.1.2~~Fig. 1b) and run a 30 kyr-long simulation using parameterisations described above~~. Ensemble~~, fixing ensemble-varying parameters ~~are set~~ to their mid-range values (Table 1). After 30 kyr ~~of simulation~~ with a static climate (from 24 kyr BP), modelled surface and basal ice velocities are stable across the domain, while mass flux rates in glacierised areas are near zero. Basal mass flux for grounded and sub-shelf ice as well as surface melt, accumulation and runoff rates all reach steady state. The spun-up grounded GrIS area reaches 2.27 10^6 km^2, while grounded-ice volume approximates 8.22 m sea-level-equivalent (SLE), ~0.8 m above ~~the~~its present-day ~~GrIS~~ volume (7.42 ± 0.05 m SLE; Morlighem et al., 2017). In this study, grounded GrIS volume calculations (in m SLE) exclude ice under floatation~~, computed~~ (using the PISM-derived time-dependent ~~floatation~~flotation criterion~~. The calculation also excludes~~), the ISS, ~~periphery~~peripheral glaciers and icecaps, and any ice thinner than 10 m (after Albrecht et al., 2020). We use ice density, ~~sea water~~seawater density, and ~~static~~ ocean surface area values of 910 kg m^{-3}, 1027 kg m^{-3}, and 3.618 x 10^8 km^2 (Menard and Smith, 1966), respectively. This spun up GrIS is used as ~~the initial condition for all ensemble transient simulations.~~ initial condition for all ensemble transient simulations. The 30 kyr equilibrium spinup limited us computationally to this single initial state at 24 kyr BP with ensemble-varying parameters fixed to mid-range values. Although adjusting parameters in subsequent transient runs can generate instabilities in the first simulation years, equilibrium with parameterisations is likely reached within the first centuries and should not significantly affect the modelled lLGM or deglacial dynamics.

2.3 Ensemble design

Numerical ice-sheet modelling is governed by a plethora of parameters, many of which are poorly constrained by physical processes or empirical data. Uncertainties ~~associated with~~from subjective parameter configurations are large, and generally greater in paleo simulations, due to a lack of observational data (Tarasov et al., 2012). To minimise biases in parameter choices and to assess model-data fit (see section 2.4)

using a wide range of parameter configurations, we perturbate an ensemble of 100 simulations with 10 varying parameters (Table 1). We use ~~the~~ Latin hypercube sampling~~ technique~~ (Iman, 2008; Stein, 1987) with the maximin criterion (van Dam et al., 2007) to ensure homogeneous sampling of the high-dimensionality parameter space, while minimising potential redundancies. The 10 ensemble-varying parameters were drawn from five ~~main~~ groups:

-Ice dynamics: we alter the flow law (Eq. 1) enhancement factor (E) uniformly for both the SIA and SSA using a range (0.5 - 3) bracketing the value E = 1.25 found to produce best fit with contemporary GrIS flow speeds (Aschwanden et al., 2016). We vary the sliding law exponent q (Eq. 3) between 0.01 and 1, permitting to continuously alter the dependency of basal shear stress on sliding velocity from nearly purely-plastic to linear.

-Basal yield stress: to alter the impact of bed elevation (and bed strength) on basal yield stress between simulations, we vary ϕ_{min} and ϕ_{max} (Eq. 4) between 4 - 15° and 20 - 45°, respectively, which bracket values obtained by Aschwanden et al. (2016) for present-day GrIS hindcasting.

-SMB: Based on present-day GrIS surface melt, PDD snow and ice melt factors vary between 2 - 5 and 5 - 12 mm *we* d^{-1} $°C^{-1}$, respectively (Braithwaite, 1995; Fausto et al., 2009; Aschwanden et al., 2019). We also vary coefficient a in Eq. 5 between -0.25 and -0.1, thus modifying the impact of temperature change on the standard deviation of daily temperature variability (σ), following the relationship established by Seguinot and Rogozhina (2014).

-Calving: preliminary testing revealed that varying the minimum thickness threshold of ice shelf fronts had a greater impact on modelled GrIS extent than modifying the eigen calving law constant, K (Eq. 6). The thickness threshold was thus retained as an ensemble parameter and is varied between 25 and 200 m, based on observations (Motyka et al., 2011; Morlighem et al., 2014).

-Climate forcing: paleo-climate data from earth-system models can have biases, for instance due to their own paleo-ice-sheet forcings displaying inaccurate geometries (Buizert et al., 2014; Erb et al., 2022; He et al., 2021a). To account for ~~potential biases~~these, we apply ~~variations in input~~perturbations to climate fields using space-independent temperature and precipitation offsets as ensemble-varying parameters (Table 1). Based on surface air temperature variability over Greenland (1 stdev) in Osman et al. (2021)'s ensemble, we vary temperature fields by -3.5 to +3.5 °C (Table 1). ~~Furthermore, preliminary~~Preliminary simulations showed a high sensitivity of modelled GrIS extent and volume to precipitation changes. We thus vary precipitation ~~between simulations and choose~~using a wide range of offsets, *i.e.* between 20 and 200 % input precipitation.

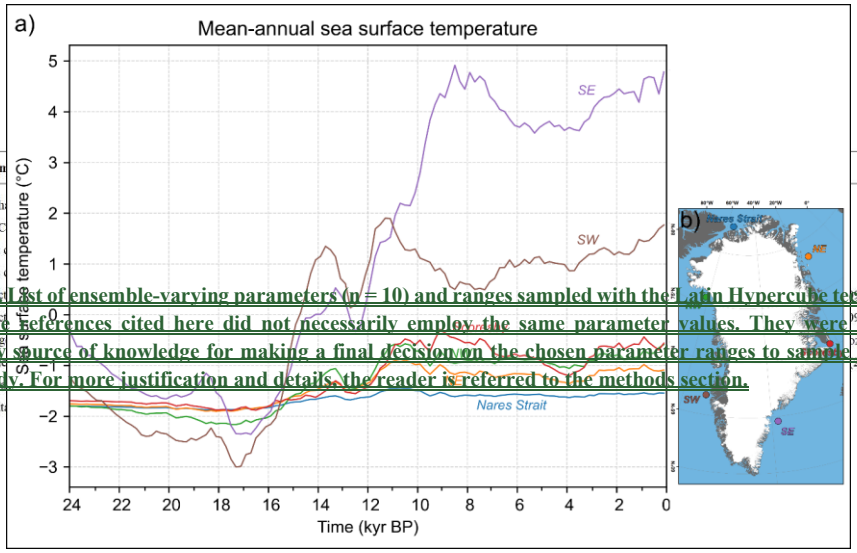

Table 1. List of ensemble-varying parameters (n = 10) and ranges sampled with the Latin Hypercube technique. Note the references cited here did not necessarily employ the same parameter values. They were used as primary source of knowledge for making a final decision on the chosen parameter ranges to sample from in this study. For more justification and details, the reader is referred to the methods section.

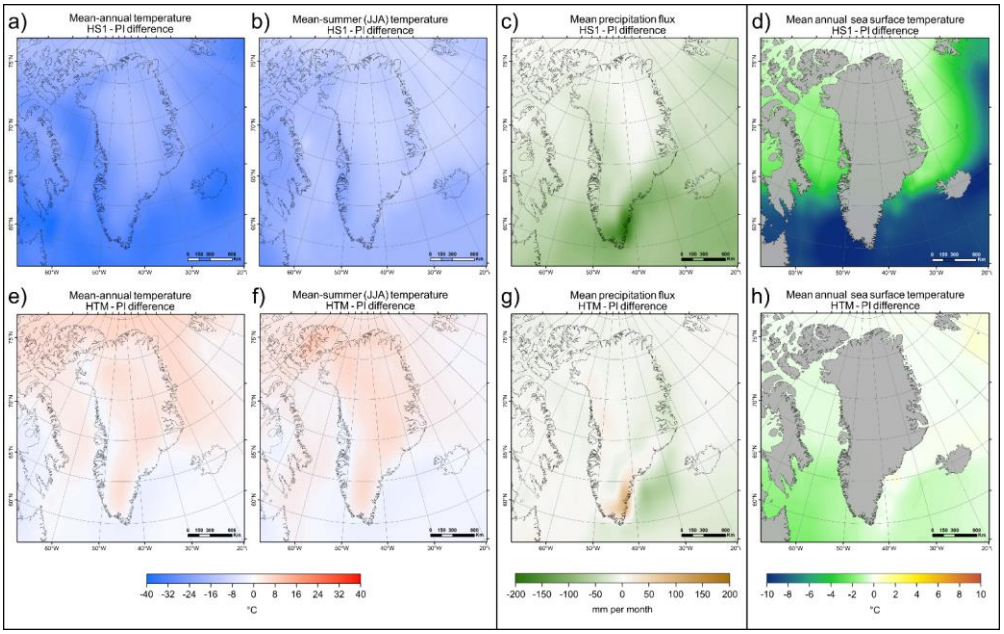

Formatted: Font: +Headings CS (Times New Roman), 11 pt

Formatted: Space After: 8 pt, Add space between paragraphs of the same style, Line spacing: single

~~**Figure 7. Time series of mean annual sea-surface temperature input data (panel a) (Osman et al., 2021) extracted from our two-dimensional input forcing fields, for five distinct locations taken from different ocean basins offshore the present-day GrIS (as shown by the inset: panel b).**~~

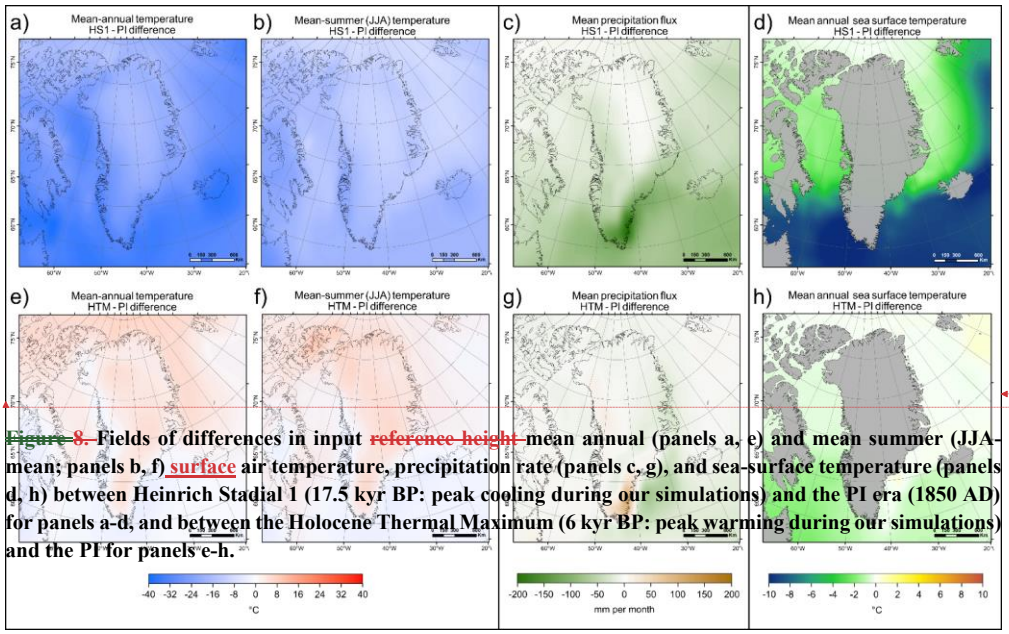

~~Figure 8.~~ **Fields of differences in input ~~reference height~~ mean annual (panels a, e) and mean summer (JJA-mean; panels b, f) surface air temperature, precipitation rate (panels c, g), and sea-surface temperature (panels d, h) between Heinrich Stadial 1 (17.5 kyr BP: peak cooling during our simulations) and the PI era (1850 AD) for panels a-d, and between the Holocene Thermal Maximum (6 kyr BP: peak warming during our simulations) and the PI for panels e-h.**

2.4 Model-data comparison scheme

Formatted: Justified, Space After: 8 pt, Add space between paragraphs of the same style, Line spacing: Multiple 1,15 li

Formatted: Font: 12 pt, Ligatures: Standard + Contextual

Formatted: Line spacing: Multiple 1,08 li

Formatted: Font: +Headings CS (Times New Roman), 12 pt, Ligatures: Standard + Contextual

Formatted: Space After: 8 pt, Add space between paragraphs of the same style, Line spacing: Multiple 1,08 li

Formatted: Font: 12 pt, Ligatures: Standard + Contextual

Formatted: Left, Line spacing: Multiple 1,08 li

Isolating ~~ensemble~~ best-fit ensemble simulations requires a quantitative assessment of model-data agreement ~~with data~~ on past GrIS behaviour. Here, each ~~ensemble~~ simulation is scored ~~based on~~using three chronologically- distinct tests, described below. ~~Prior to conducting these tests, floating ice,~~Before testing, we remove the IIS~~,~~ and ice thinner than 10 m~~, and modelled peripheral icecaps and glaciers are removed~~ from modelled ~~ice~~ thickness fields. Because former GrIS ice-shelf extent is poorly constrained, and empirical datasets used here only constrain grounded GrIS extent, we also exclude floating ice (post-simulation) and restrict all ice-extent analyses to grounded ice for the remainder of the study. Modelled ice shelf extent at selected time periods is nonetheless shown in Figures 22 and 23.

-The *local-LGM extent* test~~; assesses~~: This test evaluates the fit between simulations and grounded GrIS extent during the ~~local LGM, reached between ~~lLGM (~21~~ and ~~–15 kyr BP, depending on ~~regions (~~region; *e.g.* Funder et al., 2011; Ó Cofaigh et al., 2013; ~~;~~Hogan et al., 2016; Jennings et al., 2017; ~~; Ó Cofaigh et al., 2013;~~ Sbarra et al., 2022). ~~As~~Because the GrIS was ~~then~~ fully marine-terminating, data constraining its past ~~ice~~ extent are rare and challenging to obtain ~~and rare~~ (Sbarra et al., 2022a). Given this uncertainty, we ~~produce~~define a conservative ~~local LGM extent~~ lLGM mask ~~covering~~spanning the area between the outermost PaleoGrIS 1.0 isochrone (~14-13 kyr BP) (Leger et al., 2024), ~~reconstructing GrIS~~which reconstructs margins following initial deglaciation, and the continental shelf break, a likely maximum ~~extent constraint~~limit (Fig. ~~9). Due to numerous~~ 8). Given dating challenges ~~in dating the GrIS's local LGM~~ (Jennings et al., 2017), no chronology is considered in this test, rather only absolute extent. For each simulation, we compute the percentage of mask pixels covered by ~~modelled~~ grounded ice at any ~~point in~~ time~~. These percentages are~~, then ~~normalised~~normalise these values to ~~compute~~produce a 0-1 score ~~per simulation (0-1)~~ (Fig. ~~10~~9). High-scoring simulations ~~model an~~ reconstruct a more extensive grounded GrIS, covering ~~more~~larger parts of the mid- to outer continental shelves, thus ~~reconstructing~~yielding a more accurate ~~local LGM~~lLGM geometry (Fig. ~~10~~9).

-The *deglaciation extent* test~~; assesses the simulations' ability to fit~~: This test evaluates simulations against an empirical reconstruction of GrIS retreat during the last deglaciation (~15 - 5 kyr BP). ~~To do so, we~~We use ATAT v1.1 (Ely et al., 2019) to score simulations against the PaleoGrIS 1.0 isochrone reconstruction (Leger et al., 2024), ~~which spans~~spanning 13 ± 1 kyr BP to 7 ± 0.5 kyr BP. We use the 'isochrone buffer' product, a mask-based version of the ~~margin~~ reconstruction ~~designed~~suited for ~~comparison~~models with >1 km- resolution ~~models~~ (see Fig. 15 in Leger et al., 2024). ~~Here, three~~Three ATAT output statistics are equally weighted ~~in~~into a final normalised 0-1 score ~~(0-1);~~ i) the percentage of ~~pixels from~~ PaleoGrIS 1.0 ~~buffers~~ buffer pixels covered by ~~modelled~~ grounded ice~~,~~ (periphery glaciers removed), ii) the percentage of these pixels ~~that agree~~matching within chronological error, and iii) the Root-Mean Squared Error in retreat timing ~~for the latter~~ (see ~~Table 4 in~~ Ely et al., 2019~~). Consequently, this~~: Table 4). This test ~~assesses~~thus evaluates whether modelled GrIS margins retreat ~~over~~across the correct regions~~,~~ and at ~~both~~ the correct time and rate (Figs. 8, 9~~, 10~~).

-**The *Pre-Industrial extent* test**~~; assesses the simulations' ability to reproduce~~: This test evaluates simulations against the PI (1850 AD) GrIS extent. ~~To do so, we~~We compute the difference in grounded ice extent between the present-day GrIS (BedMachine v4 re-sampled to 5 km~~, periphery glaciers removed~~) and ~~our simulations' last~~ each simulation's final frame (1850 AD). ~~While~~Although these ~~two products represent GrIS~~ states ~~at times differing~~differ by ~150 years, we ~~consider this difference to be~~ assume the offset is negligible ~~given our~~ relative to the 24 kyr ~~long simulations~~ simulation length and the 5 ~~x 5~~ km spatial uncertainty ~~inherent to~~of both products, which likely exceeds the ~~offset between the two extents. We thus integrate the number of~~true extent difference. We then count pixels ~~over which modelled~~where simulated PI grounded ~~GrIS margins are both~~ice is either more ~~and~~or less extensive than the present-day margin (Figs. 8, ~~9, 10~~). The total ~~number of~~ misfit ~~pixels~~pixel count is ~~then~~ normalised ~~to produce~~into a final ~~relative~~0-1 score ~~(0 – 1).~~.

To isolate overall best-fit simulations, we ~~follow~~apply a chronologically-ordered sieving approach and sequentially remove simulations that do not meet ~~threshold values~~thresholds at each test. ~~Starting with~~Simulations first pass the *local-LGM extent* test~~, only simulations with~~ if mask pixel ~~cover percentages~~ coverage exceeds >40~~% are retained.~~%. Of ~~those~~these, only ~~simulations yielding normalized scores~~runs scoring >0.8 (out of 1) at the *deglaciation extent* test are retained. Of ~~those~~these, only simulations ~~presenting a total number of~~with <19800 misfit pixels ~~<19800~~ at the *Pre-Industrial extent* test are retained. ~~These thresholds~~ Thresholds were ~~selected~~set such that 60 - 70% of simulations are removed by each sieve while ~~keeping~~retaining five ~~overall~~ best-fit ~~simulations~~runs (upper 95th percentile of ~~model-data~~ comparison scores). This ~~sequential sieving~~ strategy ~~enables us to avoid retaining~~avoids selecting simulations ~~which may model~~that fit the ~~most recent ice-sheet state more accurately (*i.e.*~~ present-day ~~GrIS)~~state well but ~~for the wrong reasons, *e.g.* when their previous~~achieve it through unrealistic paleo- -evolution ~~strongly disagrees with empirical data.~~.

Formatted: Font: +Body (Calibri), 11 pt

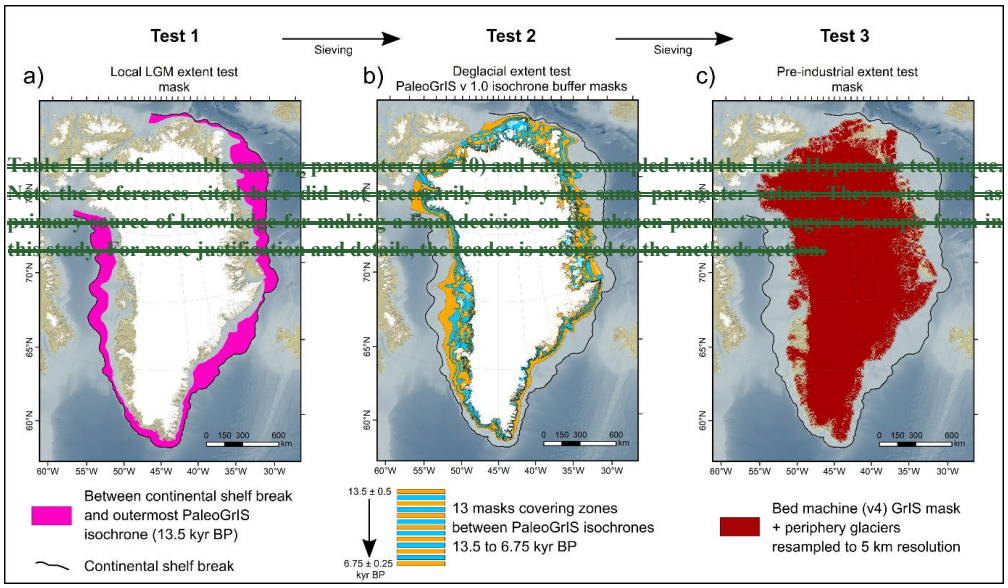

~~Table 1. List of ensemble sampling parameters (n = 10) and ranges sampled with the Latin Hypercube technique. Note the references cited here did not necessarily employ the same parameter values. They were used as primary sources of knowledge for making a final decision on the chosen parameter ranges to sample from in this study. For more justification and details, the reader is referred to the methods section.~~

Model parameter *(PISM parameter name)*	Range	Unit	Source
Flow law enhancement factor (*sia_e* and *ssa_e*)	[0.5 - 3]	n/a	Aschwanden (2016)
Regularized Coulomb sliding law exponent (*q*)	[0.01 - 1]	n/a	Zoet and Iverson (2020)
Topographic control on Yield Stress: lower ϕ treshold (ϕ_{min})	[4 - 15]	angle degree	Aschwanden (2016)
Topographic control on Yield Stress: upper ϕ treshold (ϕ_{max})	[20 - 45]	angle degree	Aschwanden (2016)
PDD melt factor for ice (*surface.pdd.factor_ice*)	[5 - 12]	mm *we* $.d^{-1}.°C^{-1}$	Braithwaite (1995); Fausto *et al*. (2009)
PDD melt factor for snow (*surface.pdd.factor_snow*)	[2 - 5]	mm *we* $.d^{-1}.°C^{-1}$	Braithwaite (1995); Fausto *et al*. (2009)
Rate of change in Stdev of daily temperature variability as function of elevation (*param_a*)	[-0.25 - -0.1]	n/a	ERA 40 re-analysis: Seguinot & Rogozhina (2014)
Minimum thickness of terminal floating ice shelf (*thickness_calving_threshold*)	[25 - 200]	m	Albrecht *et al*. (2021); Pittard *et al*. (2022)
Input temperature forcing: Temperature scalar offset (*delta_T*)	[-3.5 - 3.5]	°C	Osman *et al*. (2021)
Input precipitation forcing: % precipitation scaling (*frac_P*)	[0.2 - 2.0]	scalar multiplier	Initial sensitivity tests

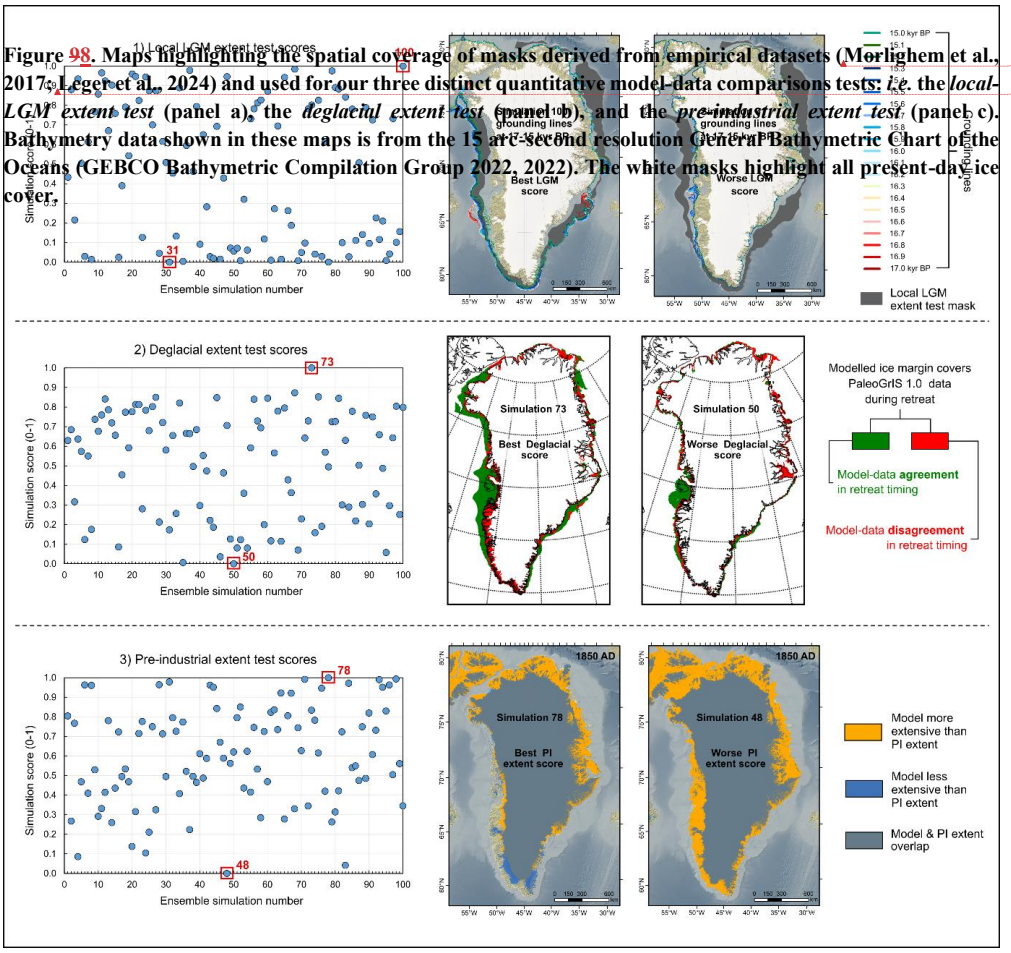

Figure ~~98~~. Maps highlighting the spatial coverage of masks derived from empirical datasets (Morlighem et al., 2017; Leger et al., 2024) and used for our three distinct quantitative model-data comparisons tests: *i.e.* the *local-LGM extent test* (panel a), the *deglacial extent test* (panel b), and the *pre-industrial extent test* (panel c). Bathymetry data shown in these maps is from the 15 arc-second resolution General Bathymetric Chart of the Oceans (GEBCO Bathymetric Compilation Group 2022, 2022). The white masks highlight all present-day ice cover.

Formatted: Font: Bold

Formatted: Font: Bold

Figure ~~10~~9. Ensemble simulation scores at our three model-data comparison tests (*local-LGM extent test*, *deglacial extent*, and *PI extent test*) and example results illustrated for both the best-scoring and worse-scoring ensemble simulations, at each test. Note that for the *PI-extent test*, the 2D mask used as empirical data and described in this figure as the "PI extent" is the grounded ice extent of the present-day GrIS mask from BedMachine v4 (Morlighem et al., 2017) re-sampled to 5 km resolution, with periphery glaciers removed. While the true PI and present-day extents represent GrIS states that differ by ~150 years, we here consider this difference to be negligible given our 24 kyr-long simulations and the 5 x 5 km spatial uncertainty inherent to both products. That uncertainty, once propagated, likely exceeds the extent offset between the two states. Bathymetry and topography data shown in these maps are from the 15 arc-second resolution General Bathymetric Chart of the Oceans (GEBCO Bathymetric Compilation Group 2022, 2022).

Formatted: Font: Bold

3 Insights ~~on~~into past Greenland-Ice-Sheet history

3.1 Modelled Greenland Ice Sheet during the local LGM

3.1.1 Ensemble-wide trends

All ensemble simulations (n=100) model an increase (of up to ~23%) in grounded GrIS extent between the global LGM (*i.e.* 24 - 21 kyr BP) and the ~~GrIS-wide local LGM~~lLGM, here modelled between 17.5 and 16 kyr BP (Fig. ~~11~~10). This is consistent with the timing of maximum GrIS volume and extent in other recent modelling studies (*e.g.* 16.5 kyr BP in Lecavalier et al., 2014; 17 - 17.5 kyr BP in Yang et al., 2022). Here, modelled GrIS maximum expansion is synchronous with the Heinrich Stadial 1 (HS1: ~18 - 14.7 kyr BP: He et al., 2021) cooling event. In our prescribed climate forcing (iCESM-derived), HS1 is associated with decreases in mean annual air temperatures of between 5 °C and 7 °C over the GrIS (Figs. 4, 5), and reductions in sea surface temperatures of up to 1 °C in ocean basins surrounding Greenland (Figs. 6~~, 7~~). In nearly all ensemble simulations, HS1 cooling forces modelled surface accumulation rates to increase between 24 and

16 kyr BP (by up to 200% for certain simulations) and causes reduced sub-shelf melt (by up to 350%), between 18 and 16 kyr BP (Fig. ~~12~~11).

3.1.2 Insights from local LGM best-fit simulations

In this section, we refer to 'lLGM best-fit simulations' as the five best-scoring ~~ensemble~~ simulations at the *local-LGM extent* test (Figs. 12, 13, 14~~, 15, 17~~-16).

Grounded GrIS extent during ~~local LGM~~lLGM

Our lLGM best-fit simulations yield maximum ~~total~~ grounded GrIS areas that range between 2.80 and 2.85 million km^2 (excluding the IIS) (Fig. ~~13), an extent~~12), ~1.65 times ~~greater than~~ the present-day ~~ice sheet~~area (1.71 million km^2; Morlighem et al., 2017). ~~For these simulations, agreement~~Agreement with empirical data on ~~the local LGM ice~~lLGM extent is relatively good~~. Our lLGM best fit~~: our simulations are 4 ± 0.7% and 10 ± 0.6% less extensive than the minimum and maximum lLGM GrIS extents reconstructed ~~by the~~in PaleoGrIS 1.0 ~~database for the local LGM, respectively~~ (Leger et al., 2024)(Figs. ~~14, 17). The remaining~~13, 16). Remaining misfits ~~are~~occur mainly ~~located~~ in NE Greenland, where no ~~ensemble~~ simulation produces grounded ice ~~reaching~~extending to the mid-to-outer continental shelf during the ~~local LGM~~lLGM (Figs. ~~14~~13, 16, 17~~, 18~~), contrary to recent empirical ~~data~~evidence (*e.g.* Hansen et al., 2022; Davies et al., 2022; Roberts et al., 2024~~). Indeed, these~~; Ó Cofaigh et al., 2025). These studies ~~suggest local LGM~~indicate grounded ~~ice~~ margins reached ~~between~~ ~100~~ and ~~ 200 km ~~further East~~farther east than in our most extensive simulations. This ~~implies~~suggests the true ~~local LGM~~lLGM (~17 - 16.5 kyr BP) ~~areal extent of the~~ grounded GrIS area was likely ~~closer to~~ 2.9 - 3.1 million km^2, consistent with the Huy3 model (Lecavalier et al., 2014).

Along the Western GrIS margin, from offshore Uummannarsuaq in the South (Cape Farewell) to offshore Kangaarasuk in the North (Cape Atholl), all lLGM best-fit simulations (and ~~a large proportion~~much of ~~our~~the ensemble) model a grounded ~~GrIS~~ margin ~~that reaches~~reaching the continental shelf edge during the ~~local LGM~~lLGM (Figs. 13, 14, ~~15, 17~~16). This ~~is consistent~~agrees with empirical constraints on the ~~Western~~western GrIS ~~local~~ LGM extent (*e.g.* Ó Cofaigh et al., 2013; Rinterknecht et al., 2014; Sbarra et al., 2022)~~. Therefore,~~, whereby both ~~empirical~~data and modelling ~~studies~~ increasingly suggest the grounded GrIS ~~likely~~ reached the ~~continental~~ shelf edge along its entire ~~Western~~western margin ~~during the local LGM. Furthermore, our~~. Our lLGM best-fit simulations also produce extensive ice shelves extending across Baffin Bay during that time. As the LGM LIS ~~was~~ also ~~contributing significant~~contributed major ice flux into Baffin Bay from the ~~West around that time~~west (Dalton et al., 2023), it seems ~~possible for Baffin Bay to be~~ plausible the bay was fully covered by ice shelves ~~during the local LGM,~~ between 18 and 16 kyr BP. ~~We also note that towards~~Toward the relatively shallow Davis strait saddle (500 - 600 m below present-day sea level~~) Davis strait saddle,~~), offshore CW Greenland, four ~~out~~ of five lLGM best-fit simulations model grounded ice ~~that~~

Formatted: Font: 12 pt
Formatted: Font: 12 pt
Formatted: French (Switzerland)
Formatted: French (Switzerland)
Formatted: French (Switzerland)
Formatted: French (Switzerland)
Formatted: French (Switzerland)
Formatted: English (United Kingdom)
Formatted: English (United Kingdom)
Formatted: English (United Kingdom)
Formatted: English (United Kingdom)
Formatted: English (United Kingdom)

~~extends~~extending beyond the ~~continental~~ shelf break and onto the saddle~~, during the local LGM~~ (Fig. ~~14). Assuming~~13). If the LIS ~~flowing eastwards~~similarly extended east from Baffin Island ~~was able to extend over the saddle by a similar extent, it seems possible that~~, grounded ice from ~~the two~~both ice sheets ~~was able to coalesce~~may have coalesced over Davis Strait, as modelled in some previous studies (*e.g.* Patterson et al., 2024; Gandy et al., 2023).

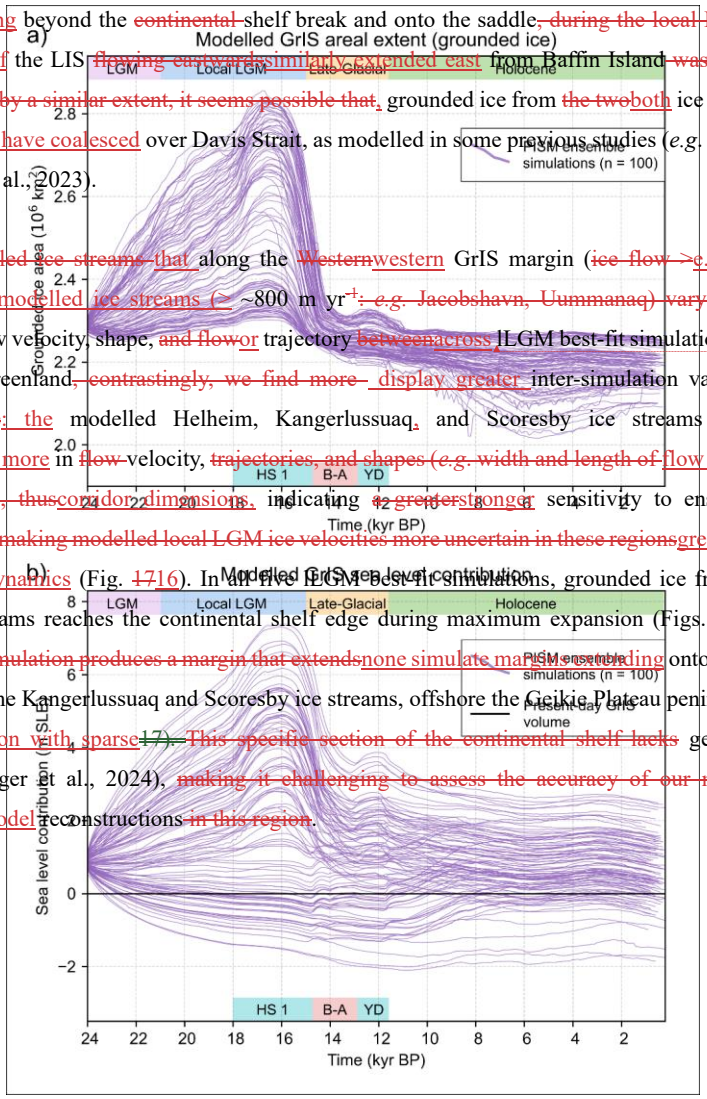

We find ~~modelled ice streams that~~ along the ~~Western~~western GrIS margin (~~ice flow >~~e.g. Jakobshavn, Uummannaq), ~~modelled ice streams (>~~ ~800 m yr^{-1}~~; *e.g.* Jacobshavn, Uummanaq) vary~~ $^{-1}$) show little variation in flow velocity, shape, ~~and flow~~or trajectory ~~between~~across lLGM best-fit simulations. In contrast, SE and CE Greenland~~, contrastingly, we find more~~ display greater inter-simulation variability ~~in ice dynamics. The~~; the modelled Helheim, Kangerlussuaq, and Scoresby ice streams ~~show greater variations~~differ more in ~~flow~~ velocity, ~~trajectories, and shapes (*e.g.* width and length of~~ flow paths, and fast-flow ~~corridors), thus corridor dimensions,~~ indicating ~~a greater~~ stronger sensitivity to ensemble ~~varying~~ parameters and ~~making modelled local LGM ice velocities more uncertain in these regions~~greater uncertainty in lLGM ice dynamics (Fig. ~~17~~16). In all five lLGM best-fit simulations, grounded ice from these three eastern ice streams reaches the continental shelf edge during maximum expansion (Figs. ~~14, 17~~13, 16). However, ~~no simulation produces a margin that extends~~none simulate margins extending onto the ~~continental~~ shelf between the Kangerlussuaq and Scoresby ice streams, offshore the Geikie Plateau peninsula (Figs. ~~14,~~ 13, 16), a region ~~with sparse~~17). ~~This specific section of the continental shelf lacks~~ geochronological constraints (Leger et al., 2024), ~~making it challenging to assess the accuracy of our models'~~limiting validation of model reconstructions ~~in this region~~.

Formatted: Font: Times New Roman

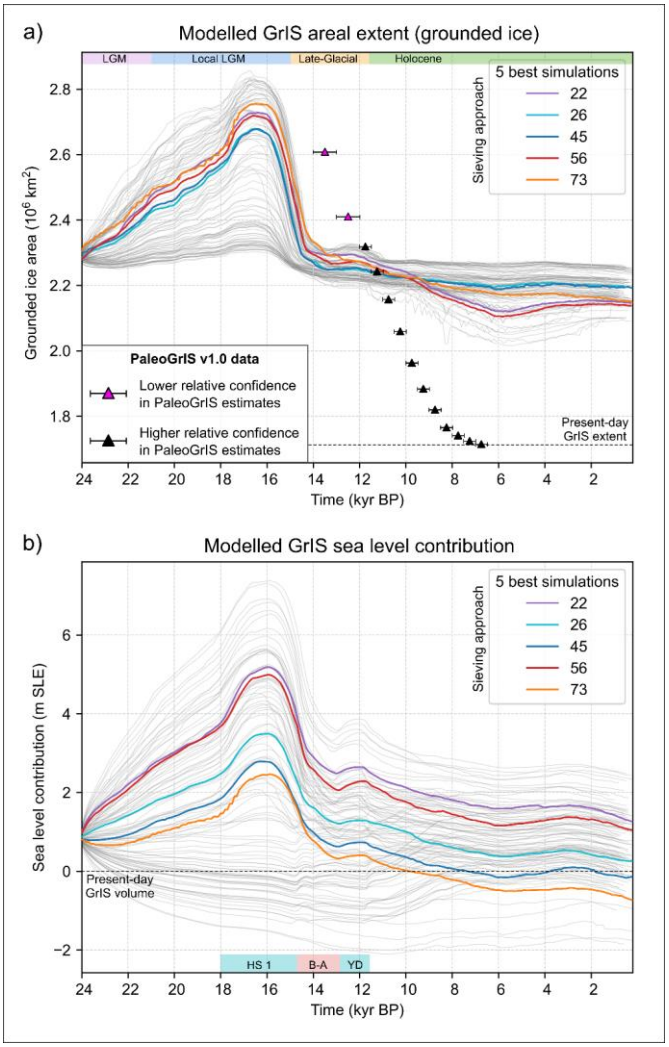

Figure ~~11~~10. Modelled grounded ice area (panel a) and ice volume (panel b) for the 100 transient PISM ensemble simulations of the GrIS (light grey time series) from 24 kyr BP to the PI era (1850 AD). Here, the modelled grounded GrIS volume (in m SLE) is expressed in 'sea level contribution' by subtracting the estimated present-day GrIS volume from our results (7.42 m SLE; Morlighem et al., 2017). GrIS volume calculations ~~moreover~~ exclude ice under floatation computed using the PISM-derived time-dependent floatation criterion. The calculation also excludes the Innuitian ice sheet (IIS), periphery glaciers and icecaps, and any ice thinner than 10 m (after Albrecht et al., 2020). We use ice density, sea water density, and static ocean surface area values of 910 kg m^{-3}, 1027 kg m^{-3}, and 3.618 x 10^8 km^2, respectively. The five overall best-fit simulations (which pass all sieves) are highlighted with thicker coloured time series. The PaleoGrIS v1.0 isochrones data reconstructing the GrIS's former grounded ice extent are shown with triangle symbols on panel a (Leger et al., 2024). Note the GrIS-wide model-data misfit in ice extent apparent here can be misleading as it is spatially heterogeneous and heavily influenced by a few regions concentrating most of the misfit (*i.e.* NO, NE, and CE Greenland); see Fig. 17. Note the five overall best-fit simulations highlighted here, while passing all sieves, are not the best-scoring simulations at each individual model-data comparison test (see Fig. 12), but rather they score better than other simulations when combining all tests. For instance, their volume during the lLGM (panel

Formatted: Font: Bold

Formatted: Font: Bold

b: ~16 kyr BP) is lower and less realistic than values of best-scoring simulations at the *local-LGM extent* test (see Fig. 12d).

GrIS volume and thickness during the ~~local LGM~~lLGM

lLGM best-fit simulations ~~produce~~yield maximum grounded GrIS volumes (ice above floatation, excluding the IIS and peripheral glaciers) ~~that are between 6 and~~6 - 7.5 m SLE greater than ~~the present-day volume~~today (~7.42 m, Morlighem et al., 2017) (Fig. ~~13d~~12d). These ~~lLGM volumes are distinctly higher than~~values exceed most previous estimates ~~from the literature~~, generally comprised between 2 and 5.5 m SLE (Bradley et al., 2018; Yang et al., 2022; Simpson et al., 2009; Clark and Mix, 2002; Huybrechts, 2002; Niu et al., 2019; Fleming & Lambeck, 2004; Quiquet et al., 2021; Buizert et al., 2018; Tabone et al., 2018; Khan et al., 2016) (Fig. ~~19~~18). We however note that ~~published~~ volume estimates display an increasing trend in time, with ~~more~~ recent studies more often reporting values between 4 and 5.5 m SLE. ~~Moreover, reported GrIS LGM volume estimates~~ Reported volumes are ~~negatively correlated with~~ also inversely related to model resolution (~~power regression~~ R^2 = 0.5), ~~suggesting models using a~~ with higher-resolution ~~grid tend~~models tending to produce a thicker GrIS ~~during the local LGM~~ (Fig. ~~19). All previous~~ 18). Previous ensemble studies producing ~~an ensemble of GrIS~~ LGM-to-present ~~model~~GrIS simulations with model-data comparison (Simpson et al., 2009; Lecavalier et al., 2014~~; Simpson et al., 2009)~~) used ~~substantially~~much coarser ~~grid resolutions~~grids (15-20 km~~) than this study (~~ vs. our 5 km). ~~Of these~~Past modelling studies~~, moreover, few~~ also rarely include floating ice shelves ~~in their models, which are known to often provide a~~whose buttressing effect ~~leading to~~reduces ice-flux ~~lowering~~ and ~~thus~~ increases ~~in~~ grounded ice ~~sheet~~ thickness (Pritchard et al., 2012). Each of these studies also use different climate/ocean forcings and ice flow approximations, and those nudging the model to a specific ice extent may use different data-informed lLGM masks. Together, these differences may help explain the higher volumes obtained in our results. ~~Moreover, it~~

It can also be challenging to directly compare previously reported GrIS LGM volume estimates as different methods are used to compute this number (Albrecht et al., 2020). ~~Various studies~~Studies use different present-day GrIS volume estimates, ice and ocean water densities, global ocean areas, and do not always exclude floating ice nor ice under floatation using a time-~~dependent~~varying relative sea-level ~~output~~. However, we believe our workflow follows a method close to that of Lecavalier et al. (2014) when reporting ~~the modelled local LGM volume~~lLGM volumes of the Huy3 model ~~(in m SLE). Computing the~~. That model's ratio of ~~modelled GrIS-wide~~ grounded ~~ice~~GrIS volume (in 10^{15} m^3 unit) to areal extent (in 10^{12} m^2 unit) ~~reveals that,~~ during the ~~local LGM~~lLGM (~16.5 kyr BP~~), the Huy3 model features a ratio of~~) is ~1.73 (see Fig. 15 in Lecavalier et al., 2014). In comparison, our five overall best-fit simulations (which pass all sieves)

~~display volume/area~~ produce ratios of ~~between~~ 2.10 ~~and~~ 2.25, thus 20 - 30% ~~greater than the Huy3 model~~higher. Our best-fit simulations ~~thus~~ produce a much thicker lLGM GrIS than the Huy3 model ~~during the local LGM~~, despite ~~our results producing~~modelling LGM GrIS summit elevations ~~that are~~ comparable to the present-day ice sheet (Fig. ~~15~~14). We ~~thus~~ hypothesise that previous modelling studies may have underestimated the thickness, ~~mean~~ surface slope, and volume of the grounded GrIS during the ~~local LGM~~lLGM, although we acknowledge this ~~hypothesis~~ will require more testing in future work.

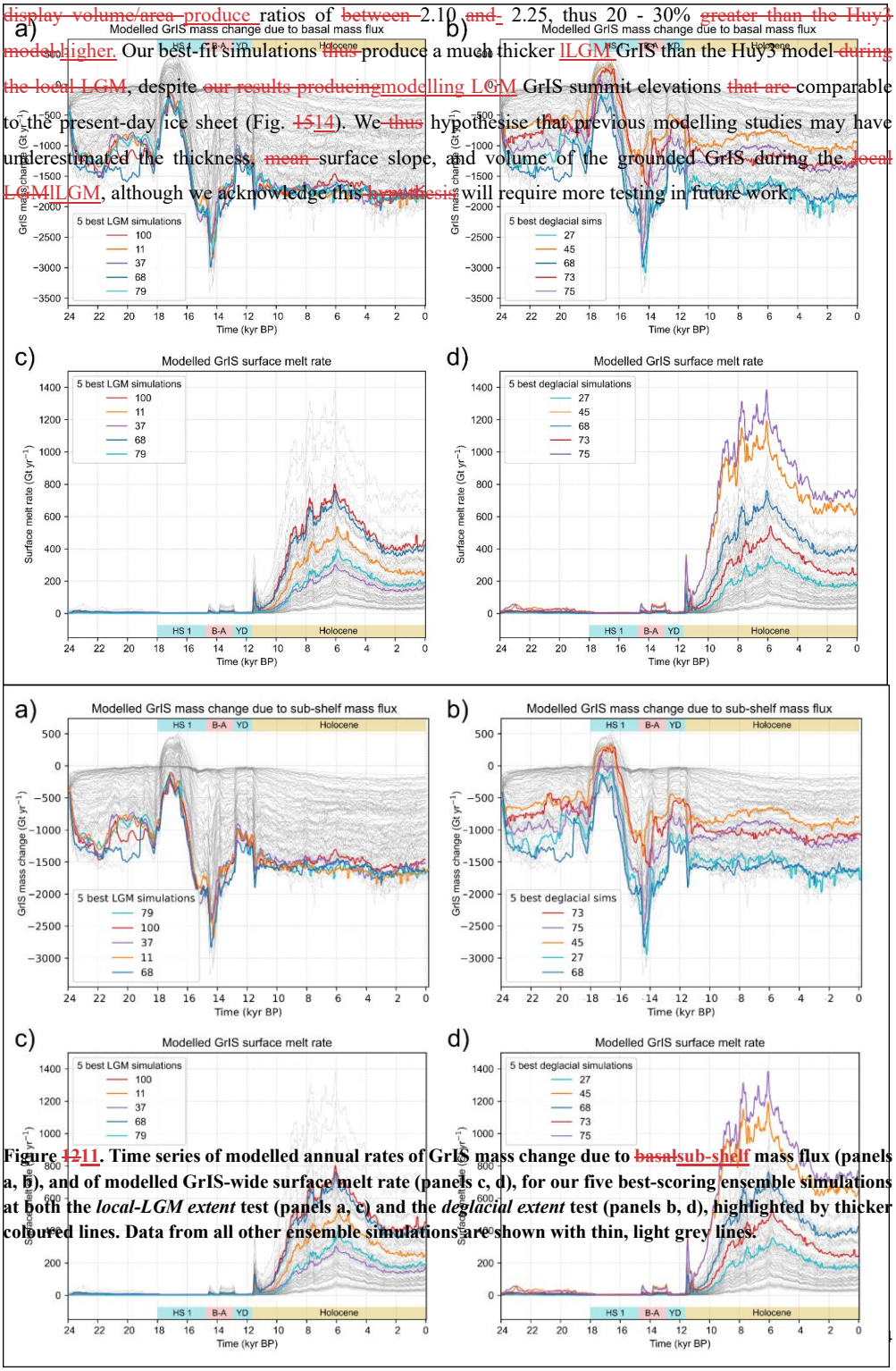

Figure ~~12~~11. Time series of modelled annual rates of GrIS mass change due to ~~basal~~sub-shelf mass flux (panels a, b), and of modelled GrIS-wide surface melt rate (panels c, d), for our five best-scoring ensemble simulations at both the *local-LGM extent* test (panels a, c) and the *deglacial extent* test (panels b, d), highlighted by thicker coloured lines. Data from all other ensemble simulations are shown with thin, light grey lines.

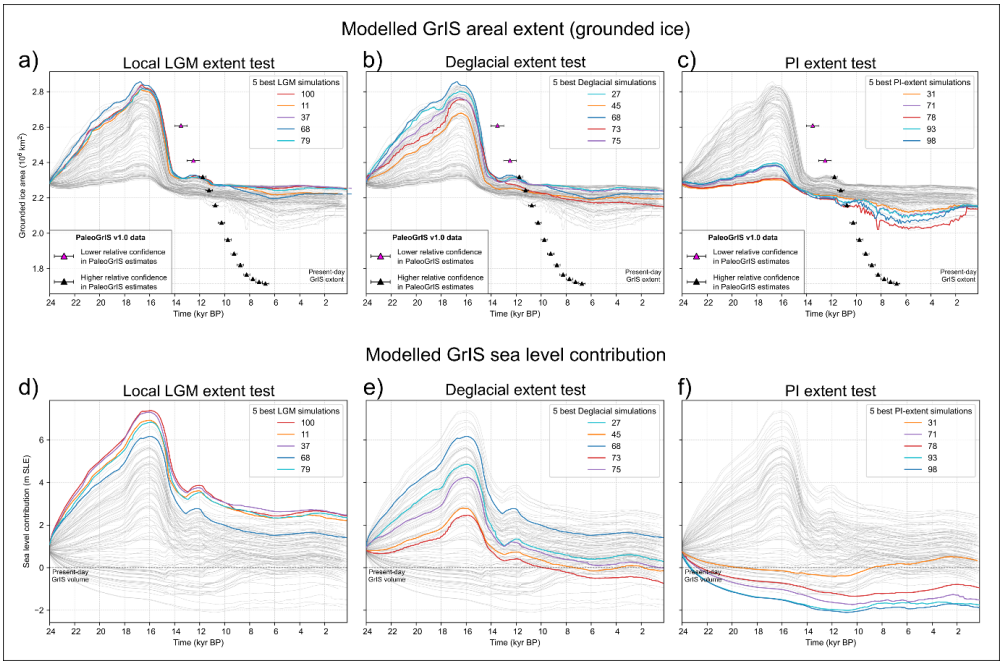

Figure ~~13~~12. Modelled grounded ice area (panels a-c) and volume (in m SLE, expressed as sea level contribution; panels d-f) for the 100 ensemble simulations (light grey time series). The five best-scoring simulations at each of our three model-data comparison tests are highlighted by thicker coloured time series : panels a, d for the *local ~~–~~LGM extent* test, panels b, e for the *deglacial extent* test, and panels c, f for the *PI extent* test. Data from the PaleoGrIS v1.0 isochrone reconstruction of GrIS former grounded ice extent (Leger et al., 2024) are shown with triangle symbols. Note the GrIS-wide model-data misfit in ice extent apparent here can be misleading as it is spatially heterogeneous and heavily influenced by a few regions concentrating most of the misfit (*i.e.* NO, NE, and CE Greenland): see Fig. ~~22~~17.

Formatted: Font: Bold

In our lLGM best-fit simulations, maximum GrIS volume is associated with spatially- heterogeneous ~~magnitudes of~~ GIA-induced bed subsidence ~~during the local LGM~~ (Supplementary Fig. 1). ~~Highest modelled bed~~The largest subsidence values ~~reach~~, reaching ~500 m below ~~the~~ present-day topography, ~~and~~consistently occur ~~systematically towards~~ in CW Greenland, around ~~the~~ Disko Bay and Sisimiut. Three additional regions~~.~~ ~~Three secondary regions of high GIA-induced bed~~ of pronounced subsidence (~400 m) are also modelled~~,~~ ~~reaching values of ~400 m below the present-day bed. These are located~~ in CE Greenland (~~the~~ inner Scoresby Sund ~~region~~), upper NE Greenland (~~The~~ Danmark Fjord region), and central Ellesmere Island (Supplementary Fig. 1). The resulting pattern of total ~~glacial~~ isostatic loading (non-local and local components combined) during the ~~local LGM is~~lLGM broadly ~~consistent~~agrees with previous modelling efforts focusing on GIA signals ~~and model-data comparison using~~calibrated against relative sea level indicators (*e.g.* Simpson et al., 2009; Lecavalier et al., 2014; Bradley et al., 2018).

LGM ice geometry at the locations of ice cores

In Southern Greenland, and following modelled flowlines from the location of the DYE-3 ice core, lLGM best-fit simulations produce a notably different ice-sheet geometry during the ~~local LGM~~lLGM than today (Fig. ~~15~~14). Modelled ice surface elevations ~~are greater by ~300 - 500 m~~ at the local summit are ~300 - 500 m higher than present, despite ~~increased~~greater isostatic loading and ~400 m of bed subsidence ~~(of ~400 m) relative to today. In this region, maximum~~. Maximum modelled ice thickness in this region is thus ~~modelled to be~~ ~700 - 900 m greater ~~during the local LGM~~ than ~~is estimated for~~ the present-day GrIS (Morlighem et al., 2017a). ~~Furthermore, towards~~Toward DYE-3, ~~our~~ lLGM best-fit simulations also suggest a notable ~~shift~~westward migration of the main East/West ice divide~~, here modelled to be located further West than the present-day's by approximately 100 km~~ by ~100 km relative to today (Figs. ~~15, 16). Such a~~14, 15). If confirmed, such glacial-interglacial ice-divide ~~migration, if further validated, could~~shifts would have

implications for the DYE-3 ice core record (Dansgaard et al., 1982), which may not have remained as close to the ~~local~~ GrIS ~~summit~~divide as previously thought during Quaternary glacial maxima ~~as previously thought.~~. Instead, ice from the drill site may have been located further ~~East and well~~east within the Helheim glacier catchment ~~during glacial maxima~~, where higher flow velocities and stronger layer deformation could ~~produce~~induce irregularities in the ice core profile and complicate chronological ~~interpretations~~interpretation (Rasmussen et al., 2023).

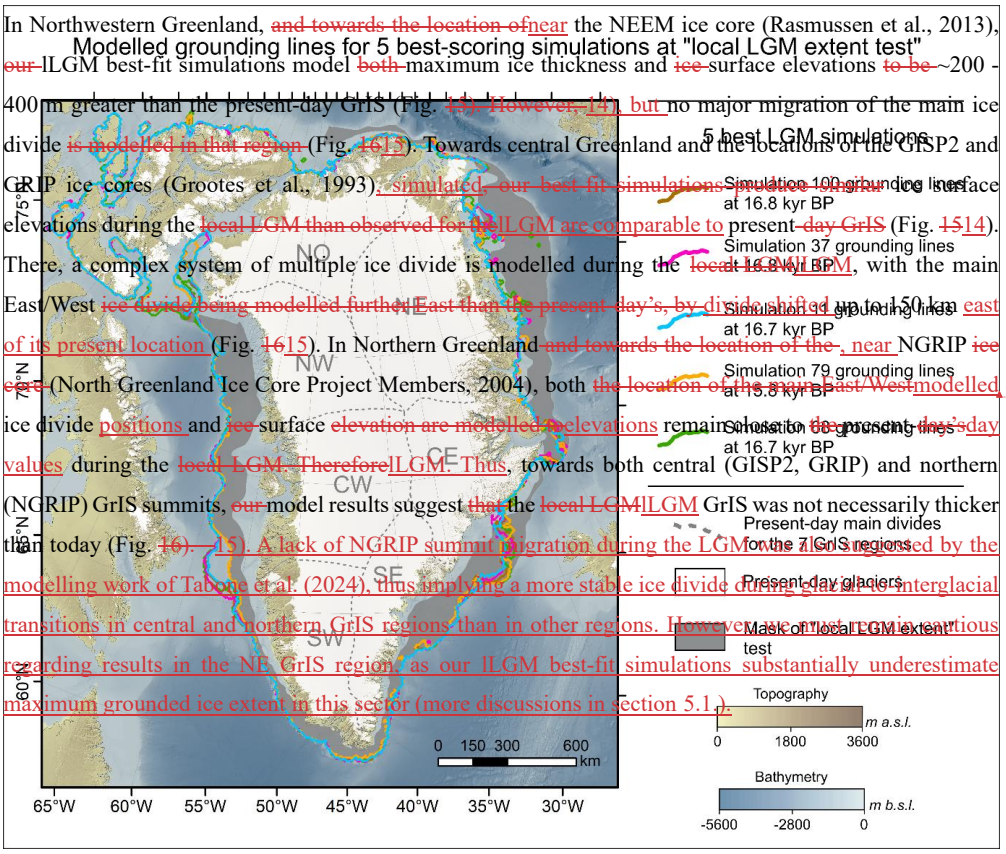

In Northwestern Greenland, ~~and towards the location of~~near the NEEM ice core (Rasmussen et al., 2013), ~~our~~ lLGM best-fit simulations model ~~both~~ maximum ice thickness and ~~ice~~ surface elevations ~~to be~~ ~200 - 400 m greater than the present-day GrIS (Fig. ~~13~~). ~~However, 14~~), but no major migration of the main ice divide ~~is modelled in that region~~ (Fig. ~~1613~~). Towards central Greenland and the locations of the GISP2 and GRIP ice cores (Grootes et al., 1993), ~~simulated, our best-fit simulations produce similar~~ ice surface elevations during the ~~local LGM than observed for the~~lLGM are comparable to present ~~day GrIS~~ (Fig. ~~15~~14). There, a complex system of multiple ice divide is modelled during the ~~local LGM~~lLGM, with the main East/West ~~ice divide being modelled further East than the present-day's, by divide shifted~~ up to 150 km east of its present location (Fig. ~~16~~15). In Northern Greenland ~~and towards the location of the~~, near NGRIP ~~ice cap~~ (North Greenland Ice Core Project Members, 2004), both ~~the location of the main East/West~~modelled ice divide positions and ~~ice~~ surface ~~elevation are modelled~~ elevations remain close to the present ~~day's~~day values during the ~~local LGM. Therefore~~lLGM. Thus, towards both central (GISP2, GRIP) and northern (NGRIP) GrIS summits, ~~our~~ model results suggest ~~that~~ the ~~local LGM~~lLGM GrIS was not necessarily thicker than today (Fig. ~~16~~). ~~15~~). A lack of NGRIP summit migration during the LGM was also suggested by the modelling work of Tabone et al. (2024), thus implying a more stable ice divide during glacial-to-interglacial transitions in central and northern GrIS regions than in other regions. However, we must remain cautious regarding results in the NE GrIS region, as our lLGM best-fit simulations substantially underestimate maximum grounded ice extent in this sector (more discussions in section 5.1).

Formatted: Font: +Body (Calibri), 11 pt, Ligatures: None

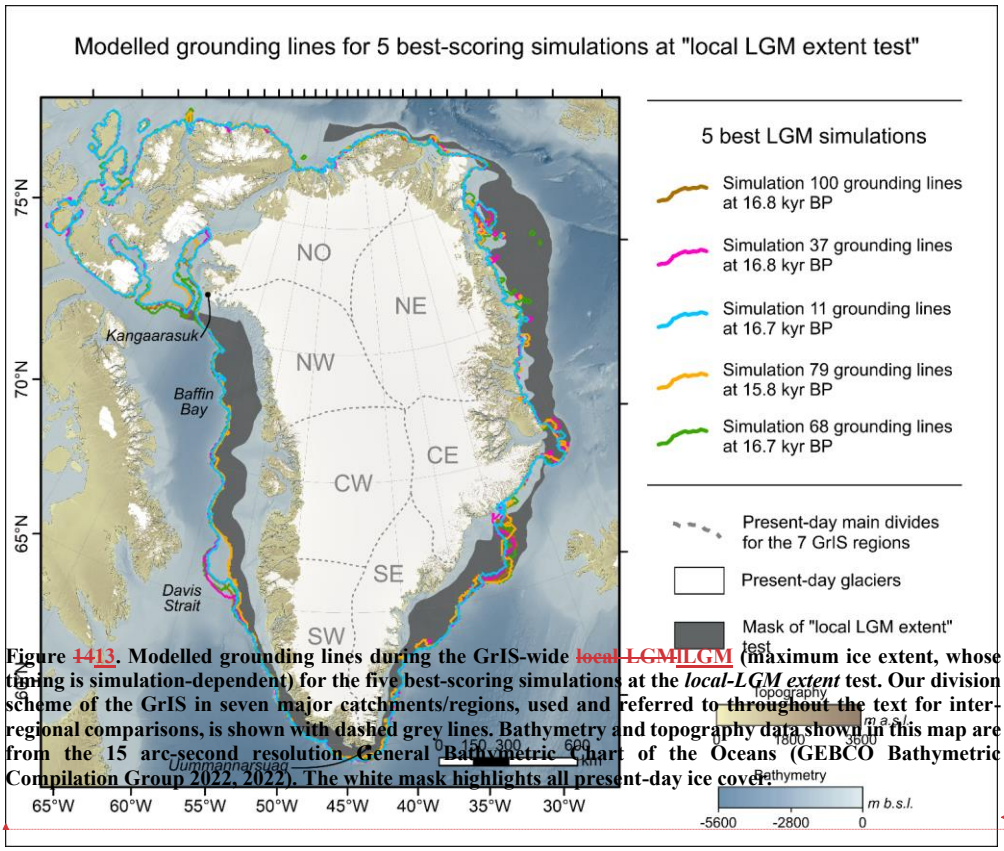

Figure 1413. Modelled grounding lines during the GrIS-wide ~~local LGM~~lLGM (maximum ice extent, whose timing is simulation-dependent) for the five best-scoring simulations at the *local-LGM extent* test. Our division scheme of the GrIS in seven major catchments/regions, used and referred to throughout the text for inter-regional comparisons, is shown with dashed grey lines. Bathymetry and topography data shown in this map are from the 15 arc-second resolution General Bathymetric Chart of the Oceans (GEBCO Bathymetric Compilation Group 2022, 2022). The white mask highlights all present-day ice cover.

GrIS discharge during the ~~local LGM~~lLGM

Our lLGM best-fit simulations produce a faster-flowing GrIS during the ~~local LGM~~lLGM than today. In these ~~simulations, the glaciated~~runs, areas covered by ice streams (>800 m yr^{-1} surface velocities: Bennett, 2003) are ~~between~~ 6.8 ~~and~~ 10.7 times greater during the ~~local LGM, relative to today~~lLGM than at present (Joughin et al., 2018a) (Fig. ~~17). Such an increase in flow velocities combined with the greater ice extent~~

Formatted: Font: +Headings CS (Times New Roman), 11 pt, Bold, Ligatures: None

Formatted: Space After: 8 pt, Add space between paragraphs of the same style, Line spacing: single

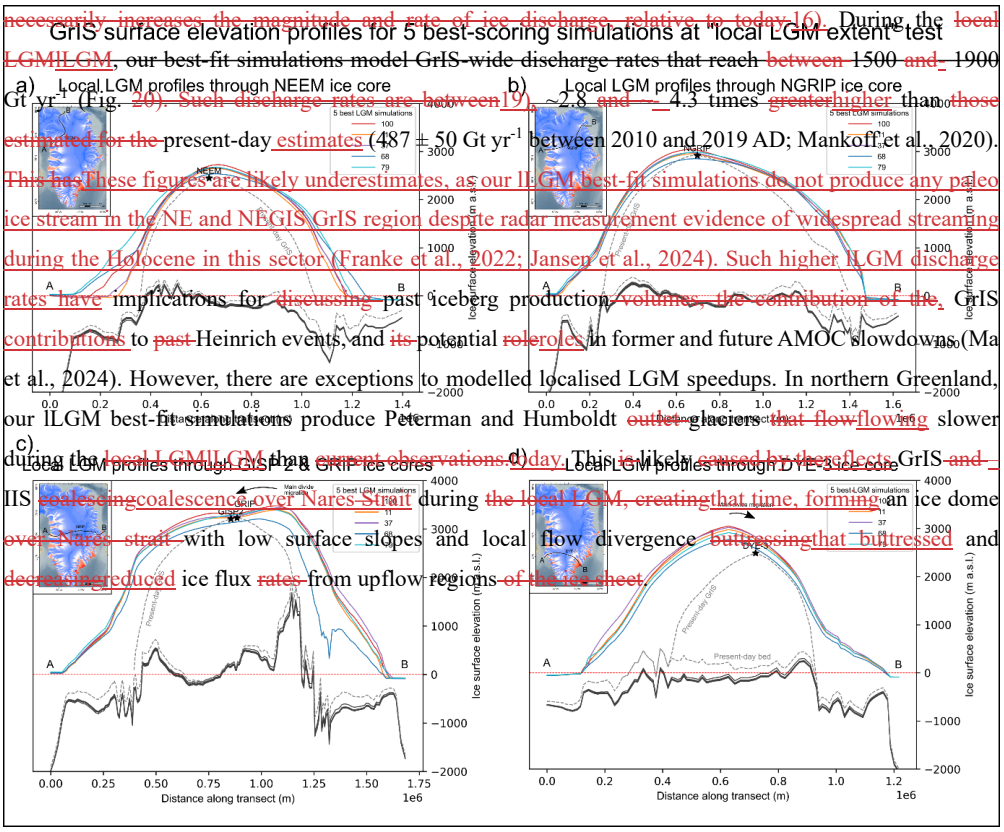

necessarily increases the magnitude and rate of ice discharge relative to today.16). During the local LGMlLGM, our best-fit simulations model GrIS-wide discharge rates that reach between 1500 and 1900 Gt yr^{-1} (Fig. 20). Such discharge rates are between19), ~2.8 and ~ 4.3 times greaterhigher than those estimated for the present-day estimates (487 ± 50 Gt yr^{-1} between 2010 and 2019 AD; Mankoff et al., 2020). This hasThese figures are likely underestimates, as our lLGM best-fit simulations do not produce any paleo ice stream in the NE and NEGIS GrIS region despite radar measurement evidence of widespread streaming during the Holocene in this sector (Franke et al., 2022; Jansen et al., 2024). Such higher lLGM discharge rates have implications for discussing past iceberg production volumes, the contribution of the GrIS contributions to past Heinrich events, and its potential roleroles in former and future AMOC slowdowns (Ma et al., 2024). However, there are exceptions to modelled localised LGM speedups. In northern Greenland, our lLGM best-fit simulations produce Petermann and Humboldt outlet glaciers that flow flowing slower during the local LGMlLGM than current observations of today. This is likely caused by thereflects GrIS and IIS coalescingcoalescence over Nares Strait during the local LGM, creatingthat time, forming an ice dome over Nares strait with low surface slopes and local flow divergence buttressingthat buttressed and decreasinereduced ice flux rates from upflow regions of the ice sheet.

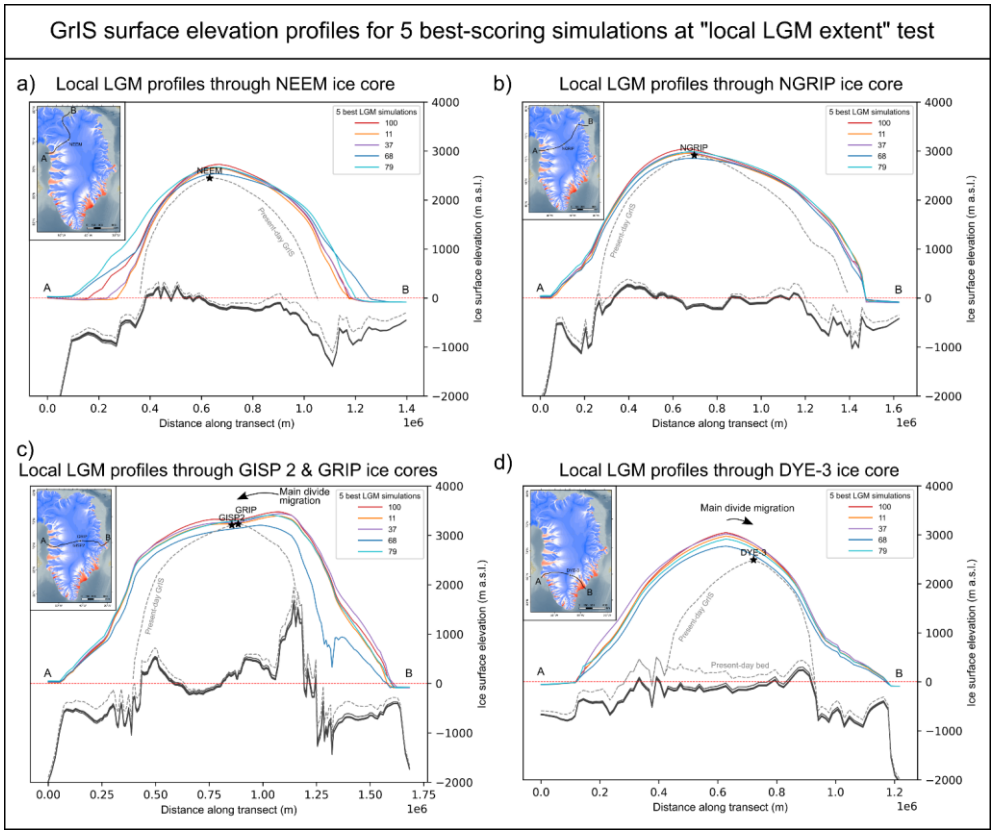

Figure ~~15~~14. Modelled ice surface and bed elevations during the ~~local LGM~~LGM extracted across four different transects for our five best-scoring simulations at the *local-LGM extent* test (thicker coloured lines), and for the present-day GrIS (dashed grey lines). The four transects were drawn following modelled ice flow lines while ensuring to cross the NEEM (panel a), NGRIP (panel b), GISP 2 and GRIP (panel c), and the DYE-3 (panel d) ice core locations, as shown by the black lines in the inset maps.

3.2 Modelled Greenland Ice Sheet during the ~~Late Glacial~~last deglaciation

3.2.1 Ensemble-wide trends

Following the ~~local LGM~~lLGM, nearly all ensemble simulations produce rapid ~~and~~, high-magnitude retreat of GrIS margins between 16 and 14 kyr BP, during ~~the~~ late HS1 and the *Bølling–Allerød* warming ~~event~~ (B-A; ~14.7-12.9 kyr BP; He et al., 2021) (Fig. ~~11~~10). Depending on regions, this ~~sudden~~abrupt warming ~~is associated with increases in~~raises mean annual and ~~mean~~ summer air temperatures ~~of between~~by 5 ~~and~~ 12 °C ~~in our forcing data~~ (Fig. 5~~), while our input~~) and sea surface temperatures ~~increase~~ by ~~between~~ 0.2 ~~and~~ 3.8 °C (Fig. ~~7). For~~6) in our forcing data. In simulations ~~that model an expansion of the grounded~~ where the GrIS ~~over~~advanced onto continental shelves between 24 and 16 kyr BP, ~~subsequent~~ retreat during the B-A causes ~~a~~ near-~~-~~complete deglaciation of continental shelf covers. ~~During the late HS1 and B-A warming (16-14 kyr BP), we~~We find nearly no modelled surface melt across any simulations~~,~~ during the late HS1, B-A warming (16 - 14 kyr BP), and until ~12 kyr BP (Fig. ~~12). Modelled~~11). Instead, modelled margin retreat and mass losses between 16 and 14 kyr BP are ~~instead~~ associated with more negative (up to tenfold) ~~basal~~sub-shelf mass fluxes~~, caused~~ driven by ocean warming increasing sub-shelf melt rates (Fig. ~~12~~11). A ~30% decrease in modelled ice accumulation rates during that time also plays a smaller role. These mechanisms lead to ~~substantial~~ ice sheet thinning of up to 800 m in 2 kyr ~~during that period~~ (Supplementary Fig. 2). ~~Our~~Consistent with Tabone et al. (2018), our ensemble ~~thus~~ suggests that during ~~the~~ late HS1 and B-A warming, ~~between 16 and 14 kyr BP,~~ ocean forcing ~~likely caused the~~drove rapid GrIS ~~to~~ retreat ~~rapidly~~ and ~~lose most~~near-total loss of its ~~glaciated~~ continental-shelf ~~areas~~cover, despite air temperatures remaining too cold to produce ~~any~~ surface melt (Fig. ~~12~~11).

At the ice-sheet scale, ensemble simulations produce little or no GrIS margin re-advance during the Younger Dryas stadial (YD: ~12.9 - 11.7 kyr BP). ~~For~~In the few ~~simulations that demonstrate some~~runs where grounded ~~margin~~margins do re-advance ~~during the YD~~, they recover less than ~3% of the area lost during deglaciation just prior (~16 - 14 kyr BP). ~~Towards~~In the north Atlantic region, the YD was a high-~~-~~magnitude but ~~relatively~~ short-lived (~1.2 kyr) cooling event, with our ~~input climate~~ forcing data suggesting mean annual temperatures over the GrIS decreasing by ~7 °C~~,~~ relative to 13 kyr BP (Fig. 5). ~~-~~In our simulations, the ~~modelled~~ GrIS is likely still adjusting to ~~the substantial~~major mass and extent loss ~~experienced just prior,~~ during the preceding B-A warming. ~~We find that despite~~ Despite large parameter and climate perturbations between simulations (Table 1), ~~the~~ this post B-A inertia ~~and memory from the B-A warming phase~~ combined with the ~~relatively~~ short~~-lived nature~~ duration of the YD ~~event prevented any simulation from producing~~prevents substantial margin re-advances in most regions. Modelled GrIS volume, however,

Formatted: Font: +Body (Calibri), 11 pt, Ligatures: None

Formatted: Font: +Body (Calibri), 11 pt, Ligatures: None

responds more dynamically to YD cooling ~~than extent~~, with some simulations recovering up to 8% of the mass ~~loss experienced just prior (~~lost between 16 ~~-~~and 13 kyr BP~~)~~ (Figs. ~~11, 13~~10, 12). During the YD, these simulations display ~~highly~~ spatially heterogeneous ~~variations in~~ ice ~~-~~ thickness changes: with some thickening of up to ~200 m ~~mainly modelled~~ in CE and Southern GrIS regions, while other ~~regions display continued~~areas continue thinning (Supplementary Fig. 2). ~~Nevertheless~~Overall, despite ~~the high magnitude of~~strong cooling, our ensemble suggests large ~~re-advances of~~ GrIS ~~margins~~margin re-advances during the YD ~~are~~were unlikely and would have required ~~a~~ more sustained ~~cooling event.~~forcing. This ~~finding is consistent~~aligns with ~~a~~the general lack of geomorphological ~~and~~or geochronological evidence for GrIS ~~margin readvances~~re-advances during the YD (Leger et al., 2024), and ~~confirms that~~highlights the ~~ice sheet's~~substantial inertia of the ice sheet following millennial-scale ~~warming and~~ retreat ~~can be substantial.~~ Contrastingly, numerous ~~periphery Greenland~~peripheral icecaps and glaciers ~~best~~ scoring simulations due to lower ~~ice~~ volumes and ~~extent~~extents, were ~~found to be~~ more sensitive and ~~to have~~did re-~~advanced~~advance during the YD (*e.g.* Larsen et al., 2016; Biette et al., 2020).

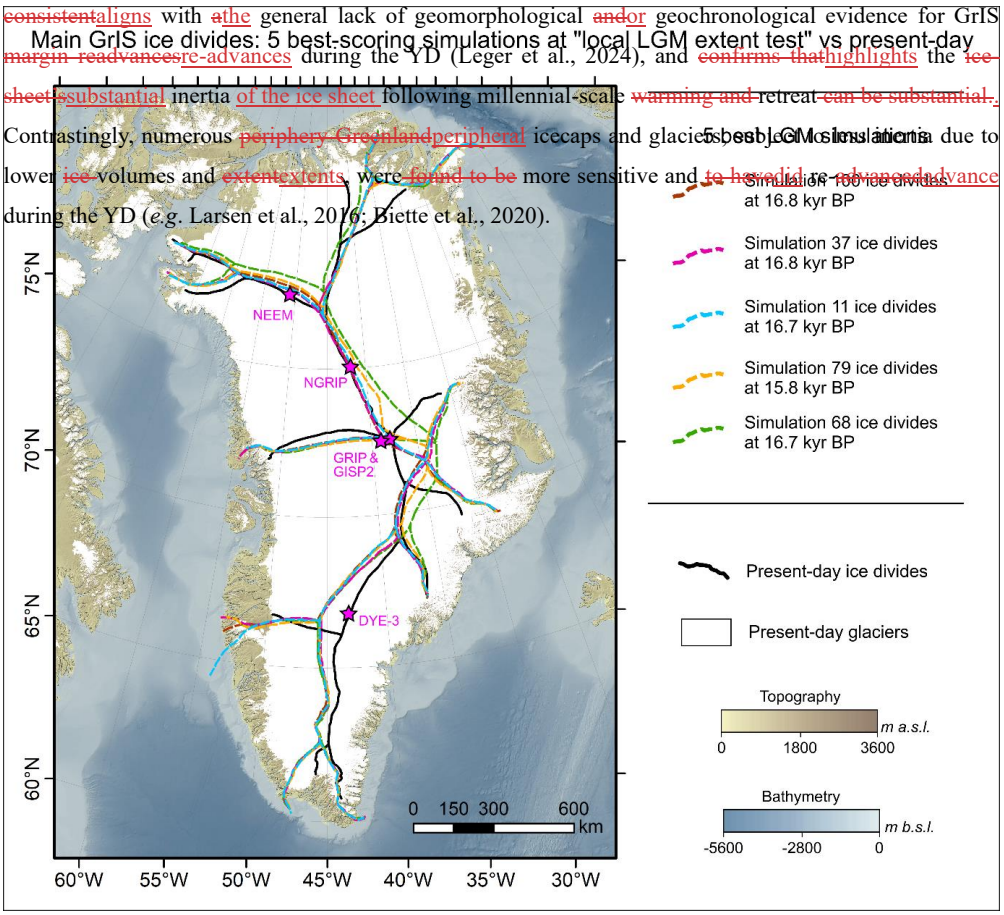

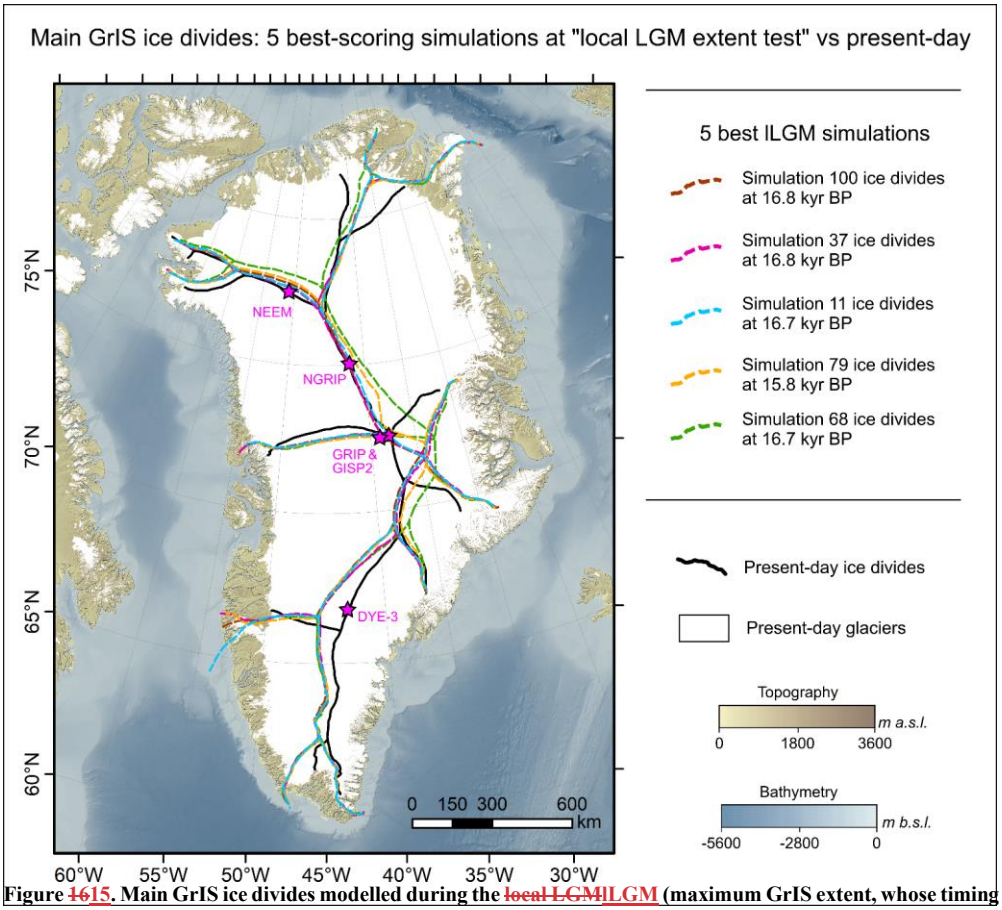

Figure ~~16~~15. Main GrIS ice divides modelled during the ~~local LGM~~lLGM (maximum GrIS extent, whose timing is simulation-dependent) for our five best-scoring ensemble simulations at the *local-LGM extent* test (dashed coloured lines). These are compared against the present-day GrIS main ice divides (continuous black line) extracted from surface ice velocity observations (Joughin et al., 2018). The locations of main Greenland ice cores discussed in this study are highlighted by the pink stars. Note the potent offset between the location of the DYE-3 ice core and modelled ice divides during the ~~local LGM~~lLGM (more details in section 3.1.2.). Bathymetry and topography data shown in this map are from the 15 arc-second resolution General Bathymetric Chart of the Oceans (GEBCO Bathymetric Compilation Group 2022, 2022).

Formatted: Font: Bold

3.2.2 Insights from deglacial best-fit simulations

In this section, we refer to our 'deglacial best-fit simulations' as the five best-scoring ensemble simulations at the *Deglacial extent* test (Figs. ~~10, 13~~9, 12).

Deglacial best-fit simulations produce spatially heterogeneous mass-change patterns ~~of mass change~~ during the last deglaciation (16 - 8 kyr BP) (Supplementary Fig. 2). ~~For instance, during~~During the YD stadial (~~13~~14 - 12 kyr BP), only small peripheral regions of CE, SE, and SW Greenland ~~experience~~gain mass ~~gain~~, while other ~~regions of the modelled ice sheet experience either~~sectors show no ~~mass~~ change~~,~~ or ~~instead~~ mass loss. During peak B-A warming (16 - 14 kyr BP), ~~we find~~ modelled mass loss is most ~~prominent~~pronounced in NW, CW, SW, and SE Greenland (Supplementary Fig. 2). At the ice-sheet scale, ~~our~~ deglacial best-fit simulations generate maximum mass loss rates during ~~the~~ late HS1 and B-A warming ~~periods~~ (16~~-~~ - 14 kyr BP) ~~that reach maximum values of between~~reaching ~500 ~~and ~-~~ 1400 Gt yr^{-1}~~, equivalent to between ~~~ (~~1 ~~and ~-~~ 3 mm SLE yr^{-1}~~, at around 14.5 kyr BP)~~ (Fig. ~~21). Comparatively, between 2003 and 2020 AD~~20). By comparison, the GrIS ~~is~~lost an estimated ~~to have lost~~ 200 ~~to~~ 300 Gt yr^{-1}~~, equivalent to approximately~~ (0.57 mm SLE yr^{-1}) between 2003 and 2020 AD (Simonsen et al., 2021). ~~Therefore, our deglacial best-fit simulations model between 2.5 and 7 times greater mass loss rates~~ Thus, during peak deglaciation (~14.5 kyr BP), best-fit simulations model 2.5 - 7 times greater mass loss rates than ~~is estimated for the last two decades~~present estimates (Fig. ~~21). Such mechanisms lead~~20). This leads to substantial ice-sheet thinning between 16 and 14 kyr BP in these simulations, especially-pronounced over the CW GrIS (Supplementary Fig. ~~2). During this event, moreover, the modelled rates of~~2), and causes maximum areal-extent loss ~~reach maximum values~~rates of ~~between~~ 300 ~~and~~ 450 km^2 yr^{-1} (Supplementary Fig. 3). ~~We note that these~~These modelled area loss rates ~~during peak B-A warming, here mostly related~~, primarily linked to ocean~~-~~ forcing, ~~notably~~ exceed the ~~near-constant rate of~~ 170 ± 27 km^2 yr^{-1} estimated ~~by~~from the ~~landform-derived~~ PaleoGrIS 1.0 reconstruction for the ~14 - 8.5 kyr BP period (Leger et al., 2024). This ~~may suggest~~suggests that grounded GrIS retreat ~~rates~~ during peak B-A warming ~~were greater~~was faster than during the YD-to-early Holocene transition, the period covered by most data compiled in PaleoGrIS 1.0, when a ~~higher proportion~~larger fraction of the ~~deglaciating~~ GrIS was land-terminating.

Including Ellesmere Island in our model domain ~~enables to potentially reconstruct and better understand the important mechanisms~~allows reconstruction of coalescence during advance and ~~the~~ subsequent unzipping of the ~~Greenland~~GrIS and ~~Innuitian ice sheets~~IIS over Nares Strait~~,~~ during deglaciation. ~~Here, we find that some of our~~Some deglacial best-fit simulations (*e.g.* simulation 73) ~~do~~ capture this behaviour (Fig. ~~23~~21). In these ~~simulations, the majority of~~runs, most grounded ice over Nares Strait ~~is deglaciated~~deglaciates between 10 and 8 kyr BP, ~~approximately in line~~broadly consistent with geochronological ~~empirical~~ evidence (Jennings et al., 2011) (Fig. 21). For ~~23). We note that for~~ simulations successfully modelling ~~the~~ full grounded-ice unzipping of the two ice sheets, final separation (although modelled too late) occurs

Formatted: Font: Times New Roman

consistently offshore Peterman glacier~~, towards~~ near Hall basin, while ~~the~~ Kane Basin ~~further Southwest~~farther southwest (offshore Humboldt glacier) deglaciates earlier (*e.g.* Fig. ~~23~~21).

Grounded ice surface velocities for 5 best scoring simulations at 'local LGM extent' test

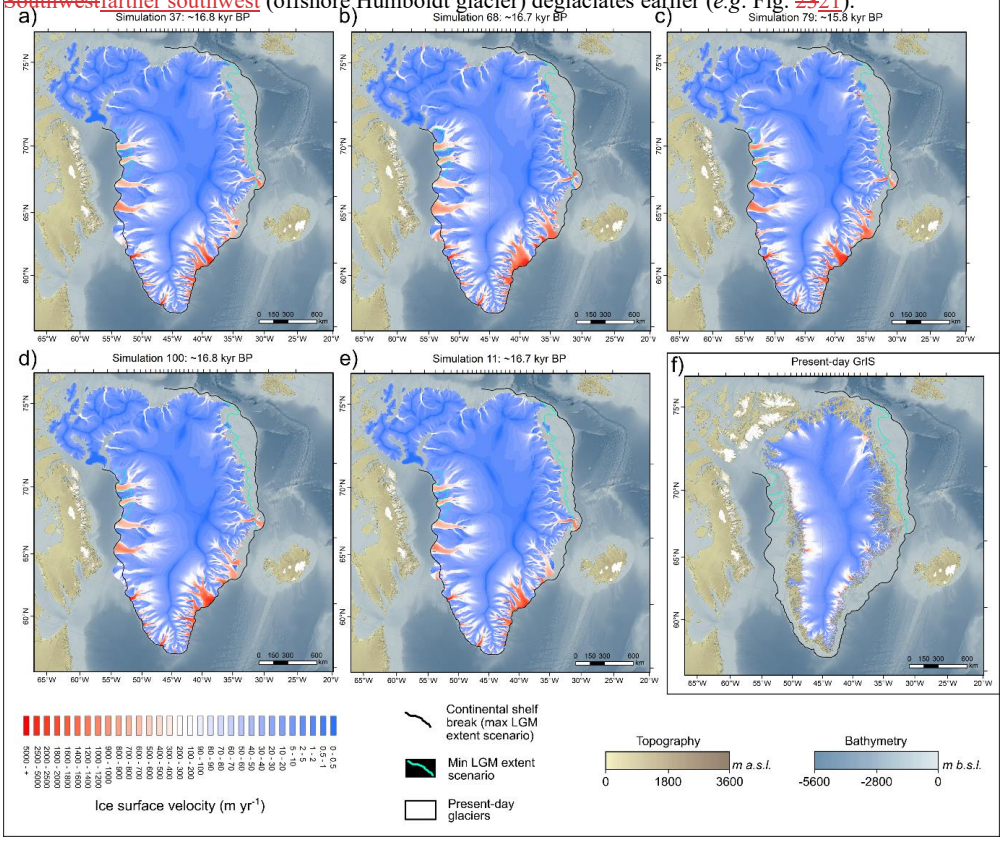

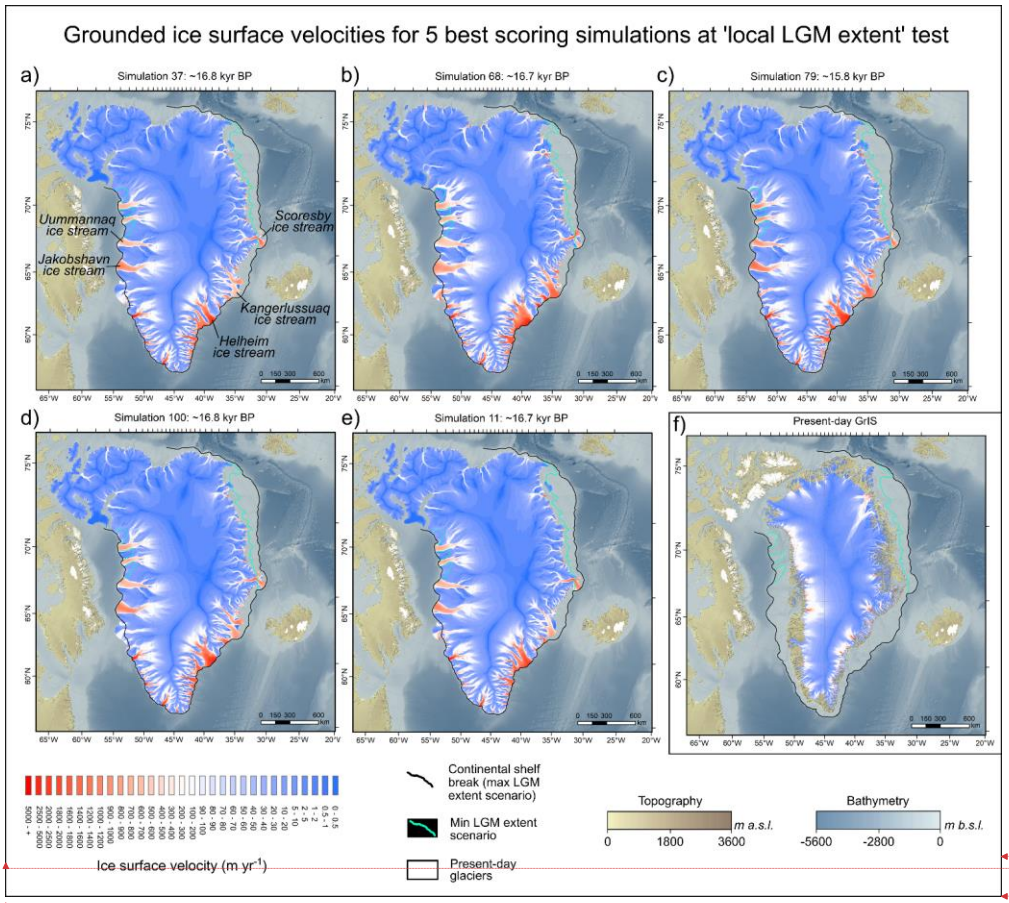

Figure ~~17~~16. Modelled grounded ice surface velocities during the ~~local LGM~~LGM (maximum Gris-wide ice extent, whose timing is simulation-dependent) for our five best-scoring ensemble simulations at the *local-LGM extent* test (panels a-e), compared with observed present-day GrIS ice surface velocities (panel f; Joughin et al., 2018). Bathymetry and topography data shown in this map are from the 15 arc-second resolution General Bathymetric Chart of the Oceans (GEBCO Bathymetric Compilation Group 2022, 2022).

Formatted: Font: +Headings CS (Times New Roman), 11 pt, Ligatures: None

Formatted: Left, Space After: 8 pt, Add space between paragraphs of the same style, Line spacing: single

Formatted: Font: Bold

Formatted: Justified

Formatted: Font: Bold

3.3 Modelled Greenland Ice Sheet during the Holocene

3.3.1 Ensemble-wide trends

~~The majority of our~~Most ensemble simulations produce a minimum in GrIS areal extent during the mid-Holocene~~, between~~ (6 ~~and~~ 5 kyr BP~~, prior to~~), before modelling margin re-advances ~~during~~in the late-Holocene and Neoglacial ~~periods~~ (5 kyr BP - 1850 AD). This ~~is consistent~~aligns with empirical reconstructions of Holocene GrIS margin evolution (Funder et al., 2011; Sinclair et al., 2016; Leger et al., 2024). The modelled mid-Holocene minimum in ~~grounded~~ GrIS extent occurs in response to the Holocene Thermal Maximum (HTM), ~~characterised by~~with mean annual and ~~mean~~ summer surface air temperatures ~~that were~~ over the GrIS up to ~~7~~ 5 - 7 °C warmer ~~relative to~~than at the PI ~~era~~ (1850 AD~~), over the GrIS ()~~(Figs. 4, 5). In our climate forcing, the HTM ~~occurs towards~~peaks at ~6 kyr BP for mean annual ~~air~~ temperatures~~,~~ and between ~9 ~~and ~~~ 6 kyr BP for ~~mean~~ summer temperatures ~~(JJA mean),~~ depending on the region. ~~In agreement~~Consistent with ~~findings of~~ the PaleoGrIS 1.0 reconstruction, ~~our~~ simulations thus ~~capture a degree of~~ produce ice-sheet inertia causing the ice extent ~~response~~ to lag ~~the~~warming cessation ~~of warming~~ and ice-thickness adjustment by ~~a few~~ centuries~~, and up~~ to a millennium~~,~~ during the early-to-mid Holocene. Furthermore, ~~we find~~ all ~~ensemble~~ simulations model a notable ~~increase in~~ ice-sheet volume increase during the late Holocene (3-2 kyr BP) and ~~produce~~ widespread thinning during the ~~neoglacial period (Fig. 11),~~Neoglacial, thus ~~following~~ reflecting trends opposite ~~trends relative~~ to ice extent~~.~~ (Fig. 10).

During most of the Holocene~~, between~~ (8 kyr BP ~~and~~ 1850 AD~~;~~), all ~~ensemble~~ simulations produce GrIS mass~~-~~change rates ~~that remain~~remaining below 100 Gt yr^{-1}, despite important variations in climate and SMB parameters between ~~simulations~~runs (Fig. 20). These~~21). Such~~ rates ~~remain below~~are lower than present-day ~~estimated~~ mass~~-~~loss ~~rates~~estimates of 200 - 300 Gt yr^{-1} (2003 - 2020 ~~period~~AD; Simonsen et al., 2021). This ~~observation is coherent~~result agrees with other GrIS modelling and ~~reconstruction efforts~~reconstructions suggesting ~~the speed of~~ contemporary and future GrIS mass loss ~~is~~rates are likely unprecedented ~~throughout~~over much of the Holocene (Briner et al., 2020). Similarly~~ for~~, our ensemble suggests that present-day GrIS~~-wide ice~~ discharge rates~~, our ensemble suggests the estimated present-day rate of~~ (487 ± 50 Gt yr^{-1}~~(~~; Mankoff et al., 2020) ~~is~~are likely unprecedented ~~for~~over the past five ~~thousand years~~millennia (Fig. ~~20).~~19).

3.3.2 Insights from Pre-Industrial best-fit simulations

In this section, we refer to our 'PI best-fit simulations' as the five best-scoring ensemble simulations at the *PI extent* test (Figs. ~~10, 13~~9, 12).

Formatted: Font: Times New Roman

Formatted: Font: Bold

~~We find that~~ PI best-fit simulations (*e.g.* simulation 31) tend to ~~produce a closer~~ fit ~~with~~ the youngest PaleoGrIS 1.0 isochrones (~~during the~~ mid-Holocene~~), relative to~~) better than other ensemble ~~simulations~~runs (Fig. ~~13~~12). They model both a pronounced minimum in grounded GrIS extent at ~5 kyr BP~~,~~ and a ~~notable~~ margin re-advance between ~5 kyr BP and the PI (1850 AD). During the Holocene minimum ~~in ice extent, our PI best-fit~~, these simulations model some retreat behind ~~the~~ present-day GrIS ~~margin, as is suggested by~~ margins, consistent with empirical evidence (*e.g.* Larsen~~Briner~~ et al., ~~2014)~~2011; 2015), but only~~. However, this is exclusively the case~~ in SE and SW Greenland ~~regions. No GrIS~~. North of 68 °N, no retreat behind present-day margins is modelled ~~north of 68.°N, with the exception of the~~except for Humboldt glacier ~~front~~ (Supplementary Fig. 4). ~~In all other GrIS regions, the~~Elsewhere, modelled ~~ice sheet margin remains close to~~ margins remain near or more extensive than ~~the~~ present-day ~~margin~~margins throughout the mid-to-late-Holocene~~, between~~ (5 kyr BP ~~and~~ 1850 AD~~. It is worth noting that ensemble simulations~~). Simulations with the lowest areal extent during the HTM (*e.g.* simulation 78; Fig. ~~13c~~12c) produce up to ~100 km ~~of~~ retreat behind ~~the~~ present-day ~~GrIS margin~~margins in southernmost Greenland (north of Narsarsuaq), ~~prior to~~before re-advancing ~~and reaching~~to present-day ~~margins by the end of the simulation (~~extents by 1850 AD~~).~~. Although this ~~result~~ may well be an overestimation ~~and should be interpreted with caution~~, our modelling suggests such a retreat magnitude ~~of retreat~~ behind present-day margins (~100 km) in response to the HTM cannot be fully ruled out~~,~~ in certain regions. This behaviour is correlated to, and likely caused by, PI best-fit simulations presenting both positive (>+1.5°C) and negative (<40% of original) temperature and precipitation offsets, respectively (Fig. 24).

Within ~~our~~ PI best-fit simulations, simulation 31 ~~yields a better match in~~ best reproduces present-day ice thickness (Morlighem et al., 2017a) and ~~ice~~ surface velocity (Joughin et al., 2018) ~~with the present-day GrIS~~ (Supplementary Figs. 5, 6). The remaining four best-fit simulations underestimate PI GrIS volume (Fig. ~~13). Nonetheless,~~12). Even in simulation 31, ~~PI~~ ice thickness is ~~still~~ underestimated ~~towards~~in the GrIS interior (~~by~~ up to ~600 m~~),~~) and overestimated ~~towards~~at the ~~ice sheet's~~ margins~~. We find our simulations produce lower~~, whilst modelled ice surface velocities ~~at the PI~~ are generally lower than present-day observations ~~in most regions~~ (Joughin et al., 2018). This is likely ~~caused by the~~ due to underestimated ~~PI~~ GrIS thickness towards its interior, ~~resulting in lower~~which reduces ice surface slopes and ~~thus underestimated~~ driving stresses (Supplementary Figs. 5, 6, ~~12~~11). The most notable examples are NEGIS and Jacobshavn Isbrae, where the present-day GrIS ~~is flowing~~flows more than 200 m yr^{-1} faster than simulation 31 during the PI. Therefore, ~~our~~ PI best-fit simulations fail ~~at~~to reproducing the particular dynamics of NEGIS. In SE Greenland, however, ~~there seems to be a higher concentration of regions where~~ simulation 31 produces faster-flowing ice ~~instead~~in several regions (by more than 200 m yr^{-1}). Interestingly, that is also the case for the terminus of Humboldt glacier (Supplementary Fig. 6).

Formatted: Font color: Black

Formatted: Font color: Black

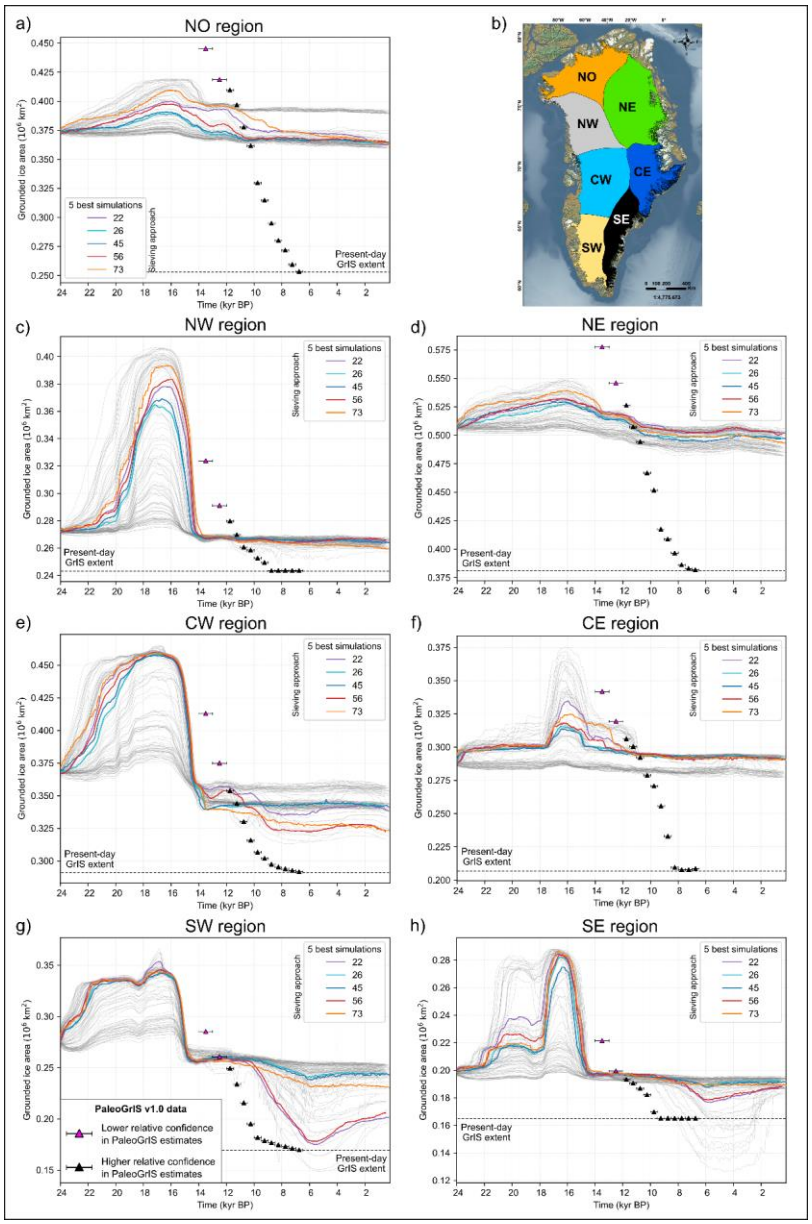
a)
NO region
b)
NO
NE
NW
CW
CE
SE
SW
c)
NW region
d)
NE region
e)
CW region
f)
CE region
g)
SW region
h)
SE region
Grounded ice area (10^6 km^2)
Time (kyr BP)
5 best simulations
22
26
45
56
73
Sieving approach
Present-day GrIS extent
PaleoGrIS v1.0 data
Lower relative confidence in PaleoGrIS estimates
Higher relative confidence in PaleoGrIS estimates

Figure ~~18~~17. Time series of modelled grounded GrIS extent for our five overall best-fit simulations (which pass all sieves, highlighted by thicker coloured lines) for each of the seven main GrIS regions (panels a, c-h) whose locations are shown by the inset map on panel b. Data from the PaleoGrIS 1.0 ice-extent reconstruction (Leger et al., 2024) are shown with triangle symbols. Data from all other ensemble simulations are shown with thin, light grey lines.

Formatted: Font: Bold

4 Insights from model-data comparison

4.1 Model agreement with empirical data

When compared against the PaleoGrIS 1.0 ice extent reconstruction (Leger et al., 2024), all ensemble simulations underestimate ~~the magnitude of~~ grounded GrIS retreat during the last deglaciation, ~~with~~missing at least 30% (~0.5 million km^2) of the ice-sheet-wide retreat signal ~~missing~~ (Figs. ~~13, 22~~10, 12). While more consistent with ~~the~~ PaleoGrIS 1.0 ~~reconstruction~~ during ~~the~~ late HS1 and B-A warming ~~events~~ (16 - 14 kyr BP), ~~both~~ modelled retreat rates and magnitudes ~~of modelled margin retreat are~~remain too low during the early-to-mid Holocene (12-8 kyr BP). ~~This remaining~~These model-data ~~misfit is apparent in~~misfits occur across all ~~ensemble~~ simulations despite ~~our~~ parameter and climate perturbations (~~Fig. 13, 22~~Figs. 10, 12). In ~~all simulations~~addition, the onset of modelled GrIS retreat ~~also~~ occurs ~2 kyr earlier than ~~is~~ suggested by PaleoGrIS 1.0~~, with an offset of nearly 2 kyr~~ (Fig. ~~22~~10). However, the 14 - 12 kyr BP PaleoGrIS 1.0 isochrones are ~~characterised~~limited by ~~significant~~ data scarcity and timing uncertainties associated with offshore samples, whose radiocarbon dating is ~~challenged~~complicated by high-latitude marine reservoir effects (Leger et al., 2024). ~~The~~Thus, time ranges ~~and error ranges~~ of oldest PaleoGrIS 1.0 isochrones should ~~thus~~ be interpreted with caution. Alternatively, as our results show the onset of modelled GrIS retreat during late HS1 and B-A is primarily controlled by sub-shelf melting (see section 3.2.1.), this offset in retreat timing may also reflect uncertainties and biases in the SST reconstruction (Osman et al., 2021; Figs. 6) used as ocean temperature forcing (see section 5.1. for more discussion).

When analysing model-data agreement at the regional scale, ~~however,~~ we find that model misfits with the PaleoGrIS 1.0 reconstruction are spatially heterogeneous (Figs. ~~18, 23, 24~~17, 21, 22). Overall best-fit

simulations (which pass all sieves) generally ~~display a~~agree better ~~fit~~ with the PaleoGrIS 1.0 reconstruction during both the ~~local LGM~~lLGM extent and ~~the~~ Lateglacial-to-mid-Holocene deglaciation in NW, CW, SW, SE Greenland, and ~~towards~~ the Kangerlussaq outlet glacier sub-region (CE Greenland ~~south of Scoresby Sund~~), relative to other regions (Fig. ~~18). In~~17). Even in these better-fitting ~~regions, our~~areas, best-fit simulations ~~still~~ underestimate ~~the reconstructed magnitudes of~~ grounded GrIS retreat magnitudes, but often by less than 50 km. ~~There are some smaller~~Smaller-scale exceptions ~~such as~~occur in the Nuuk fjord and Sisimiut regions, ~~,~~ where ~~the~~ ice-extent ~~misfit is closer to~~misfits reach 70 - 90 km~~,~~ depending on the simulation and time ~~slice~~period analysed (Figs. ~~23, 24~~21, 22).

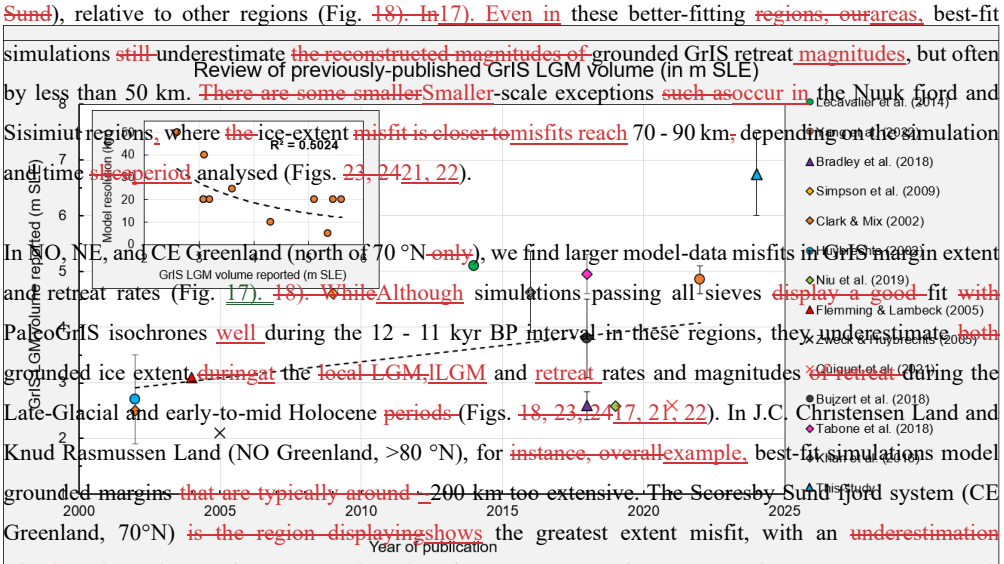

In NO, NE, and CE Greenland (north of 70 °N ~~only~~), we find larger model-data misfits in GrIS margin extent and retreat rates (Fig. ~~17). 18). While~~Although simulations passing all sieves ~~display a good~~ fit ~~with~~ PaleoGrIS isochrones well during the 12 - 11 kyr BP interval in these regions, they underestimate ~~both~~ grounded ice extent ~~during~~at the ~~local LGM,~~lLGM and retreat rates and magnitudes ~~of retreat~~ during the Late-Glacial and early-to-mid Holocene ~~periods~~ (Figs. ~~18, 23,~~24~~17, 21~~, 22). In J.C. Christensen Land and Knud Rasmussen Land (NO Greenland, >80 °N), for ~~instance, overall~~example, best-fit simulations model grounded ~~margins that are typically around ~200 km too extensive. The Scoresby Sund fjord system~~ (CE Greenland, 70°N) ~~is the region displaying~~shows the greatest extent misfit, with an ~~underestimation of~~underestimated margin retreat ~~that is~~ closer to ~230 km, at maximum. ~~Moreover, such underestimation~~Underestimation also remains ~~relatively~~ high ~~(between ~~(~90 ~~and ~~- 160 km) along the ~~entire~~ NE Greenland coast, ~~with the exception of~~except for the Nioghalvfjerdsbrae ('79N glacier') and Zachariæ Isstrøm glaciers, where ~~our~~ modelled grounded ~~ice~~ margins ~~fit the~~ agree well with PaleoGrIS 1.0 isochrones ~~well throughout~~through the early-to-mid Holocene (~11-6.5 kyr BP) (Figs. ~~23, 24~~21, 22).

Figure ~~19~~18. Review of previously modelled and/or reported GrIS volumes during the ~~local LGM~~lLGM (in m SLE, expressed as 'sea level contribution'), and compared against this study's estimates. An increasing trend of reported values through time can be observed, along with a negative correlation between model horizontal grid resolution and reported modelled LGM volumes.

Table 2: Ensemble-varying parameter values for the five overall best-fit simulations (which pass all sieves).

Ensemble-varying model parameter	Simulation 22	Simulation 26	Simulation 45	Simulation 56	Simulation 73	Unit
Flow law enhancement factor (-sia_e and ssa_e)	0.554	1.787	3.000	1.174	2.650	n/a
Regularized Coulomb sliding law exponent (q)	0.719	0.325	0.222	0.280	0.985	n/a
Topographic control on Yield Stress: lower ϕ treshold (ϕ_{min})	7.046	6.491	6.781	14.466	4.631	angle degree
Topographic control on Yield Stress: upper ϕ treshold (ϕ_{max})	36.100	22.427	20.000	31.905	41.246	angle degree
PDD melt factor for ice (*surface.pdd.factor_ice*)	10.241	7.665	12.000	10.946	10.078	mm we d^{-1} °C^{-1}
PDD melt factor for snow (*surface.pdd.factor_snow*)	4.485	2.491	4.945	4.500	3.444	mm we d^{-1} °C^{-1}
Rate of change of daily temperature variability (std) as function of elevation (*pgram_g*)	-0.148	-1.225	-0.285	-0.132	-0.240	n/a
Minimum thickness of terminal floating ice shelf (*-thickness_calving_threshold*)	84.250	125.393	74.242	190.606	176.156	m
Input temperature forcing: Temperature scalar offset (*delta_T*)	2.736	3.172	3.500	2.895	1.609	°C
Input precipitation forcing: % precipitation scaling (*frac_P*)	1.446	1.289	1.305	1.471	1.397	scalar multiplier

Although we ~~exclusively~~ use ~~data on former~~only grounded ice extent data for model-data comparison and ~~simulation~~ scoring, our results can also be ~~compared~~evaluated against ~~different~~other empirical datasets ~~used in previous studies.~~. For instance, we ~~here~~ compare modelled surface ice elevation change between 8 kyr BP and 1850 AD at ~~the location of~~ four Greenland ice ~~cores~~core sites (GRIP, NGRIP, DYE-3, and Camp Century) ~~against the~~with δ^{18}O-derived Holocene thinning curves ~~(for these sites, originally produced by (~~Vinther et al., 2009~~), and improved by~~ Lecavalier et al. ~~(~~, 2013~~)~~) (Fig. 23). ~~25). Holocene thinning~~These curves ~~provide a mean to~~ check whether modelled GrIS ~~thinning rates are in general agreement~~ align with ice-core data. We find that, despite ~~our five best-fit simulations (which pass all sieves)~~ showing ~~some~~ differences in thinning magnitudes and trends, ~~they all~~ all best-fit simulations (which pass all sieves) produce thinning signals ~~that remain~~ within the 1σ uncertainty bands of the ~~ice core -derived data~~thinning curves, for more than 80% (100% for NGRIP) of the time period analysed ~~here~~ (8 - 0 kyr BP). One exception is simulation 22 which, at the ~~location of the~~ GRIP ~~ice core~~site, models a mid-Holocene ~~surface~~ elevation offset relative to PI that remains ~~higher than~~above the upper 1σ ~~uncertainty~~ limit~~,~~ for ~~approximately~~ ~2.2 kyrs (Fig. ~~25). Contrastingly~~23). By contrast, at ~~the location of~~ DYE-3, simulation 22 matches ~~the thinning curve~~ better than the ~~remaining four~~other best-fit simulations ~~by producing~~, capturing a higher thinning rate between 8

Formatted: Font: +Headings CS (Times New Roman), 11 pt, Bold, Ligatures: None

Formatted: Left, Space After: 8 pt, Add space between paragraphs of the same style, Line spacing: single

Formatted: Font color: Auto

Formatted: Font color: Auto

and 6 kyr BP. All five ~~best-fit~~ simulations ~~seem to~~ slightly underestimate the higher thinning rate estimated at ~~the~~ Camp Century ~~ice core,~~ between 8 and 6.5 kyr BP, a misfit ~~that has~~ also ~~been observed~~seen in previous ~~paleo GrIS~~ modelling ~~efforts~~work (e.g. Huy3 model; Lecavalier et al., 2014). Overall, ~~despite not scoring~~ although our ensemble ~~simulations using comparisons was not scored~~ against ~~Holocene~~ thinning curves ~~(Vinther et al., 2009; Lecavalier et al. 2013), our~~, best-fit simulations ~~produce~~generally reproduce thinning signals ~~that generally remain~~ within ~~the uncertainty of the ice core - derived data~~ (their uncertainties between 8 kyr BP and PI ~~(~~Fig. ~~25~~23). This ~~finding~~ suggests that ~~best scoring~~GrIS simulations ~~isolated~~constrained by model-data ~~comparison using detailed scoring against~~ ice-extent reconstructions tend to also ~~result in appropriate~~yield realistic Holocene ~~GrIS~~ thinning ~~signals~~histories. However, ~~it must be noted that, although~~ while some ensemble ~~simulations are~~members clearly ~~not in agreement~~disagree with the ~~ice core - derived~~ thinning curves (Lecavalier et al., 2013), ~~the majority~~most of the ensemble remains ~~close to, or~~ within~~, the~~ their 1σ uncertainty bands ~~of these data~~ (Fig. ~~25).~~23). It must also be noted that whilst we here focus on the 8 - 0 kyr BP interval, GrIS thinning histories during the early Holocene (12 – 8 kyr BP) are known to be more challenging to both i) replicate in models and ii) recover in original ice-core derived data (Lecavalier et al., 2017; Tabone et al., 2024). This is due to the demise of the LIS and IIS and unzipping from the GrIS during this interval, and the important impacts of these events on GrIS thinning and bed isostatic adjustment.

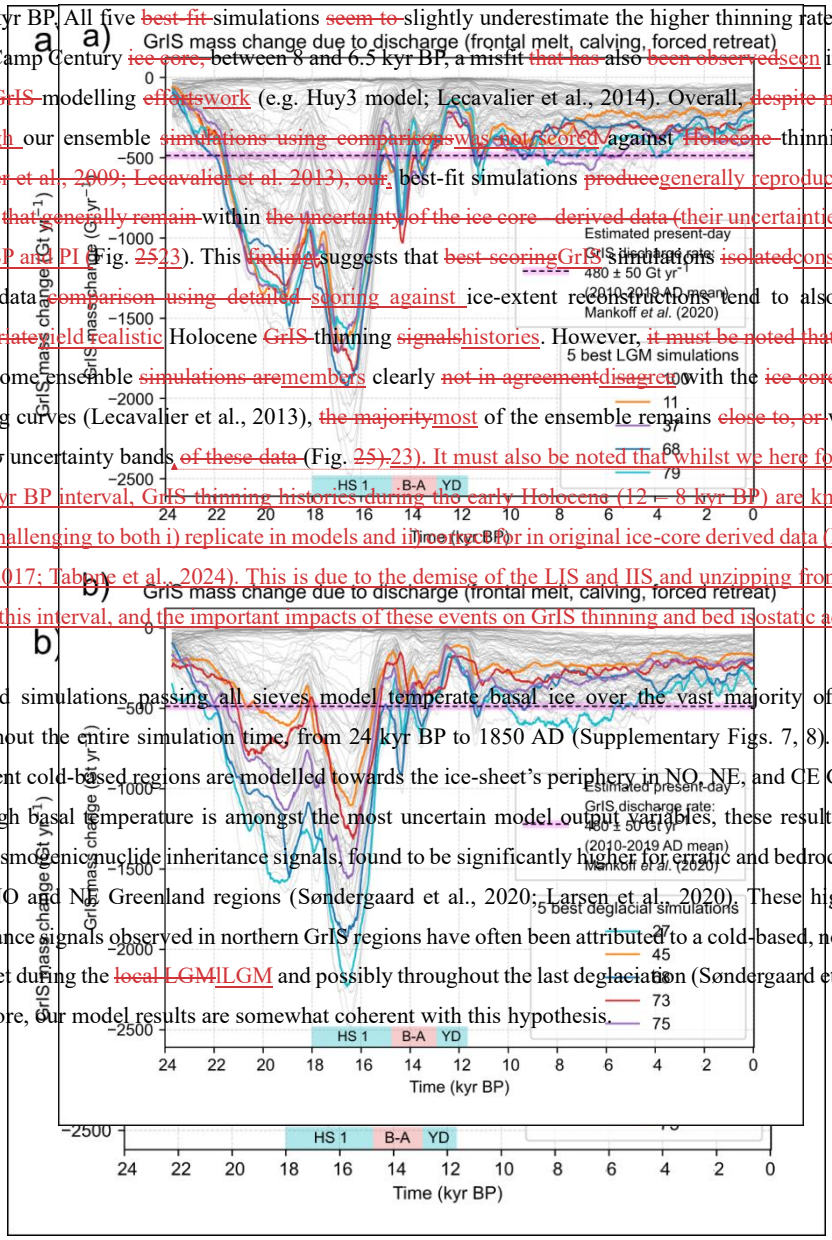

We find simulations passing all sieves model temperate basal ice over the vast majority of the GrIS throughout the entire simulation time, from 24 kyr BP to 1850 AD (Supplementary Figs. 7, 8). However, persistent cold-based regions are modelled towards the ice-sheet's periphery in NO, NE, and CE Greenland. Although basal temperature is amongst the most uncertain model output variables, these results coincide with cosmogenic nuclide inheritance signals, found to be significantly higher for erratic and bedrock samples from NO and NE Greenland regions (Søndergaard et al., 2020; Larsen et al., 2020). These high nuclide inheritance signals observed in northern GrIS regions have often been attributed to a cold-based, non-erosive ice sheet during the ~~local LGM~~LLGM and possibly throughout the last deglaciation (Søndergaard et al., 2020). Therefore, our model results are somewhat coherent with this hypothesis.

Formatted: Font color: Auto

Figure ~~20~~19. Time series of modelled GrIS mass change due to ice discharge for our five best-scoring ensemble simulations at both the *local-LGM extent* test (panel a) and the *deglacial extent* test (panel b), highlighted by thicker coloured lines, and compared with an estimated present-day GrIS ice discharge rate (Mankoff et al., 2020)**. Data from all other ensemble simulations are shown with thin, light grey lines.**

4.2 No perfect ensemble simulation

Our model-data comparison scheme ~~generates a~~yields different ~~list~~sets of five best-fit simulations for each of ~~our~~the three tests, ~~suggesting~~indicating no single simulation consistently matches empirical data ~~better~~

than others throughout across the full modelled timeframe (24 - 0 kyr BP), period and across all GrIS regions. (Fig. 1312). Instead, specific ensemble simulations need toruns must be selected and analysed to address research questions regarding certainon particular time periods and/or certain Greenland regions. Consequently, producing a high-resolution (≤ 5 km) simulation of the LGM-to-present GrIS evolutionsimulation that remainsis both consistent with physics and that shows good andin spatially/temporally homogeneous agreement with a detailed empirical datasetreconstruction such as PaleoGrIS 1.0, remains a major challenge.

More specifically, we find that *deglacial extent* and *local-LGM extent* test scores are positively correlated (Supplementary Fig. 9). Thus, simulations showing aSimulations that better relative match with data during the local LGMlLGM tend to also generate afit better fit during the deglaciation, mostly because as continental shelves need tomust first be ice-covered in order to deglaciate subsequently deglaciate (Fig. 109). However, both the *deglacial extent* and *local-LGM extent* test scores are negatively correlated with *PI extent* test scores. Ensemble; simulations yielding higher scoresperforming well during the local LGMlLGM and deglaciation tend to score worse at reproducingreproduce the PI GrIS extent less accurately, with a few exceptions (Supplementary Fig. 9). This is caused by a large proportion ofoccurs because many simulations not successfully producing anyfail to produce significant GrIS advance noror retreat prior tobefore the Holocene, but instead remaining closer tonear the present-day GrIS extent throughout the simulation (Fig. 1312), and thus scoring betterhigher at the *PI extent test*. This finding highlights the importance of applying a chronologically- ordered sieving of an ensemble usingacross multiple model-data comparison tests when isolating best-fit simulations. Indeed, this ordering of sieves helps to avoidprevents overrating a simulation that produces a better PI (or present-day) ice-sheet state, but for the wrong reasons. More generally, this result highlights that a model initialisationinitialisations successfully reproducing thepresent-day GrIS PI geometry isgeometries are not guaranteed to be an ideal initial statestates for forward modelling, as such parameterisationthey may not necessarily capture the transient longer-term ice-sheet behaviour, inertia, and memory inherited from the last glaciation and subsequent retreat.

Formatted: Font: Italic

Formatted: Font: +Body (Calibri), 11 pt, Ligatures: None

4.3 Are certain parameter values better than others?

We here analysed ensemble-varying parameter values (n = 10) for the five best-scoring simulations at each of our three model-data comparisons tests (Figs. 10, 269, 24, Table 1), and find the following:

Three out of 10 ensemble-varying parameters, *i.e.* the precipitation offset, the air temperature offset, and the flow law enhancement factor (Table 1), present someshow clustering in best-fit parameter values. For these three parameters,, meaning specific values may lead toyield better model-data fit (Table 2, Fig. 2624). Here, a 'cluster' is defined as when parameter values of the five best-scoring simulations at each test (Table 2) cover a range that isspan less than 50% of the original sampled parameter range (Table 1). For two ensemble-

varying parameters, *i.e.* the precipitation offset and ~~the~~ flow law enhancement factor, values leading to better model-data fit appear ~~to be~~ test-specific and thus time-dependent. ~~Parameter clusters suggest, for~~ For instance, ~~that~~ flow law enhancement factors lower than 1 may lead to better ~~relative~~ model-data fit in GrIS extent during the ~~local LGM~~lLGM (Table 2, Fig. ~~26). This may imply that better model-data fit during~~ 24), suggesting maximum expansion ~~requires to model~~is better captured when modelling a GrIS with harder, less deformable, ~~and~~ more viscous ice (or ~~with~~ lower impurity contents~~),~~) than ~~is~~ modelled ~~with~~by default flow law constants (E=1, n=3). ~~Parameter clusters moreover~~However, this may also represent a compensating adjustment from our modelled ice temperatures, which are warmer (thus possibly resulting in too soft ice) and produce more widespread warm-based conditions over greater proportions of the GrIS than most other GrIS models (e.g. Tabone et al., 2024; MacGregor et al., 2022) and this across all best-fit simulations (e.g. Supplementary Figs. 7, 8). Parameter clusters further suggest that better ~~model data~~ fit ~~may require between~~ requires 1.3 ~~to~~ 2 times higher precipitation during the ~~local LGM~~lLGM and deglacial periods, ~~and instead between~~but 2 ~~to~~ 5 times lower precipitation during the PI (1850 AD), ~~than is obtained with~~compared to our default climate forcing (Table 1, Figs. ~~6, 8, 26~~4, 5, 7, 24). However, ~~we acknowledge that~~ due to complex parameter interactions~~,~~ and the simplicity of our SMB parameterisation (PDD), ~~these~~such trends may not necessarily ~~help detect biases in~~ indicate input climate biases but ~~may~~ instead hide ~~more~~ impactful misrepresentations of ice dynamics and/or boundary conditions, ~~thus~~ precluding ~~any~~ definitive interpretations linked to individual model parameters.

For seven out of 10 ensemble-varying parameters (~~impacting~~affecting SMB, yield stress, sliding, or calving), no best-fit clusters ~~could be~~were identified, ~~suggesting~~indicating that better model-data fit can ~~be achieved~~occur with highly variable parameter values ~~covering more than~~ spanning ≥50% of the sampled ranges (Tables 1, 2, Fig. ~~26~~24). This ~~result either~~ suggests that: **i**) these seven parameters may not ~~significantly~~strongly impact the transient evolution of grounded GrIS extent; ~~and/~~or **ii**) ~~the various~~ interactions between ~~these seven parameters~~them may be more impactful than individual parameter perturbations; or **iii**) ~~identifying~~detecting best-fit clusters for ~~some of~~ these ~~seven~~ parameters may require a larger-than-100-simulation ensemble and a ~~more comprehensive~~broader exploration of the parameter space. ~~This result justifies~~These findings support the use of ~~an~~ ensemble ~~approach~~approaches when attempting to match ~~a~~ paleo-GrIS model ~~reconstruction~~simulations with empirical data, as ~~we find~~ highly ~~variable~~diverse parameter configurations can ~~generate~~still yield relatively ~~better~~good model-data fit.

Formatted: Justified

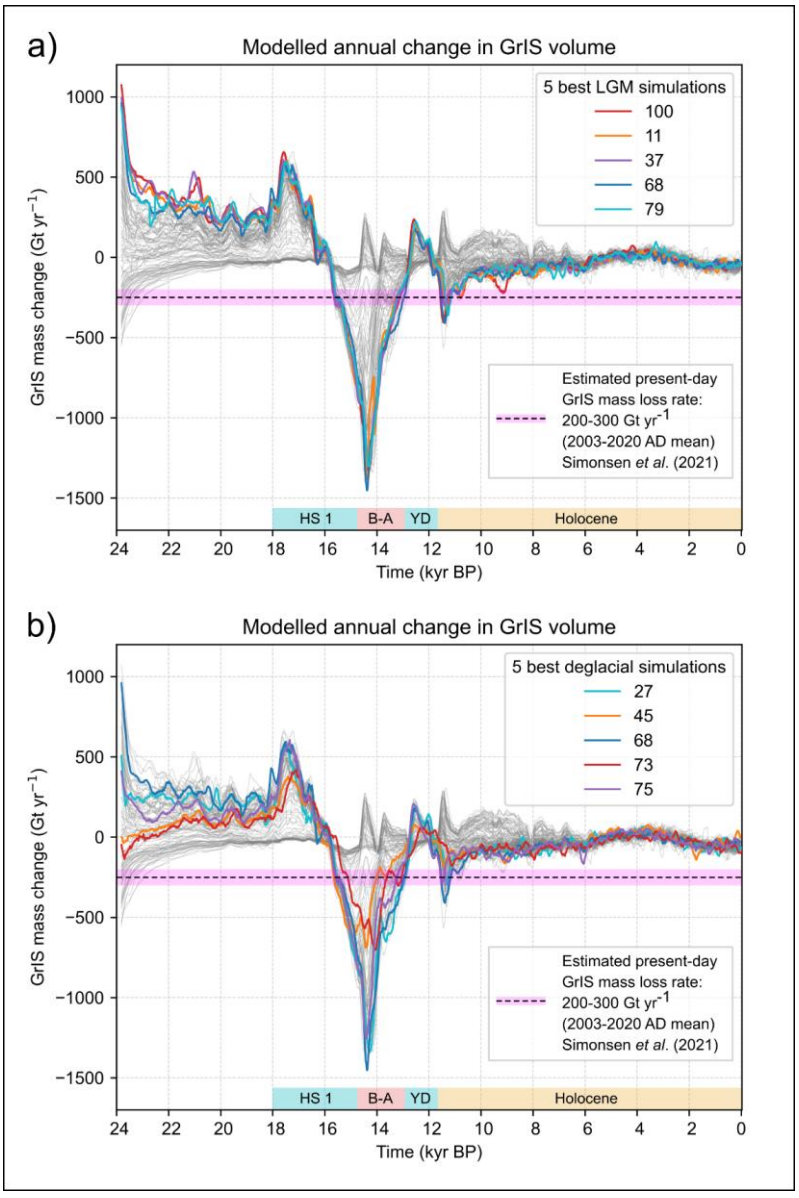
a)
Modelled annual change in GrIS volume
5 best LGM simulations
100
11
37
68
79
Estimated present-day
GrIS mass loss rate:
200-300 Gt yr-1
(2003-2020 AD mean)
Simonsen et al. (2021)
GrIS mass change (Gt yr-1)
1000
500
0
−500
−1000
−1500
HS 1
B-A
YD
Holocene
24
22
20
18
16
14
12
10
8
6
4
2
0
Time (kyr BP)
b)
Modelled annual change in GrIS volume
5 best deglacial simulations
27
45
68
73
75
Estimated present-day
GrIS mass loss rate:
200-300 Gt yr-1
(2003-2020 AD mean)
Simonsen et al. (2021)
GrIS mass change (Gt yr-1)
HS 1
B-A
YD
Holocene
Time (kyr BP)

Figure ~~21~~20. Time series of modelled annual rates of GrIS mass change for our five best-scoring ensemble simulations at both the *local-LGM extent* test (panel a) and the *deglacial extent* test (panel b) highlighted by thicker coloured lines. The time series are compared against an estimate of present-day GrIS mass loss rate (2003-2020 AD mean; Simonsen et al., 2021**). Data from all other ensemble simulations are shown with thin, light grey lines.**

5 Remaining misfits: possible causes

As mentioned above (see section 4.1.), ~~we find~~ model-data misfits in grounded ice extent display strong inter-regional heterogeneities, and are larger in the NO, NE, and CE Greenland regions (Figs. ~~18, 23, 24~~17, 21, 22). Additionally, ~~we find ensemble~~ simulations passing all sieves (see Methods section) present the most dynamic ice-extent responses ~~in ice extent~~ through time. They display both higher and lower grounded GrIS extents than ensemble-mean values during the ~~local LGM~~lLGM and mid-Holocene periods, respectively (Fig. ~~22~~10). This ~~may suggest that~~suggests remaining ~~model-data~~ misfits are related to ~~our model~~simulations not capturing ~~certain~~ mechanisms that would enable shorter response times to ~~changes in~~ boundary ~~conditions~~condition changes and produce higher-amplitude transitional advance and retreat phases. In the following sections, we discuss ~~and hypothesise~~ in more detail the possible mechanisms leading to remaining misfits by dividing them into: ~~1) Misfits~~i) misfits in GrIS advance during the ~~local LGM~~lLGM; and ~~2) Misfits~~ii) misfits in GrIS retreat during the Late-Glacial and Holocene periods.

5.1 Underestimated LGM advance in NE and NO Greenland

Along the NE Greenland coast (81-71°N), our simulations underestimate the magnitude of grounded ice advance during the ~~local LGM~~lLGM (~17.5-16 kyr BP) (Figs. ~~10, 14~~9, 13, 16, 17~~, 18). Empirical investigations~~). Investigations producing new geomorphological and geochronological reconstructions of GrIS thinning histories (*e.g.* Roberts et al., 2024~~)~~) and offshore ice extent (*e.g.* Arndt et al., 2017; Davies et al., 2022; Hansen et al., 2022) suggest that ~~local LGM~~lLGM grounded GrIS margins reached ~~between~~ ~100 ~~and ~~~ 200 km further ~~East~~east than ~~is modelled by~~ our best-~~scoring~~fit simulations (Figs. ~~14, 17~~13, 16).

~~A possible cause of~~These model-data misfit during the ~~local LGM~~lLGM may be related to our model initialisation (spinup) procedure reaching a steady-state that does not produce an extensive and/or thick enough GrIS at 24 kyr BP (*i.e.* the starting time of our transient simulations). This could be due to an inappropriate model parameterisation (*e.g.* SMB), or to biases in our static input atmospheric or oceanic forcings at 24 kyr BP (see section 2.2.). In the NO and NE regions, the GrIS may require a longer cooling

period than the 7.5 kyrs modelled in transient ensemble simulations (between 24 and 16.5 kyr BP) to fully re-adjust to the new parameterisation and switch from a margin location provided by the unique initial state (here close to the present-day GrIS margin) to a margin that needs to reach the mid-to-outer continental shelf. If this is the case, a bias in our model initialisation at 24 kyr BP may be responsible for the underestimated grounded ice advance during the ~~local~~ ~~BGM~~ILCM in NO and NE Greenland.

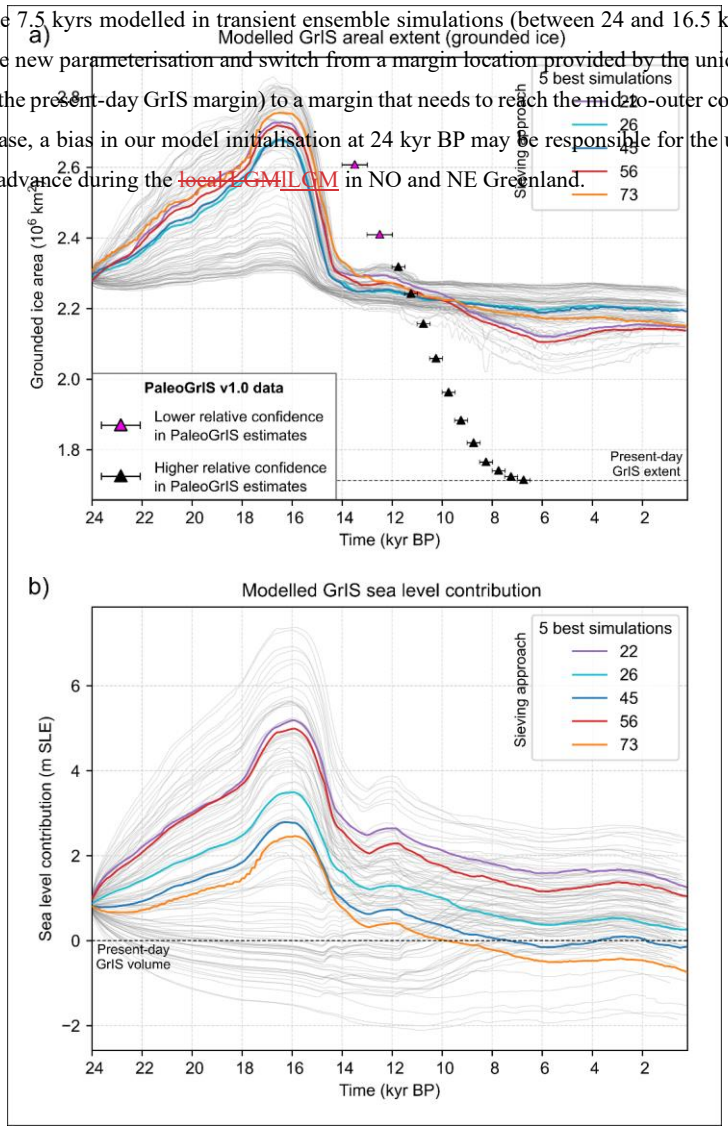

~~**Figure 22: Modelled grounded ice area (panel a) and volume (panel b; in m SLE, expressed as sea level contribution) for the 100 ensemble simulations (light grey time series), with the five overall best-fit simulations (which pass all sieves) highlighted with thicker coloured time series. The PaleoGrIS v1.0 isochrones data reconstructing the GrIS's former grounded ice extent are shown with triangle symbols on panel a (Leger et al., 2024). Note the GrIS-wide model-data misfit in ice extent apparent here can be misleading as it is spatially heterogeneous and heavily influenced by a few regions concentrating most of the misfit (*i.e.* NO, NE, and CE Greenland): see Fig. 18. Note the five overall best-fit simulations highlighted here, while passing all sieves, are not the best-scoring simulations at each individual model-data comparison test (see Fig. 13), but rather they score better than other simulations when combining all tests. For instance, their volume during the local LGM (panel b: ~16 kyr BP) is lower and less realistic than values of best-scoring simulations at the *local LGM extent* test (see Fig. 13d).**~~

Another potential source of ~~model-data~~ misfit could be biases in ~~our~~ input climate forcing causing either too low precipitation rates, or too high sea-surface temperatures (SST) across NO and NE Greenland. We do not expect biases in ~~input~~ air temperature forcing to have a meaningful impact at this stage, as despite ~~our~~ conservative ensemble parameter perturbations, we find no PDD-derived surface melt is produced until 12 kyr BP, ~~thus~~ several millennia after the ~~local LGM~~lLGM and initial deglaciation, due to mean annual and summer temperatures remaining ~~below~~ ≤0°C (Figs. 4, 5). We note that during HS1 cooling, input mean-annual SST drops to lower minimum values (-2 to -3 °C) offshore SE and SW Greenland than offshore NE Greenland (-1.5 to -2 °C) (~~Figs~~Fig. 6~~, 7~~), which may ~~highlight a possible~~reflect an overestimation of ~~our~~ sea-surface temperature forcing ~~(from Osman et al., 2021)~~ in NE Greenland during the ~~local LGM~~lLGM. This 0.5~~-~~ ~~-~~ 2°C drop in SST at around 18-17 kyr BP, which occurs in response to HS1, is a key driver of modelled GrIS expansion during the ~~local LGM~~lLGM, as it is associated with sharp reductions in GrIS-wide sub-shelf melt rates and thus basal mass loss ~~rates~~ (Fig. ~~12~~11). A small underestimation in HS1 sea-surface cooling offshore NE Greenland~~,~~ in the order of 1~~-~~ ~~-~~ 2°C ~~for instance,~~ may be enough to deter ~~the~~ modelled GrIS margins from advancing extensively. This hypothesis may ~~also~~ be reinforced by the general lack ~~of spatial coverage~~ of SST proxy records used in the data-assimilation scheme of Osman et al. (2021) north of 65°N, offshore Greenland coasts. Biases may also ~~be introduced by~~result from our interpolation scheme used for resampling from the nominal 1° horizontal resolution of the original data (Osman et al., 2021), equivalent to a ~20 x 27 km grid offshore NE Greenland, to our 5 x 5 km model grid. This highlights that our experiment ~~may be~~is limited by a lack of variation in SST input fields between ensemble simulations. A future experiment using an ensemble-varying parameter introducing spatial and temporal perturbations to the input ocean forcing may help test this hypothesis and possibly increase model-data fit.

Our simulations may also underestimate grounded ice extent in the NO and NE due to too low accumulation rates, largely controlled by our input precipitation forcing. Throughout these regions, iCESM-derived forcing suggests precipitation rates below 20 mm per month during HS1 (Fig. 6). ~~We note that although~~Although

iTRACE represents an improvement from the former CESM-derived transient global simulation of the last deglaciation (TRACE-21, Liu et al., 2009), it may still be subject to ~~CESM~~ biases that ~~can sometimes~~could misrepresent present-day and former precipitation rates over certain GrIS regions (van Kampenhout et al., 2020; Lofverstrom et al., 2020). In the case of NO and NE Greenland, input precipitation biases in the iTRACE simulation can also originate from global ice-sheet reconstruction used as forcing within iCESM (ICE-6G: Peltier et al., 2015), which ~~may~~ provide slightly incorrect geometries in these regions, impacting the modelled climate used here as input (*e.g.* Bouttes et al., 2023). More specifically, the ICE-6G reconstruction does not produce a GrIS that extends much beyond the present-day Greenland coastlines, which likely introduces regional biases in CESM simulations due to missing GrIS-atmosphere feedbacks ~~between the ice sheet and the earth system~~ (Bradley et al., 2024). Although we use an ensemble-varying parameter introducing precipitation perturbations of up to +200% (Table 1), ~~such an increase~~this is not space-dependent and may still be too low over NE Greenland. This may be ~~suggested~~shown by our lLGM best-fit simulations all displaying precipitation offset values that are clustered towards the upper parameter-range threshold, between 1.8 and 2.0 (Fig. ~~26~~24). Thus, better model-data scores at the *local-LGM extent* test could potentially be achieved with precipitation offset values ~~above +200%.~~> +200%. We compared our precipitation forcings with the paleoclimate data assimilation reconstruction of Badgeley et al. (2020), who extended ice-core derived climate reconstructions across Greenland using TRACE-21 (Liu et al., 2009), and also made comparisons with raw data from TraCE-21ka and Buizert et al. (2018)'s reconstruction. This analysis suggests notably lower precipitation rates in our iTRACE-derived climate forcing during HS1, and this in numerous regions across Greenland (Fig. 25b).

Alternatively, our ensemble may be too small to fully explore the full impacts of our climate correction parameters on grounded GrIS extent evolution. As a test, we conducted an additional simulation using default (mid-range) values for all ensemble-varying parameters excluding the precipitation scalar offset (Table 1), here set to 2.0 (+200% precipitation rate). This test simulation successfully produces an extensive HS1 advance of the grounded GrIS margin offshore NE Greenland, reaching a mid-shelf position. This modelled ~~local LGM~~lLGM advance is more extensive than any ~~of our~~ ensemble simulations, and suggests ~~a~~our 100 ~~simulation~~ member ensemble ~~is too small to~~did not explore the parameter-space region that ~~models~~produces this ~~preferable GrIS behaviour.~~specific model response. Therefore, although computationally unfeasible here, running a larger ensemble while keeping perturbed parameter ranges identical ~~to our setup~~ may ~~likely~~already produce simulations yielding a better model-data ~~fits~~fit in ice extent~~,~~ during the ~~local LGM.~~lLGM. Alternatively, future experiments running several ensemble waves (e.g. Lecavalier and Tarasov, 2025), with a first ensemble exclusively focused on more widely exploring different climate and ocean forcings with different perturbations schemes, may achieve more data-consistent GrIS LGM-to-present simulations.

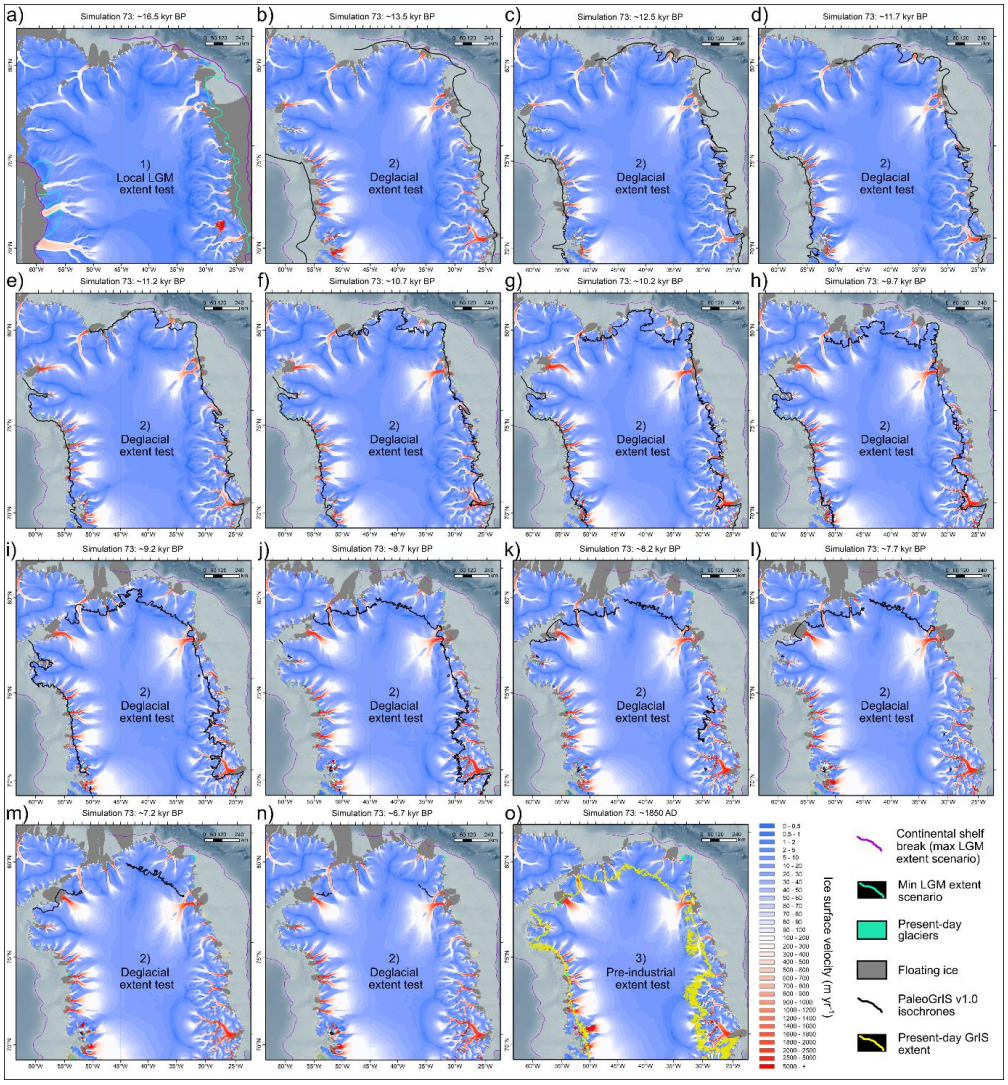
a)
Simulation 73: ~16.5 kyr BP
1)
Local LGM
extent test
b)
Simulation 73: ~13.5 kyr BP
2)
Deglacial
extent test
c)
Simulation 73: ~12.5 kyr BP
2)
Deglacial
extent test
d)
Simulation 73: ~11.7 kyr BP
2)
Deglacial
extent test
e)
Simulation 73: ~11.2 kyr BP
2)
Deglacial
extent test
f)
Simulation 73: ~10.7 kyr BP
2)
Deglacial
extent test
g)
Simulation 73: ~10.2 kyr BP
2)
Deglacial
extent test
h)
Simulation 73: ~9.7 kyr BP
2)
Deglacial
extent test
i)
Simulation 73: ~9.2 kyr BP
2)
Deglacial
extent test
j)
Simulation 73: ~8.7 kyr BP
2)
Deglacial
extent test
k)
Simulation 73: ~8.2 kyr BP
2)
Deglacial
extent test
l)
Simulation 73: ~7.7 kyr BP
2)
Deglacial
extent test
m)
Simulation 73: ~7.2 kyr BP
2)
Deglacial
extent test
n)
Simulation 73: ~6.7 kyr BP
2)
Deglacial
extent test
o)
Simulation 73: ~1850 AD
3)
Pre-industrial
extent test
Ice surface velocity (m yr-1)
Continental shelf break (max LGM extent scenario)
Min LGM extent scenario
Present-day glaciers
Floating ice
PaleoGrIS v1.0 isochrones
Present-day GrIS extent

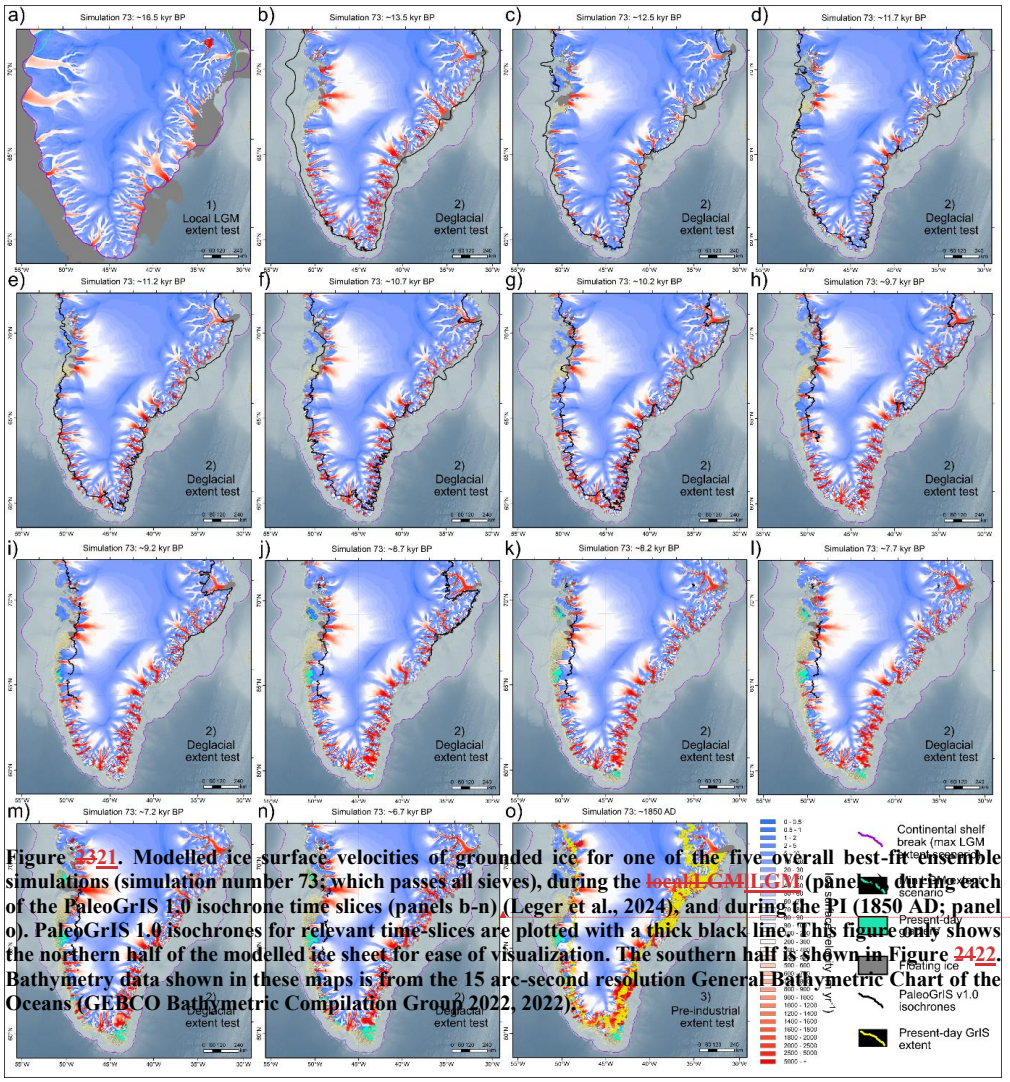

Figure 2321. Modelled ice surface velocities of grounded ice for one of the five overall best-fit ensemble simulations (simulation number 73; which passes all sieves), during the ~~local~~LGM~~LGM~~ (panel a), during each of the PaleoGrIS 1.0 isochrone time slices (panels b-n) (Leger et al., 2024), and during the PI (1850 AD; panel o). PaleoGrIS 1.0 isochrones for relevant time-slices are plotted with a thick black line. This figure only shows the northern half of the modelled ice sheet for ease of visualization. The southern half is shown in Figure ~~2422~~. Bathymetry data shown in these maps is from the 15 arc-second resolution General Bathymetric Chart of the Oceans (GEBCO Bathymetric Compilation Group 2022, 2022).

Formatted: Font: Bold

Figure ~~24~~22. Modelled ice surface velocities of grounded ice for one of the five overall best-fit ensemble simulations (simulation number 73; which passes all sieves), during the ~~local LGM~~lLGM (panel a), during each of the PaleoGrIS 1.0 isochrone time slices (panels b-n) (Leger et al., 2024), and during the PI era (1850 AD; panel o). PaleoGrIS 1.0 isochrones for relevant time-slices are plotted with a thick black line. This figure only shows the southern half of the ice sheet for ease of visualization. The northern half is shown in Figure ~~25~~21. Bathymetry data shown in these maps is from the 15 arc-second resolution General Bathymetric Chart of the Oceans (GEBCO Bathymetric Compilation Group 2022, 2022).

Formatted: Font: Bold

5.2 Underestimated deglacial retreat

We note that the CE and NE GrIS regions, where ~~the greatest~~ model-data misfits with PaleoGrIS 1.0 are ~~found~~largest (Figs. ~~18, 23, 24), also~~17, 21, 22), present the highest concentration of high elevations and ~~steep topographies~~relief (1500 - 3000 m a.s.l~~.) in Greenland (Morlighem et al., 2017). We hypothesise that coarse model resolution may be a factor contributing to the higher relative ice extent misfits observed in these regions during the Late Glacial and Holocene deglaciation. Indeed, a large portion of the Eastern Greenland~~

coast features the steepest and highest mountain ranges of the continent, stretching from 67 °N (Schweizerland Alps) to 77.9°N (Halle range), and dissected by a complex network of overdeepened valleys. This topographic setting leads to the highest concentration of deglaciated and relatively long (>100 km), narrow (<15 km), deep.), steep topographies, and steep-sided fjords in Greenland ((Swift et al., 2008); Morlighem et al., 2017). With. These major fjord systems include the Kangertittivaq (Scoresby Sund), Kangerluk Kong Oscar, Kangerluk Kejser Franz Joseph (Fig. 27), Gael Hamke Bay, Shannon Bay and Dove Bay (76°N) complexes. According to geochronological reconstructions, the retreat of GrIS outlet glaciers from the outer mouths of these CE and NE Greenland fjords to near their present day positions occurred mainly between ~12 and ~8.5 kyr BP (*e.g.* Marienfeld, 1990; Bennike et al., 1999; Håkansson et al., 2007; Leger et al., 2024). However, the majority of this retreat is missing in our ensemble simulations. A 5 x 5 km horizontal resolution may not be fine enough to capture the complexity of GrIS margin retreat into the complex network of over deepened fjords and steep valleys of these regions. By drawing topographic elevation profiles across one the region's main fjords 5 km resolution, we find that even towards one of the widest (~20 km) fjords in NE Greenland (Kangerluk Kejser Franz Joseph, 73.2°N; 23.2°W), we find that even for one of the widest NE Greenland fjords (~ 20 km), formerly acting as the main topographic conduit for the Waltershausen Glacier, the topography is heavily flattened at 5 km resolution ((Supplementary Fig. 27). Across the profile, summit 13). Summit elevations of fjord side mountains are underestimated by 30 - 50%, and average slope along the a cross-fjord transect is 40% and 35% lower than for if using 150 m and 1 km resolution grids, respectively (Fig. 27). Thus, at 5 x 5 km resolution, the modelled GrIS is less topographically constrained than it should be during deglacial margin retreat and thinning (Fig. 27). A better resolved topography (*e.g.* see Supplementary Fig. 13). In such rough topographies, a finer model resolution (*e.g.* 1 x 1 km or lower) would likely lead to both higher ice flux rates within narrow valleys, due to higher summits, steeper bed slopes, and greater ice flow convergence, but also (as shown by Leger et al., 2025), and to deeper fjords enabling more water ingress as modelled tidewater glaciers retreat. Both mechanisms, unlikely to be captured at 5 x 5 km, would together likely enhance modelled GrIS thinning and retreat rates during deglaciation. This is supported by the Late Glacial and early to mid Holocene in these regions. In such steep terrain, higher resolution modelling may lead to better model-data fit for a given parameter configuration (Leger et al., 2025). This was in part shown by Aschwanden et al. (2016) who, using PISM, found that better matched observed flow velocities of main present-day GrIS outlet glaciers (*e.g.* Nuussuup Sermia, Sermeq Kujalleq) were better matched using resolutions of 600 and 1500 m, relative to 3600 and 4500 m, with the latter causing underestimations of maximum flow velocities to be underestimated by factors of 4 - 7. Therefore, while the inability to resolve fine topographies generates biases across the domain, we argue its negative impact on we hypothesise that coarse model resolution may contribute to our higher relative ice-extent model-data fit is likely to be greater in CE and NE Greenland, relative to other regions, due to the greater concentration of steep and high-relief topographies. misfits observed in the CE and NE regions during the last deglaciation.

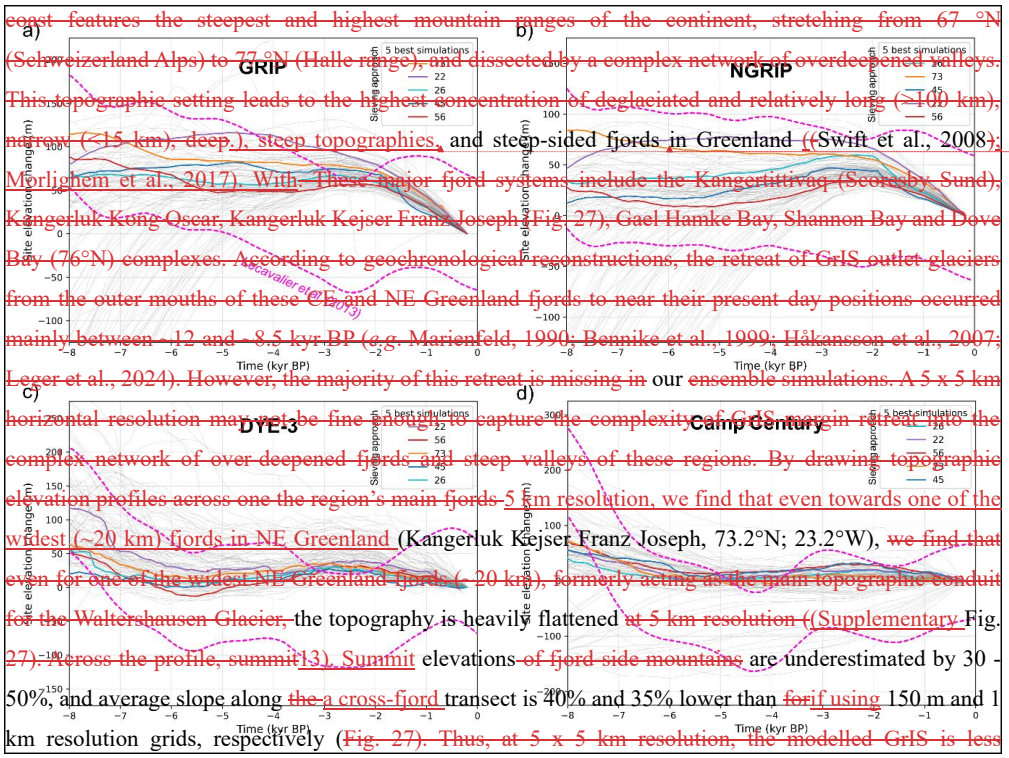

Formatted: Font: +Headings CS (Times New Roman)

Formatted: Font: +Headings CS (Times New Roman)

Formatted: Font color: Auto

Formatted: Font: Times New Roman, Font color: Black

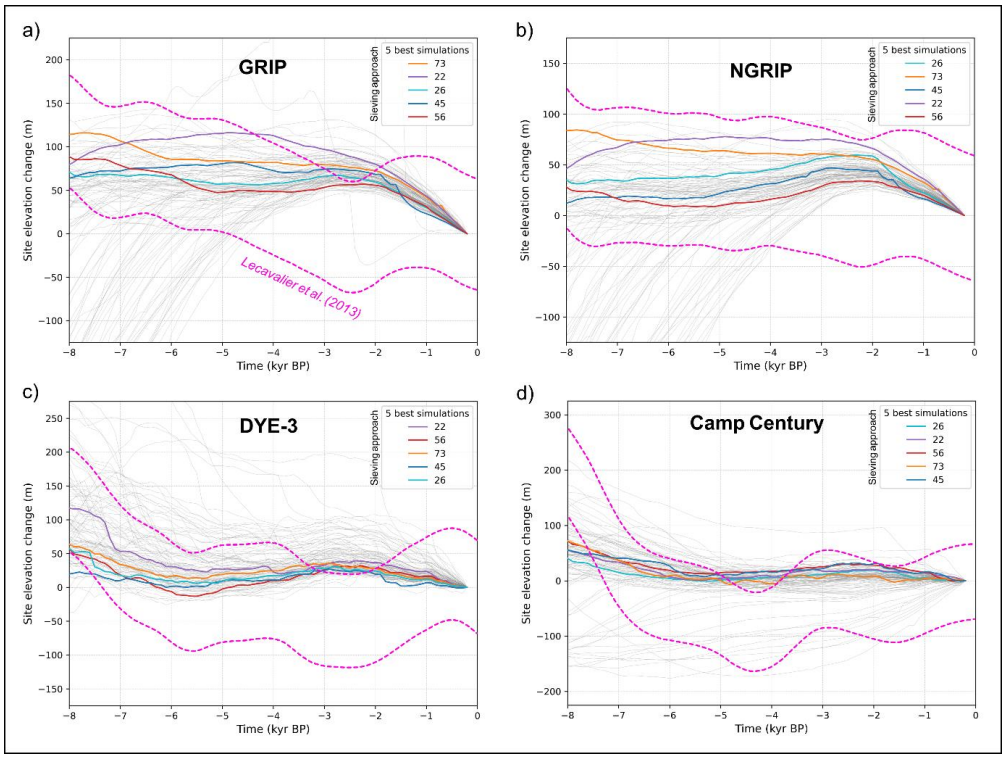
a)
GRIP
5 best simulations
Sieving approach
73
22
26
45
56
Lecavalier et al. (2013)
Site elevation change (m)
Time (kyr BP)
b)
NGRIP
5 best simulations
Sieving approach
26
73
45
22
56
Site elevation change (m)
Time (kyr BP)
c)
DYE-3
5 best simulations
Sieving approach
22
56
73
45
26
Site elevation change (m)
Time (kyr BP)
d)
Camp Century
5 best simulations
Sieving approach
26
22
56
73
45
Site elevation change (m)
Time (kyr BP)

Figure ~~25~~23. Comparison between ice elevation change modelled by our five overall best-fit simulations (which pass all sieves; thicker coloured lines) and the 1σ uncertainty band of the Holocene thinning curves (dashed pink lines), derived from ice core $\delta^{18}O$ records. Holocene thinning curves were produced by Lecavalier et al. (2013), improving from Vinther et al. (2009) following an elevation correction for thickness changes at the Agassiz and Renland ice caps. Data from all other ensemble simulations from this study are shown with thin, light grey lines.

Formatted: Font: 11 pt, Bold, Not Italic, Ligatures: None

Formatted: Space After: 8 pt, Line spacing: Multiple 1,15 li

Formatted: Font: 11 pt, Not Italic, Ligatures: None

Formatted: Font: Bold

Formatted: Font: Bold

Larger model-data misfits in the magnitude and rates of GrIS retreat during the Late-Glacial and early-to-mid Holocene in NO, NE, and CE Greenland ~~could~~are also ~~be~~likely associated with biases in our input climate forcing, including possible underestimations of sea-surface and atmospheric warming (~14 - 6 kyr BP). As mentioned above, biases in iTRACE-derived climate are possible, especially towards the margins of the former GrIS. For instance, an overestimation of the ice thickness and extent reconstruction used as forcing within iCESM (ICE-6G: Peltier et al., 2015) during the last deglaciation in NO, NE, and CE Greenland, would lead to unrealistically high albedo feedbacks impeding the atmospheric warming required to model appropriate GrIS thinning and retreat rates. Our experiment features an ensemble-varying temperature offset parameter (Table 1) with maximum space-independent warming of up to +3.5 °C, along with ensemble-varying snow and ice PDD melt factors that can reach 5 and 12 mm *w.e.* d^{-1} $°C^{-1}$, respectively. However, ~~if significant~~with important input climate biases ~~exist~~ in the regions of concern, these perturbations may still underestimate the resulting surface melt during deglaciation~~.~~ (see Fig. 25a,c). We note that a cold temperature bias during the Late-Glacial and early-to-mid Holocene is not supported by comparison against the climate reconstruction (and its associated uncertainty range) of Badgeley et al. (2020), which instead suggests that our forcing produce relatively warm mean annual temperature anomalies towards the GrIS summit and NO, NE, and CE GrIS regions, between 15 and 5 kyr BP (Fig. 25c). On the other hand, this comparison reveals that our iTRACE and iCESM - derived climate forcing results in significantly higher (up

to ~100%) precipitation rates during the entire Holocene towards the GrIS summit and its vicinity, than is obtained in ice-core-data-informed reconstructions from Badgeley et al. (2020) and Buizert et al. (2018) (Fig. 25d). Although the HTM has been shown to likely be associated with higher-than-present precipitations (e.g. Downs et al., 2020), and although our experiment features an ensemble-varying precipitation offset scheme with possible reductions down to 20% input precipitations, this potential positive bias may be responsible for too high Holocene precipitation in many of our ensemble simulations, thus impeding GrIS retreat in certain regions and causing ice extent overestimations during the modelled deglaciation but also during the PI (Fig. 25d). Moreover, it is worth noting that CESM has been shown to also overestimate (by <20%) present-day snowfall precipitations over the GrIS relative to observations which my also explain our overestimations in ice extent during the PI (e.g. Lenaerts et al., 2020; Fig. 5 therein).

Alternatively, our ensemble (n=100) may be too small to explore the full impact of these temperature and PDD melt parameter perturbations on modelled GrIS retreat during deglaciation. Furthermore, our SMB parameterisation, based on on a simple PDD scheme (Calov and Greve, 2005), does not capture certain ablation mechanisms such as sublimation and wind-driven snow layer erosion, nor does it fully capture the elevation feedback between the modelled ice-sheet surface and climate forcing. These missing mechanisms may be important to model deglacial GrIS thinning and retreat accurately at high latitudes (>75°N), where mean summer air temperatures during the HTM remained close to or below 0°C (at least in our forcing data) (Fig. 5) (Plach et al., 2019). Alternatively, the underestimated modelled GrIS retreat in NO, NE, and CE Greenland could be associated with a lower-than-needed ocean temperature increase during the last deglaciation (Osman et al., 2021; Figs. 6~~-8~~, 7) offshore the present-day GrIS. ~~Importantly, we also~~We note that our ice-ocean interaction model does not consider multiple ocean layers, which are important when poorly mixed sub-surface layers of higher temperatures increase sub-shelf melt at depth and towards the grounding line (Lloyd et al., 2023). It also does not consider a seasonal cycle of ocean water temperature change as forcing, which may be important to model the necessary magnitude of deglacial sub-shelf melt in these regions. -We also note that, for instance, TrACE-21ka-derived shelf-depth ocean forcing used in Tabone et al. (2024; Fig. S3 therein) reaches above 0°C (up to 2°C) towards the NE Greenland outer shelf, between 13 and 8 kyr BP, whilst our SST forcing does not produce values above -1°C in that region and timeframe.

Today, up to ~16% of the GrIS is thought to be drained by NEGIS (Hvidberg et al., 2020), a singular ice stream that can prove challenging to model accurately (Smith-Johnsen et al., 2020). In our best-fit ~~ensemble~~ simulations, some ice streaming is modelled towards ~~and upflow from~~ both Nioghalvfjerdsbrae (79N glacier) and Zachariae Isstrom glaciers, throughout the full simulation timespan (*e.g.* Figs. ~~17, 23~~16, 21). However, a comparison between our best-fit simulations at the *PI extent* test and ~~observed~~present-day GrIS surface velocities (Joughin et al., 2018b) reveals that our model underestimates GrIS flow speeds towards NEGIS (Supplementary Fig. 6). Our simulations do not capture its singular shape featuring a relatively narrow (<100 km) and long (>500 km) band of relatively high (> 50 m yr^{-1}) surface velocities nearly reaching the ice-

sheet's central East/West divide (Supplementary Fig. 6). Although uncertainties remain regarding the timing of last NEGIS activation into its present-day configuration, recent evidence suggests it was active ~~during much of the Holocene (Franke et al., 2022).~~in its present form ~2000 years ago (Franke et al., 2022; Jansen et al., 2024), whilst the modelling study of Tabone et al. (2024) suggests that NEGIS may be up to 8000 years old. Due to its significant impact on ice flux of the entire NE GrIS region, modelling an accurate NEGIS configuration throughout the Late-Glacial and Holocene periods would produce higher regional-mean discharge and thinning rates. Over millennial timescales, this may help model greater and more data-consistent GrIS margin retreat rates during deglaciation. ~~Therefore, it is possible~~This is supported by the results of Tabone et al. (2024) which suggest that an early-Holocene activation of a present-like NEGIS, achieved through highly targeted parameterization of low basal friction along the ice stream, is crucial to drive deglacial ice thinning over the central and northern GrIS. Therefore, it is likely that not fully reproducing NEGIS may contribute to increasing model-data misfits in NE Greenland relative to other GrIS regions, where ice streams are generally less challenging to model accurately.

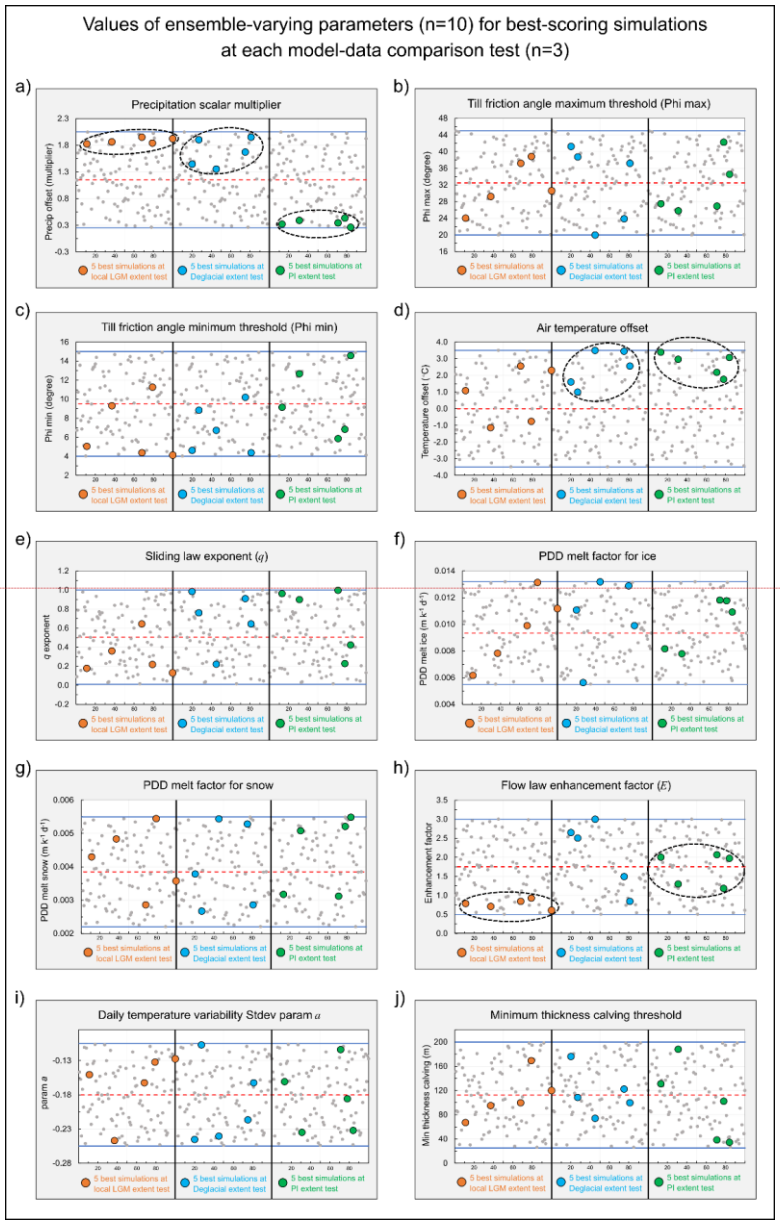

Formatted: Font: 11 pt, Ligatures: None

Formatted: Justified, Space After: 8 pt, Line spacing: Multiple 1,15 li

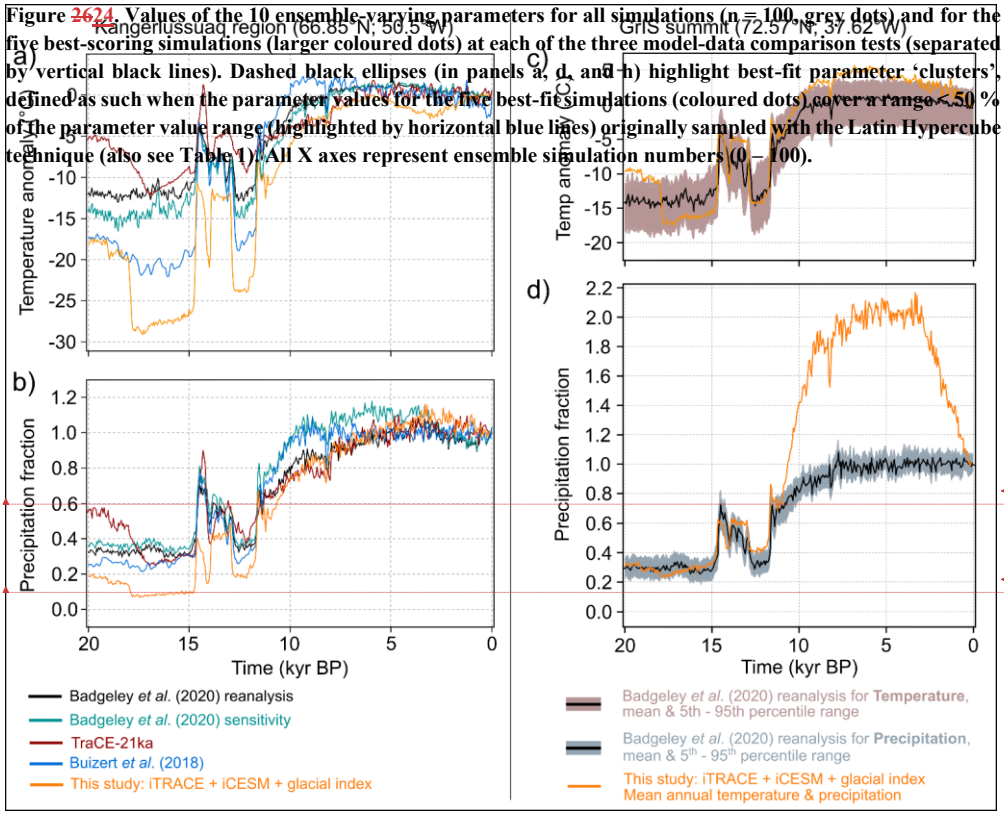

Figure ~~2624~~. Values of the 10 ensemble-varying parameters for all simulations (n = 100, grey dots) and for the five best-scoring simulations (larger coloured dots) at each of the three model-data comparison tests (separated by vertical black lines). Dashed black ellipses (in panels a, d, and h) highlight best-fit parameter 'clusters', defined as such when the parameter values for the five best-fit simulations (coloured dots) cover a range < 50 % of the parameter value range (highlighted by horizontal blue lines) originally sampled with the Latin Hypercube technique (also see Table 1). All X axes represent ensemble simulation numbers (0 – 100).

Formatted: Font: 12 pt, Ligatures: Standard + Contextual

Formatted: Line spacing: Multiple 1,08 li

Formatted: Font: +Headings CS (Times New Roman), 12 pt, Ligatures: Standard + Contextual

Formatted: Space After: 8 pt, Add space between paragraphs of the same style, Line spacing: Multiple 1,08 li

Formatted: Font: 12 pt, Ligatures: Standard + Contextual

Formatted: Left, Line spacing: Multiple 1,08 li

Figure

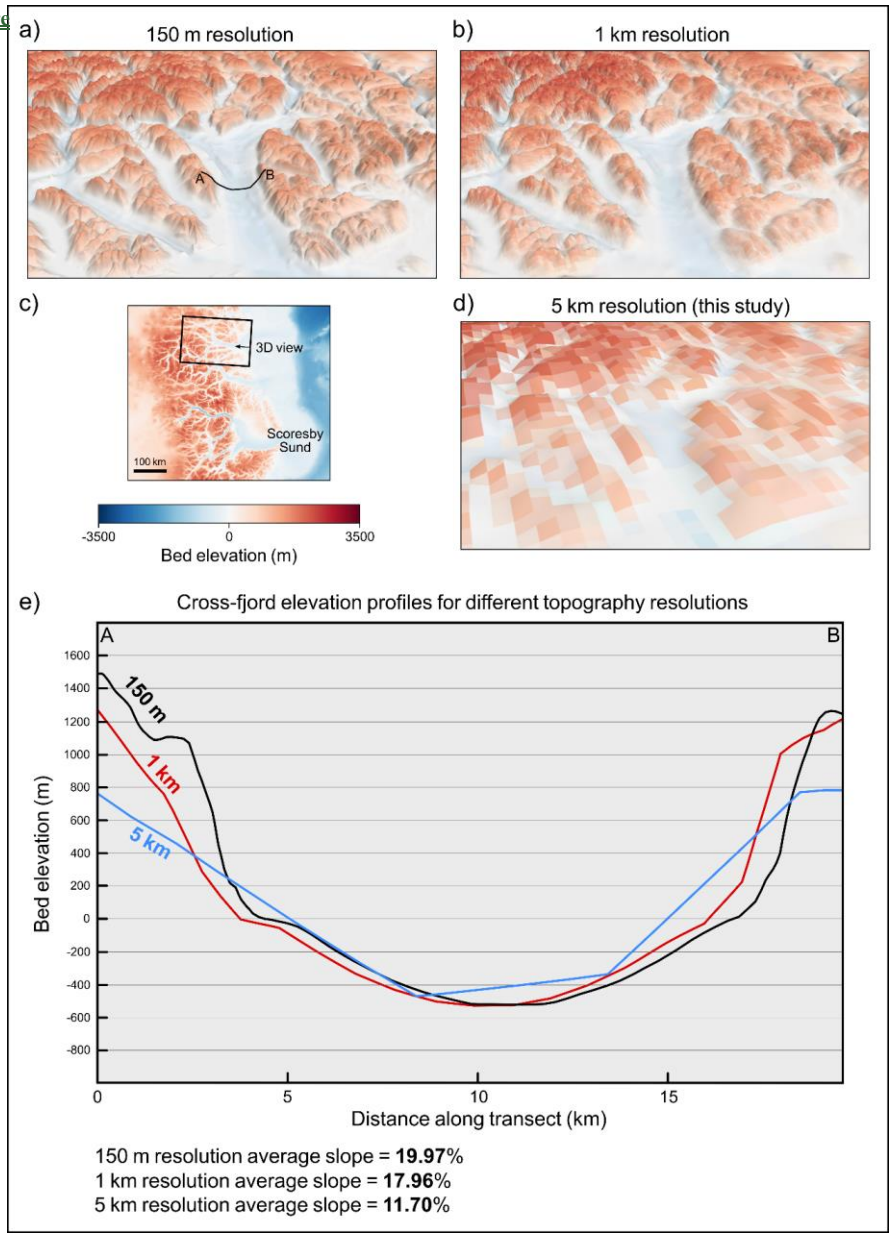

~~Figure 27. Three-dimensional views (panels a, b, and d) of bed topography (BedMachine v4 merged with GEBCO data) and cross-elevation profiles (panel c) along a transect drawn across the Kangerluk-Kejser Franz Joseph fjord (73.2°N; 23.2°W; black line in panel a). Elevation profiles are shown for three different grid resolutions (5 km, 1 km, and 150 m). While average slopes over such a terrain decreases by 10% between 150 m and 1 km resolution grids, it decreases by around 40% between 150 m and 5 km resolution grid, 5 km being the model resolution of this study. For more details regarding the bed topography used in this modelling study, the reader is referred to Figure 1 and its caption.~~ 25. Comparisons between our input mean annual temperature and precipitation forcings (orange time series) with the climate reconstructions of Badgeley et al. (2020), Buizert et al. (2018), and raw TraCE-21ka data (Liu et al., 2009). More specifically, these panels present the same data

as shown in Figures 8 and 13 in Badgeley et al. (2020). Note that precipitation fractions and temperature anomalies are here expressed with reference to the mean of 1850–2000 AD for all datasets except this study's input climate data (orange), instead expressed with reference to the mean of 1750-1850 AD, caused by our most recent iCESM simulation being 1850 AD.

Formatted: Font: +Headings CS (Times New Roman), 12 pt

Formatted: Left, Line spacing: Multiple 1,08 li

Formatted: Font: Times New Roman, 11 pt

Formatted: Justified, Space After: 8 pt, Line spacing: Multiple 1,15 li

6 Conclusions

In this study, we conducted a perturbed-parameter ensemble of 100 PISM simulations of the entire Greenland-Ice-Sheet evolution from 24,000 years ago to the pre-industrial era (1850 AD) at a spatial resolution of 5 x 5 km. Each ~~model~~ simulation was quantitatively scored against ice-sheet-wide empirical data of former grounded ice extent and its timing. We here summarize the main ~~results and~~ findings from this model-data comparison experiment.

-The maximum grounded Greenland Ice Sheet extent, *i.e.* the ~~local LGM~~lLGM, likely occurred between 17.5 and 16 kyr BP, during Heinrich Stadial 1. At that time, the grounded ice sheet reached an area of between 2.9 and 3.1 million km^2. During full glaciation, grounded ice likely reached the continental shelf break along the entire Western, Southern, and Southeastern Greenland coasts.

-Our results suggest that between the ~~local LGM~~lLGM and today, the global mean sea level rise contribution of the Greenland Ice Sheet is between 6 and 7.5 meters, a number ~~substantially~~ higher than previous estimates (see section 3.1.2.). During the ~~local LGM~~lLGM, the ice sheet was not necessarily thicker (nor higher-elevated) than today at its summits, towards the GISP2, GRIP, and NGRIP ice core ~~locations~~sites. Contrastingly, in Southern and Northwestern Greenland (DYE-3 and NEEM ice cores), the ice sheet was likely up to ~1 km thicker than today, with an ice surface up to ~500 m higher in elevation, thus causing ice divide migrations between full glacial and interglacial periods. These migrations may have important implications for the chronological interpretation of the DYE-3 ice core. During maximum extent, the ice sheet was also flowing faster and was able to discharge up to 5.1 times more ice than today, thus contributing substantially more iceberg and freshwater delivery to the north Atlantic basin than today.

-The Greenland Ice Sheet likely retreated rapidly and extensively during the late Heinrich-stadial 1 and Bølling–Allerød warming events, between 16 and 14 kyr BP. During that time, the grounded ice sheet lost the majority of its continental shelf cover. This rapid demise was ~~predominantly~~likely mainly caused by ocean warming and increased sub-shelf melt, while air temperatures likely remained too cold to generate significant surface melt. During this phase of rapid retreat, the ice sheet may have experienced up to 7 times greater mass loss rates than are currently estimated for the present-day.

-At the Greenland Ice Sheet scale, margin stabilization and readvances during the Younger Dryas cooling event were likely limited and of low magnitude, as opposed to ~~periphery~~peripheral glaciers which demonstrated a more dynamic response. We hypothesise this was caused by strong ice-sheet inertia and geometrical/thermal ice memory feedbacks associated with the potent deglaciation experienced just prior, during Bølling–Allerød warming.

-The Greenland Ice Sheet likely reached a minimum in ice extent between 6 and 5 kyr BP, and thus lagged the cessation of Holocene Thermal Maximum warming by a few centuries, and up to a millennium, prior to experiencing late-Holocene and Neoglacial readvance. During the mid-Holocene, our simulations produce up to ~100 km of margin retreat behind the present-day Greenland Ice Sheet, but only south of 68 °N.

-While best-fit simulations ~~present a~~are in reasonable agreement with the PaleoGrIS 1.0 grounded ice-extent reconstruction in Northwestern, Central-western, Southwestern, and Southeastern Greenland regions, we find larger model-data misfits remain in the Northern, Northeastern, and Central-eastern regions. There, ~~the~~ magnitudes and rates of modelled LGM advance and deglacial retreat are both underestimated, when compared to empirical data. ~~Our results suggest~~This suggests these regions are significantly more challenging to model accurately. We hypothesise these misfits are possibly related to multiple causes including biases from: surface mass balance and ice-ocean interaction parameterisations, input climate and ocean forcings, model resolution due to rougher local topographies, model initialisation, and the difficulty to reproduce the Northeast Greenland Ice Stream.

-No single ensemble simulation could achieve a better relative score at all three chronologically-distinct model-data comparison tests. Instead, we find different simulations~~,~~ and ~~thus different~~ parameter configurations~~,~~ are needed to better match empirical data in certain Greenland regions or during certain millennial-scale events (*e.g.* the early-Holocene). Thus, producing a physically-sound 3D model simulation that is data-consistent across all Greenland regions since the last glaciation, which would enable to accurately capture the ice-sheet's memory from this key period of environmental change, is still a major challenge. To achieve this, future work may need to employ larger ensembles, more appropriate parameterisations of

boundary conditions, data assimilation to reduce bias accumulations, higher resolution modelling, and more time- and space-dependent parameter and paleoclimate perturbations.

Code and data availability.

The open-access source code for PISM can be accessed and downloaded from https://github.com/pism/pism . The code specific to the PISM version used in this study, version 2.0.5, can be accessed from https://doi.org/10.5281/zenodo.7199611 .

All input data formatted for PISM (NetCDF file formats), along with shell scripts required to run each ensemble simulation (n=100), which together enable to reproduce the simulations presented in this study, as well as model output data and videos for the five overall best-fit simulations (which pass all sieves), are available for download from the following Zenodo repository; ~~https://doi.org/10.5281/zenodo.15149359~~ https://doi.org/10.5281/zenodo.15222968

Formatted: Font: +Body (Calibri), 11 pt, Ligatures: None

Supplement.

The supplement related to this article is available online at: ……..

Author contributions.

JCE and TPML conceived and guided the study. Input from SLB and CDC contributed to the design of the modelling investigation. TPML prepared the input data products and conducted the modelling on High Performance Computer clusters with technical help from JCE and REA. SLB conducted the glacial-isostatic-adjustment model and earth model simulations required to produce the non-local relative-sea-level forcing input data. JCE conducted the installation of PISM on the University of Sheffield High Performance Computing clusters. JZ provided access to- and support in interpreting- the iCESM data used as input climate forcing, with technical help from SLB. TPML conducted the post-modelling data processing and quantitative model-data comparisons, with feedback from CDC and JCE, and TPML conducted all subsequent

quantitative analyses. TPML wrote the manuscript, with feedback from JCE and SLB primarily, and other co-authors for subsequent drafts. TPML produced all maps, figures, and tables.

Competing interests.

The contact author has declared that none of the authors have any competing interests.

Acknowledgements.

We wish to thank all individuals who contributed support, ideas, and insightful discussions to this investigation including ~~Joshua Cuzzone~~Guillaume Jouvet, Jason Briner, and members of the PALGLAC team including Christiaan R. Diemont, Anna L. C. Hughes, Stephen J. Livingstone, Remy L. J. Veness, Frances E. G. Butcher, Helen E. Dulfer, and Benjamin M. Boyes. We thank the University of Sheffield Research and Innovation team in IT Services for their work and vital support in using the University High Performance Computing clusters for all computation. Finally, we are grateful to Dr. Joshua Cuzzone and an anonymous reviewer for accepting to review this manuscript which greatly improved its quality.

Financial support.

This study benefited from the PALGLAC team of researchers with funding from the European Research Council (ERC) under the European Union's Horizon 2020 research and innovation programme to Christopher D. Clark (Grant Agreement No. 787263), and which employed Tancrède P. M. Leger, Sarah L. Bradley, and Rosie E. Archer. The CESM project is supported primarily by the U.S. National Science Foundation (NSF). This material is based upon work supported by the NSF National Center for Atmospheric Research, which is a major facility sponsored by the NSF under Cooperative Agreement No. 1852977. Tancrède P. M. Leger has also received support from the Swiss National Science Foundation, through a grant (RECONCILE: project number: 213077) awarded to Guillaume Jouvet. Jeremy C. Ely has received support from a NERC independent fellowship award (grant no. NE/R014574/1).

Formatted: Font: Times New Roman, 12 pt, Ligatures: Standard + Contextual

Formatted: Font: Bold

Formatted: Justified, Space After: 0 pt

Formatted: Justified

Formatted: Font: Times New Roman, 12 pt

Formatted: Line spacing: 1,5 lines

Formatted: Font: 14 pt, Not Bold

References.

Albrecht, T. and Levermann, A.: Spontaneous ice-front retreat caused by disintegration of adjacent ice shelf in Antarctica, Earth Planet Sci Lett, 393, 26–30, https://doi.org/10.1016/j.epsl.2014.02.034, 2014.

Albrecht, T., Winkelmann, R., and Levermann, A.: Glacial-cycle simulations of the Antarctic Ice Sheet with the Parallel Ice Sheet Model (PISM)-Part 1: Boundary conditions and climatic forcing, Cryosphere, 14, 599–632, https://doi.org/10.5194/tc-14-599-2020, 2020.

Arndt, J. E., Jokat, W., and Dorschel, B.: The last glaciation and deglaciation of the Northeast Greenland continental shelf revealed by hydro-acoustic data, Quat Sci Rev, 160, 45–56, https://doi.org/10.1016/j.quascirev.2017.01.018, 2017.

Arnold, K. C. and MacKay, D. K.: Different methods of calculating mean daily temperatures, their effects on degree-day totals in the high Arctic and their significance to glaciology, Geogr Bull, 21, 123–129, 1964.

Aschwanden, A., Bueler, E., Khroulev, C., and Blatter, H.: An enthalpy formulation for glaciers and ice sheets, Journal of Glaciology, 58, 441–457, https://doi.org/10.3189/2012JoG11J088, 2012.

Aschwanden, A., Aðalgeirsdóttir, G., and Khroulev, C.: Hindcasting to measure ice sheet model sensitivity to initial states, Cryosphere, 7, 1083–1093, https://doi.org/10.5194/tc-7-1083-2013, 2013.

Aschwanden, A., Fahnestock, M. A., and Truffer, M.: Complex Greenland outlet glacier flow captured, Nat Commun, 7, 10524, https://doi.org/10.1038/ncomms10524, 2016.

Aschwanden, A., Fahnestock, M. A., Truffer, M., Brinkerhoff, D. J., Hock, R., Khroulev, C., Mottram, R., and Abbas Khan, S.: Contribution of the Greenland Ice Sheet to sea level over the next millennium, Sci Adv, 5, https://doi.org/10.1126/sciadv.aav9396, 2019.

Badgeley, J. A., Steig, E. J., Hakim, G. J., and Fudge, T. J.: Greenland temperature and precipitation over the last 20 000 years using data assimilation, Climate of the Past, 16, 1325–1346, https://doi.org/10.5194/cp-16-1325-2020, 2020.

Bennett, M. R.: Ice streams as the arteries of an ice sheet: their mechanics, stability and significance, Earth Sci Rev, 61, 309–339, https://doi.org/10.1016/S0012-8252(02)00130-7, 2003.

Bennike, O., Björck, S., Böcher, J., Hansen, L., Heinemeier, J., and Wohlfarth, B.: Early Holocene plant and animal remains from North-east Greenland, J Biogeogr, 26, 667–677, https://doi.org/10.1046/j.1365-2699.1999.t01-1-00315.x, 1999.

Berger, AndréL.: Long-Term Variations of Daily Insolation and Quaternary Climatic Changes, J Atmos Sci, 35, 2362–2367, https://doi.org/10.1175/1520-0469(1978)035<2362:LTVODI>2.0.CO;2, 1978.

Biette, M., Jomelli, V., Chenet, M., Braucher, R., Rinterknecht, V., and Lane, T.: Mountain glacier fluctuations during the Lateglacial and Holocene on Clavering Island (northeastern Greenland) from 10Be moraine dating, Boreas, 49, 873–885, https://doi.org/10.1111/bor.12460, 2020.

Born, A. and Robinson, A.: Modeling the Greenland englacial stratigraphy, Cryosphere, 15, 4539–4556, https://doi.org/10.5194/tc-15-4539-2021, 2021.

Bouttes, N., Lhardy, F., Quiquet, A., Paillard, D., Goosse, H., and Roche, D. M.: Deglacial climate changes as forced by different ice sheet reconstructions, Climate of the Past, 19, 1027–1042, https://doi.org/10.5194/cp-19-1027-2023, 2023.

Bradley, S. L., Reerink, T. J., Van De Wal, R. S. W., and Helsen, M. M.: Simulation of the Greenland Ice Sheet over two glacial-interglacial cycles: investigating a sub-ice-shelf melt parameterization and relative sea level forcing in an ice-sheet-ice-shelf model, Climate of the Past, 14, 619–635, https://doi.org/10.5194/cp-14-619-2018, 2018.

Bradley, S. L., Sellevold, R., Petrini, M., Vizcaino, M., Georgiou, S., Zhu, J., Otto-Bliesner, B. L., and Lofverstrom, M.: Surface mass balance and climate of the Last Glacial Maximum Northern Hemisphere ice sheets: simulations with CESM2.1, Climate of the Past, 20, 211–235, https://doi.org/10.5194/cp-20-211-2024, 2024.

Brady, E., Stevenson, S., Bailey, D., Liu, Z., Noone, D., Nusbaumer, J., Otto-Bliesner, B. L., Tabor, C., Tomas, R., Wong, T., Zhang, J., and Zhu, J.: The Connected Isotopic Water Cycle in the Community Earth System Model Version 1, J Adv Model Earth Syst, 11, 2547–2566, https://doi.org/10.1029/2019MS001663, 2019.

Braithwaite, R. J.: Positive degree-day factors for ablation on the Greenland ice sheet studied by energy-balance modelling, Journal of Glaciology, 41, 153–160, https://doi.org/10.1017/S0022143000017846, 1995.

Briner, J., Schaefer, J., Young, N., Keisling, B., Anandakrishnan, S., Kuhl, T., Boeckmann, G., MacGregor, J., Deconto, R., Morlighem, M., Winckler, G., and Walcott, C.: Introducing GreenDrill: Retrieving sub-glacial bedrock cores in North Greenland to test ice sheet response to interglacial warmth (and supporting your research?), in: AGU Fall Meeting Abstracts, C31A-07, 2021.

Briner, J. P., Kaufman, D. S., Bennike, O., and Kosnik, M. A.: Amino acid ratios in reworked marine bivalve shells constrain Greenland Ice Sheet history during the Holocene, Geology, 42, 75–78, https://doi.org/10.1130/G34843.1, 2014.

Briner, J. P., Cuzzone, J. K., Badgeley, J. A., Young, N. E., Steig, E. J., Morlighem, M., Schlegel, N. J., Hakim, G. J., Schaefer, J. M., Johnson, J. V., Lesnek, A. J., Thomas, E. K., Allan, E., Bennike, O., Cluett, A. A., Csatho, B., de Vernal, A., Downs, J., Larour, E., and Nowicki, S.: Rate of mass loss from the Greenland Ice Sheet will exceed Holocene values this century, Nature, 586, 70–74, https://doi.org/10.1038/s41586-020-2742-6, 2020.

Bueler, E. and Brown, J.: Shallow shelf approximation as a “sliding law” in a thermomechanically coupled ice sheet model, J Geophys Res Earth Surf, 114, 1–21, https://doi.org/10.1029/2008JF001179, 2009.

Bueler, E., Lingle, C. S., and Brown, J.: Fast computation of a viscoelastic deformable Earth model for ice-sheet simulations, Ann Glaciol, 46, 97–105, https://doi.org/10.3189/172756407782871567, 2007.

Formatted: Font: Times New Roman, 12 pt, Ligatures: Standard + Contextual

Buizert, C., Gkinis, V., Severinghaus, J. P., He, F., Lecavalier, B. S., Kindler, P., Leuenberger, M., Carlson, A. E., Vinther, B., Masson-Delmotte, V., White, J. W. C., Liu, Z., Otto-Bliesner, B., and Brook, E. J.: Greenland temperature response to climate forcing during the last deglaciation, Science (1979), 345, 1177–1180, https://doi.org/10.1126/science.1254961, 2014.

Buizert, C., Keisling, B. A., Box, J. E., He, F., Carlson, A. E., Sinclair, G., and DeConto, R. M.: Greenland-Wide Seasonal Temperatures During the Last Deglaciation, Geophys Res Lett, 45, 1905–1914, https://doi.org/10.1002/2017GL075601, 2018.

Calov, R. and Greve, R.: A semi-analytical solution for the positive degree-day model with stochastic temperature variations, Journal of Glaciology, 51, 173–175, https://doi.org/10.3189/172756505781829601, 2005.

Calov, R., Robinson, A., Perrette, M., and Ganopolski, A.: Simulating the Greenland ice sheet under present-day and palaeo constraints including a new discharge parameterization, Cryosphere, 9, 179–196, https://doi.org/10.5194/tc-9-179-2015, 2015.

Clark, C. D., Ely, J. C., Hindmarsh, R. C. A., Bradley, S., Ignéczi, A., Fabel, D., Ó Cofaigh, C., Chiverrell, R. C., Scourse, J., Benetti, S., Bradwell, T., Evans, D. J. A., Roberts, D. H., Burke, M., Callard, S. L., Medialdea, A., Saher, M., Small, D., Smedley, R. K., Gasson, E., Gregoire, L., Gandy, N., Hughes, A. L. C., Ballantyne, C., Bateman, M. D., Bigg, G. R., Doole, J., Dove, D., Duller, G. A. T., Jenkins, G. T. H., Livingstone, S. L., McCarron, S., Moreton, S., Pollard, D., Praeg, D., Sejrup, H. P., Van Landeghem, K. J. J., and Wilson, P.: Growth and retreat of the last British–Irish Ice Sheet, 31 000 to 15 000 years ago: the BRITICE-CHRONO reconstruction, Boreas, 51, 699–758, https://doi.org/10.1111/bor.12594, 2022.

Clark, P. U. and Mix, A. C.: Ice sheets and sea level of the Last Glacial Maximum, Quat Sci Rev, 21, 1–7, https://doi.org/10.1016/S0277-3791(01)00118-4, 2002.

Cuffey, K. M. and Paterson, W. S. B.: The Physics of Glaciers, Academic Press, 2010.

Dalton, A. S., Dulfer, H. E., Margold, M., Heyman, J., Clague, J. J., Froese, D. G., Gauthier, M. S., Hughes, A. L. C., Jennings, C. E., Norris, S. L., and Stoker, B. J.: Deglaciation of the north American ice sheet complex in calendar years based on a comprehensive database of chronological data: NADI-1, Quat Sci Rev, 321, 108345, https://doi.org/10.1016/j.quascirev.2023.108345, 2023.

van Dam, E. R., Husslage, B., den Hertog, D., and Melissen, H.: Maximin Latin Hypercube Designs in Two Dimensions, Oper Res, 55, 158–169, https://doi.org/10.1287/opre.1060.0317, 2007.

Dansgaard, W., Clausen, H. B., Gundestrup, N., Hammer, C. U., Johnsen, S. F., Kristinsdottir, P. M., and Reeh, N.: A New Greenland Deep Ice Core, Science (1979), 218, 1273–1277, https://doi.org/10.1126/science.218.4579.1273, 1982.

Davies, J., Mathiasen, A. M., Kristiansen, K., Hansen, K. E., Wacker, L., Alstrup, A. K. O., Munk, O. L., Pearce, C., and Seidenkrantz, M.-S.: Linkages between ocean circulation and the Northeast Greenland Ice Stream in the Early Holocene, Quat Sci Rev, 286, 107530, https://doi.org/10.1016/j.quascirev.2022.107530, 2022a.

Davies, J., Mathiasen, A. M., Kristiansen, K., Hansen, K. E., Wacker, L., Alstrup, A. K. O., Munk, O. L., Pearce, C., and Seidenkrantz, M.-S.: Linkages between ocean circulation and the Northeast Greenland Ice Stream in the Early Holocene, Quat Sci Rev, 286, 107530, https://doi.org/10.1016/j.quascirev.2022.107530, 2022b.

Downs, J., Johnson, J., Briner, J., Young, N., Lesnek, A., and Cuzzone, J.: Western Greenland ice sheet retreat history reveals elevated precipitation during the Holocene thermal maximum, Cryosphere, 14, 1121–1137, https://doi.org/10.5194/tc-14-1121-2020, 2020.

Edwards, T. L., Nowicki, S., Marzeion, B., Hock, R., Goelzer, H., Seroussi, H., Jourdain, N. C., Slater, D. A., Turner, F. E., Smith, C. J., McKenna, C. M., Simon, E., Abe-Ouchi, A., Gregory, J. M., Larour, E., Lipscomb, W. H., Payne, A. J., Shepherd, A., Agosta, C., Alexander, P., Albrecht, T., Anderson, B., Asay-Davis, X., Aschwanden, A., Barthel, A., Bliss, A., Calov, R., Chambers, C., Champollion, N., Choi, Y., Cullather, R., Cuzzone, J., Dumas, C., Felikson, D., Fettweis, X., Fujita, K., Galton-Fenzi, B. K., Gladstone, R., Golledge, N. R., Greve, R., Hattermann, T., Hoffman, M. J., Humbert, A.,

Huss, M., Huybrechts, P., Immerzeel, W., Kleiner, T., Kraaijenbrink, P., Le clec'h, S., Lee, V., Leguy, G. R., Little, C. M., Lowry, D. P., Malles, J.-H., Martin, D. F., Maussion, F., Morlighem, M., O'Neill, J. F., Nias, I., Pattyn, F., Pelle, T., Price, S. F., Quiquet, A., Radić, V., Reese, R., Rounce, D. R., Rückamp, M., Sakai, A., Shafer, C., Schlegel, N.-J., Shannon, S., Smith, R. S., Straneo, F., Sun, S., Tarasov, L., Trusel, L. D., Van Breedam, J., van de Wal, R., van den Broeke, M., Winkelmann, R., Zekollari, H., Zhao, C., Zhang, T., and Zwinger, T.: Projected land ice contributions to twenty-first-century sea level rise, Nature, 593, 74–82, https://doi.org/10.1038/s41586-021-03302-y, 2021.

Ely, J. C., Clark, C. D., Small, D., and Hindmarsh, R. C. A.: ATAT 1.1, the Automated Timing Accordance Tool for comparing ice-sheet model output with geochronological data, Geosci Model Dev, 12, 933–953, https://doi.org/10.5194/gmd-12-933-2019, 2019.

Ely, J. C., Clark, C. D., Bradley, S. L., Gregoire, L., Gandy, N., Gasson, E., Veness, R. L. J., and Archer, R.: Behavioural tendencies of the last British–Irish Ice Sheet revealed by data–model comparison, J Quat Sci, 39, 839–871, https://doi.org/10.1002/jqs.3628, 2024.

Erb, M. P., Mckay, N. P., Steiger, N., Dee, S., Hancock, C., Ivanovic, R. F., Gregoire, L. J., and Valdes, P.: Reconstructing Holocene temperatures in time and space using paleoclimate data assimilation, Climate of the Past, 18, 2599–2629, https://doi.org/10.5194/cp-18-2599-2022, 2022.

Fausto, R. S., Ahlstrøm, A. P., Van As, D., Bøggild, C. E., and Johnsen, S. J.: A new present-day temperature parameterization for Greenland, Journal of Glaciology, 55, 95–105, https://doi.org/10.3189/002214309788608985, 2009.

Fleming, K. and Lambeck, K.: Constraints on the Greenland Ice Sheet since the Last Glacial Maximum from sea-level observations and glacial-rebound models, Quat Sci Rev, 23, 1053–1077, https://doi.org/10.1016/j.quascirev.2003.11.001, 2004.

Franke, S., Bons, P. D., Westhoff, J., Weikusat, I., Binder, T., Streng, K., Steinhage, D., Helm, V., Eisen, O., Paden, J. D., Eagles, G., and Jansen, D.: Holocene ice-stream shutdown and drainage basin reconfiguration in northeast Greenland, Nat Geosci, 15, 995–1001, https://doi.org/10.1038/s41561-022-01082-2, 2022.

Funder, S., Kjeldsen, K. K., Kjær, K. H., and Ó Cofaigh, C.: The Greenland Ice Sheet During the Past 300,000 Years: A Review, in: Developments in Quaternary Science, vol. 15, 699–713, https://doi.org/10.1016/B978-0-444-53447-7.00050-7, 2011a.

Funder, S., Kjeldsen, K. K., Kjær, K. H., and Ó Cofaigh, C.: The Greenland Ice Sheet During the Past 300,000 Years: A Review, in: Developments in Quaternary Science, vol. 15, 699–713, https://doi.org/10.1016/B978-0-444-53447-7.00050-7, 2011b.

Gandy, N., Astfalck, L. C., Gregoire, L. J., Ivanovic, R. F., Patterson, V. L., Sherriff-Tadano, S., Smith, R. S., Williamson, D., and Rigby, R.: De-Tuning Albedo Parameters in a Coupled Climate Ice Sheet Model to Simulate the North American Ice Sheet at the Last Glacial Maximum, J Geophys Res Earth Surf, 128, https://doi.org/10.1029/2023JF007250, 2023.

GEBCO Bathymetric Compilation Group 2022: The GEBCO_2022 Grid - a continuous terrain model of the global oceans and land, 2022.

Goelzer, H., Robinson, A., Seroussi, H., and van de Wal, R. S. W.: Recent Progress in Greenland Ice Sheet Modelling, Curr Clim Change Rep, 3, 291–302, https://doi.org/10.1007/s40641-017-0073-y, 2017.

Goelzer, H., Nowicki, S., Payne, A., Larour, E., Seroussi, H., Lipscomb, W. H., Gregory, J., Abe-Ouchi, A., Shepherd, A., Simon, E., Agosta, C., Alexander, P., Aschwanden, A., Barthel, A., Calov, R., Chambers, C., Choi, Y., Cuzzone, J., Dumas, C., Edwards, T., Felikson, D., Fettweis, X., Golledge, N. R., Greve, R., Humbert, A., Huybrechts, P., Le Clec'H, S., Lee, V., Leguy, G., Little, C., Lowry, D., Morlighem, M., Nias, I., Quiquet, A., Rückamp, M., Schlegel, N. J., Slater, D. A., Smith, R., Straneo, F., Tarasov, L., Van De Wal, R., and Van Den Broeke, M.: The future sea-level contribution of the Greenland ice sheet: A multi-model ensemble study of ISMIP6, Cryosphere, 14, 3071–3096, https://doi.org/10.5194/tc-14-3071-2020, 2020.

Gowan, E. J.: Paleo sea-level indicators and proxies from Greenland in the GAPSLIP database and comparison with modelled sea level from the PaleoMIST ice-sheet reconstruction, GEUS Bulletin, 53, 1–17, https://doi.org/10.34194/geusb.v53.8355, 2023.

Grootes, P. M., Stuiver, M., White, J. W. C., Johnsen, S., and Jouzel, J.: Comparison of oxygen isotope records from the GISP2 and GRIP Greenland ice cores, Nature, 366, 552–554, https://doi.org/10.1038/366552a0, 1993.

~~Håkansson, L., Briner, J., Alexanderson, H., Aldahan, A., and Possnert, G.: 10Be ages from central east Greenland constrain the extent of the Greenland ice sheet during the Last Glacial Maximum, Quat Sci Rev, 26, 2316–2321, https://doi.org/10.1016/j.quascirev.2007.08.001, 2007.~~

He, C., Liu, Z., Otto-Bliesner, B. L., Brady, E. C., Zhu, C., Tomas, R., Buizert, C., and Severinghaus, J. P.: Abrupt Heinrich Stadial 1 cooling missing in Greenland oxygen isotopes, Sci Adv, 7, 1007–1023, https://doi.org/10.1126/sciadv.abh1007, 2021a.

He, C., Liu, Z., Otto-Bliesner, B. L., Brady, E. C., Zhu, C., Tomas, R., Clark, P. U., Zhu, J., Jahn, A., Gu, S., Zhang, J., Nusbaumer, J., Noone, D., Cheng, H., Wang, Y., Yan, M., and Bao, Y.: Hydroclimate footprint of pan-Asian monsoon water isotope during the last deglaciation, Sci Adv, 7, 1–12, https://doi.org/10.1126/sciadv.abe2611, 2021b.

Hellmer, H., Jacobs, S. S., and Jenkins, A.: Oceanic erosion of a floating Antarctic glacier in the Amundsen Sea, in: American Geophysical Union, 1998.

Hogan, K. A., Ó Cofaigh, C., Jennings, A. E., Dowdeswell, J. A., and Hiemstra, J. F.: Deglaciation of a major palaeo-ice stream in Disko Trough, West Greenland, Quat Sci Rev, 147, 5–26, https://doi.org/10.1016/j.quascirev.2016.01.018, 2016.

Holland, D. M. and Jenkins, A.: Modeling Thermodynamic Ice–Ocean Interactions at the Base of an Ice Shelf, J Phys Oceanogr, 29, 1787–1800, https://doi.org/10.1175/1520-0485(1999)029<1787:MTIOIA>2.0.CO;2, 1999.

Huybrechts, P.: Sea-level changes at the LGM from ice-dynamic reconstructions of the Greenland and Antarctic ice sheets during the glacial cycles, Quat Sci Rev, 21, 203–231, https://doi.org/10.1016/S0277-3791(01)00082-8, 2002.

Huybrechts, P. and de Wolde, J.: The Dynamic Response of the Greenland and Antarctic Ice Sheets to Multiple-Century Climatic Warming, J Clim, 12, 2169–2188, https://doi.org/10.1175/1520-0442(1999)012<2169:TDROTG>2.0.CO;2, 1999.

Hvidberg, C. S., Grinsted, A., Dahl-Jensen, D., Khan, S. A., Kusk, A., Andersen, J. K., Neckel, N., Solgaard, A., Karlsson, N. B., Kjær, H. A., and Vallelonga, P.: Surface velocity of the Northeast Greenland Ice Stream (NEGIS): assessment of interior velocities derived from satellite data by GPS, Cryosphere, 14, 3487–3502, https://doi.org/10.5194/tc-14-3487-2020, 2020.

Iman, R. L.: Latin Hypercube Sampling, in: Encyclopedia of Quantitative Risk Analysis and Assessment, Wiley, https://doi.org/10.1002/9780470061596.risk0299, 2008.

Jansen, D., Franke, S., Bauer, C. C., Binder, T., Dahl-Jensen, D., Eichler, J., Eisen, O., Hu, Y., Kerch, J., Llorens, M.-G., Miller, H., Neckel, N., Paden, J., de Riese, T., Sachau, T., Stoll, N., Weikusat, I., Wilhelms, F., Zhang, Y., and Bons, P. D.: Shear margins in upper half of Northeast Greenland Ice Stream were established two millennia ago, Nat Commun, 15, 1193, https://doi.org/10.1038/s41467-024-45021-8, 2024.

Jennings, A. E., Sheldon, C., Cronin, T. M., Francus, P., Stoner, J., and Andrews, J.: The holocene history of nares strait: transition from Glacial Bay to Arctic- Atlantic Throughflow, Oceanography, 24, 26–41, https://doi.org/10.5670/oceanog.2011.52, 2011.

Jennings, A. E., Andrews, J. T., Ó Cofaigh, C., Onge, G. S., Sheldon, C., Belt, S. T., Cabedo-Sanz, P., and Hillaire-Marcel, C.: Ocean forcing of Ice Sheet retreat in central west Greenland from LGM to the early Holocene, Earth Planet Sci Lett, 472, 1–13, https://doi.org/10.1016/j.epsl.2017.05.007, 2017.

Joughin, I., Smith, B., Howat, I., and Scambos, T.: MEaSUREs Greenland Ice Sheet Velocity Map from InSAR Data, Version 2, 2018a.

Joughin, I., Smith, B., Howat, I., and Scambos, T.: MEaSUREs Greenland Ice Sheet Velocity Map from InSAR Data, Version 2, 2018b.

Katrine Elnegaard Hansen, Lorenzen, J., Davies, J., Wacker, L., Pearce, C., and Seidenkrantz, M.-S.: Deglacial to Mid Holocene environmental conditions on the northeastern Greenland shelf, western Fram Strait, Quat Sci Rev, 293, 107704, https://doi.org/10.1016/j.quascirev.2022.107704, 2022a.

Katrine Elnegaard Hansen, Lorenzen, J., Davies, J., Wacker, L., Pearce, C., and Seidenkrantz, M.-S.: Deglacial to Mid Holocene environmental conditions on the northeastern Greenland shelf, western Fram Strait, Quat Sci Rev, 293, 107704, https://doi.org/10.1016/j.quascirev.2022.107704, 2022b.

Kendall, R. A., Mitrovica, J. X., and Milne, G. A.: On post-glacial sea level - II. Numerical formulation and comparative results on spherically symmetric models, Geophys J Int, 161, 679–706, https://doi.org/10.1111/j.1365-246X.2005.02553.x, 2005.

Keys, R.: Cubic convolution interpolation for digital image processing, IEEE Trans Acoust, 29, 1153–1160, https://doi.org/10.1109/TASSP.1981.1163711, 1981.

Khan, S. A., Sasgen, I., Bevis, M., van Dam, T., Bamber, J. L., Wahr, J., Willis, M., Kjær, K. H., Wouters, B., Helm, V., Csatho, B., Fleming, K., Bjørk, A. A., Aschwanden, A., Knudsen, P., and Munneke, P. K.: Geodetic measurements reveal similarities between post–Last Glacial Maximum and present-day mass loss from the Greenland ice sheet, Sci Adv, 2, https://doi.org/10.1126/sciadv.1600931, 2016.

Khroulev, C. and The PISM authors: PISM, a Parallel Ice Sheet Model v1.2: User's Manual., 2020.

Lambeck, K., Rouby, H., Purcell, A., Sun, Y., and Sambridge, M.: Sea level and global ice volumes from the Last Glacial Maximum to the Holocene, Proceedings of the National Academy of Sciences, 111, 15296–15303, https://doi.org/10.1073/pnas.1411762111, 2014.

Lambeck, K., Purcell, A., and Zhao, S.: The North American Late Wisconsin ice sheet and mantle viscosity from glacial rebound analyses, Quat Sci Rev, 158, 172–210, https://doi.org/10.1016/j.quascirev.2016.11.033, 2017.

Larsen, N. K., Kjær, K. H., Olsen, J., Funder, S., Kjeldsen, K. K., and Nørgaard-Pedersen, N.: Restricted impact of Holocene climate variations on the southern Greenland Ice Sheet, Quat Sci Rev, 30, 3171–3180, https://doi.org/10.1016/j.quascirev.2011.07.022, 2011.

Larsen, N. K., Kjær, K. H., Lecavalier, B., Bjørk, A. A., Colding, S., Huybrechts, P., Jakobsen, K. E., Kjeldsen, K. K., Knudsen, K. L., Odgaard, B. V., and Olsen, J.: The response of the southern Greenland ice sheet to the Holocene thermal maximum, Geology, 43, 291–294, https://doi.org/10.1130/G36476.1, 2015.

Larsen, N. K., Funder, S., Linge, H., Möller, P., Schomacker, A., Fabel, D., Xu, S., and Kjær, K. H.: A Younger Dryas re-advance of local glaciers in north Greenland, Quat Sci Rev, 147, 47–58, https://doi.org/10.1016/j.quascirev.2015.10.036, 2016.

Larsen, N. K., Søndergaard, A. S., Levy, L. B., Olsen, J., Strunk, A., Bjørk, A. A., and Skov, D.: Contrasting modes of deglaciation between fjords and inter-fjord areas in eastern North Greenland, Boreas, 49, 903–917, https://doi.org/10.1111/bor.12475, 2020.

Lecavalier, B. S. and Tarasov, L.: A history-matching analysis of the Antarctic Ice Sheet since the Last Interglacial – Part 1: Ice sheet evolution, Cryosphere, 19, 919–953, https://doi.org/10.5194/tc-19-919-2025, 2025.

Lecavalier, B. S., Milne, G. A., Vinther, B. M., Fisher, D. A., Dyke, A. S., and Simpson, M. J. R.: Revised estimates of Greenland ice sheet thinning histories based on ice-core records, Quat Sci Rev, 63, 73–82, https://doi.org/10.1016/j.quascirev.2012.11.030, 2013.

Lecavalier, B. S., Milne, G. A., Simpson, M. J. R., Wake, L., Huybrechts, P., Tarasov, L., Kjeldsen, K. K., Funder, S., Long, A. J., Woodroffe, S., Dyke, A. S., and Larsen, N. K.: A model of Greenland ice sheet deglaciation constrained by observations of relative sea level and ice extent, Quat Sci Rev, 102, 54–84, https://doi.org/10.1016/j.quascirev.2014.07.018, 2014.

Lecavalier, B. S., Fisher, D. A., Milne, G. A., Vinther, B. M., Tarasov, L., Huybrechts, P., Lacelle, D., Main, B., Zheng, J., Bourgeois, J., and Dyke, A. S.: High Arctic Holocene temperature record from the Agassiz ice cap and Greenland ice sheet evolution, Proceedings of the National Academy of Sciences, 114, 5952–5957, https://doi.org/10.1073/pnas.1616287114, 2017.

Leger, T. P. M., Clark, C. D., Huynh, C., Jones, S., Ely, J. C., Bradley, S. L., Diemont, C., and Hughes, A. L. C.: A Greenland-wide empirical reconstruction of paleo ice sheet retreat informed by ice extent markers: PaleoGrIS version 1.0, Climate of the Past, 20, 701–755, https://doi.org/10.5194/cp-20-701-2024, 2024.

Leger, T. P. M., Jouvet, G., Kamleitner, S., Mey, J., Herman, F., Finley, B. D., Ivy-Ochs, S., Vieli, A., Henz, A., and Nussbaumer, S. U.: A data-consistent model of the last glaciation in the Alps achieved with physics-driven AI, Nat Commun, 16, 848, https://doi.org/10.1038/s41467-025-56168-3, 2025.

Lenaerts, J. T. M., Camron, M. D., Wyburn-Powell, C. R., and Kay, J. E.: Present-day and future Greenland Ice Sheet precipitation frequency from CloudSat observations and the Community Earth System Model, Cryosphere, 14, 2253–2265, https://doi.org/10.5194/tc-14-2253-2020, 2020.

Levermann, A., Albrecht, T., Winkelmann, R., Martin, M. A., Haseloff, M., and Joughin, I.: Kinematic first-order calving law implies potential for abrupt ice-shelf retreat, Cryosphere, 6, 273–286, https://doi.org/10.5194/tc-6-273-2012, 2012.

Lingle, C. S. and Clark, J. A.: A numerical model of interactions between a marine ice sheet and the solid earth: Application to a West Antarctic ice stream, J Geophys Res Oceans, 90, 1100–1114, https://doi.org/10.1029/JC090iC01p01100, 1985.

Liu, Z., Otto-Bliesner, B. L., He, F., Brady, E. C., Tomas, R., Clark, P. U., Carlson, A. E., Lynch-Stieglitz, J., Curry, W., Brook, E., Erickson, D., Jacob, R., Kutzbach, J., and Cheng, J.: Transient Simulation of Last Deglaciation with a New Mechanism for Bølling-Allerød Warming, Science (1979), 325, 310–314, https://doi.org/10.1126/science.1171041, 2009.

Lloyd, J. M., Ribeiro, S., Weckström, K., Callard, L., Ó Cofaigh, C., Leng, M. J., Gulliver, P., and Roberts, D. H.: Ice-ocean interactions at the Northeast Greenland Ice stream (NEGIS) over the past 11,000 years, Quat Sci Rev, 308, 108068, https://doi.org/10.1016/j.quascirev.2023.108068, 2023.

Lofverstrom, M., Fyke, J. G., Thayer-Calder, K., Muntjewerf, L., Vizcaino, M., Sacks, W. J., Lipscomb, W. H., Otto-Bliesner, B. L., and Bradley, S. L.: An Efficient Ice Sheet/Earth System Model Spin-up Procedure for CESM2-CISM2: Description, Evaluation, and Broader Applicability, J Adv Model Earth Syst, 12, https://doi.org/10.1029/2019MS001984, 2020.

Lüthi, D., Le Floch, M., Bereiter, B., Blunier, T., Barnola, J.-M., Siegenthaler, U., Raynaud, D., Jouzel, J., Fischer, H., Kawamura, K., and Stocker, T. F.: High-resolution carbon dioxide concentration record 650,000–800,000 years before present, Nature, 453, 379–382, https://doi.org/10.1038/nature06949, 2008.

Ma, Q., Shi, X., Scholz, P., Sidorenko, D., Lohmann, G., and Ionita, M.: Revisiting climate impacts of an AMOC slowdown: dependence on freshwater locations in the North Atlantic, Sci Adv, 10, 3243, https://doi.org/10.1126/sciadv.adr3243, 2024.

MacGregor, J. A., Chu, W., Colgan, W. T., Fahnestock, M. A., Felikson, D., Karlsson, N. B., Nowicki, S. M. J., and Studinger, M.: GBaTSv2: a revised synthesis of the likely basal thermal state of the Greenland Ice Sheet, Cryosphere, 16, 3033–3049, https://doi.org/10.5194/tc-16-3033-2022, 2022.

Mankoff, K. D., Solgaard, A., Colgan, W., Ahlstrøm, A. P., Khan, S. A., and Fausto, R. S.: Greenland Ice Sheet solid ice discharge from 1986 through March 2020, Earth Syst Sci Data, 12, 1367–1383, https://doi.org/10.5194/essd-12-1367-2020, 2020.

~~Marienfeld, P.: Faziesvariationen glazialmariner Sedimente im Scoresby-Sund, Ost-Grönland, Zentralblatt für Geologie und Paläontologie, 1, 1739–1749, 1990.~~

Martin, T., Biastoch, A., Lohmann, G., Mikolajewicz, U., and Wang, X.: On Timescales and Reversibility of the Ocean's Response to Enhanced Greenland Ice Sheet Melting in Comprehensive Climate Models, Geophys Res Lett, 49, https://doi.org/10.1029/2021GL097114, 2022.

Martos, Y. M., Jordan, T. A., Catalán, M., Jordan, T. M., Bamber, J. L., and Vaughan, D. G.: Geothermal Heat Flux Reveals the Iceland Hotspot Track Underneath Greenland, Geophys Res Lett, 45, 8214–8222, https://doi.org/10.1029/2018GL078289, 2018.

Menard, H. W. and Smith, S. M.: Hypsometry of ocean basin provinces, J Geophys Res, 71, 4305–4325, https://doi.org/10.1029/JZ071i018p04305, 1966.

Meredith, M., Sommerkorn, M., Cassotta, S., Derksen, C., Ekaykin, A., Hollowed, A., Kofinas, G., Mackintosh, A., Melbourne-Thomas, J., Muelbert, M. M. C., Ottersen, G., Pritchard, H., and Schuur, E. A. G.: Polar regions. Chapter 3, IPCC Special Report on the Ocean and Cryosphere in a Changing Climate, 203–320 pp., 2019.

Millan, R., Mouginot, J., Rabatel, A., and Morlighem, M.: Ice velocity and thickness of the world's glaciers, Nat Geosci, 15, https://doi.org/10.1038/s41561-021-00885-z, 2022.

Mitrovica, J. X. and Milne, G. A.: On post-glacial sea level: I. General theory, Geophys J Int, 154, 253–267, https://doi.org/10.1046/j.1365-246X.2003.01942.x, 2003.

Morlighem, M., Rignot, E., Mouginot, J., Seroussi, H., and Larour, E.: Deeply incised submarine glacial valleys beneath the Greenland ice sheet, Nat Geosci, 7, 418–422, https://doi.org/10.1038/ngeo2167, 2014.

Morlighem, M., Williams, C. N., Rignot, E., An, L., Arndt, J. E., Bamber, J. L., Catania, G., Chauché, N., Dowdeswell, J. A., Dorschel, B., Fenty, I., Hogan, K., Howat, I., Hubbard, A., Jakobsson, M., Jordan, T. M., Kjeldsen, K. K., Millan, R., Mayer, L., Mouginot, J., Noël, B. P. Y., O'Cofaigh, C., Palmer, S., Rysgaard, S., Seroussi, H., Siegert, M. J., Slabon, P., Straneo, F., van den Broeke, M. R., Weinrebe, W., Wood, M., and Zinglersen, K. B.: BedMachine v3: Complete Bed Topography and Ocean Bathymetry Mapping of Greenland From Multibeam Echo Sounding Combined With Mass Conservation, Geophys Res Lett, 44, 11,051-11,061, https://doi.org/10.1002/2017GL074954, 2017a.

Morlighem, M., Williams, C. N., Rignot, E., An, L., Arndt, J. E., Bamber, J. L., Catania, G., Chauché, N., Dowdeswell, J. A., Dorschel, B., Fenty, I., Hogan, K., Howat, I., Hubbard, A., Jakobsson, M., Jordan, T. M., Kjeldsen, K. K., Millan, R., Mayer, L., Mouginot, J., Noël, B. P. Y., O'Cofaigh, C., Palmer, S., Rysgaard, S., Seroussi, H., Siegert, M. J., Slabon, P., Straneo, F., van den Broeke, M. R., Weinrebe, W., Wood, M., and Zinglersen, K. B.: BedMachine v3: Complete Bed Topography and Ocean Bathymetry Mapping of Greenland From Multibeam Echo Sounding Combined With Mass Conservation, Geophys Res Lett, 44, 11,051-11,061, https://doi.org/10.1002/2017GL074954, 2017b.

Motyka, R. J., Truffer, M., Fahnestock, M., Mortensen, J., Rysgaard, S., and Howat, I.: Submarine melting of the 1985 Jakobshavn Isbrae floating tongue and the triggering of the current retreat, J Geophys Res Earth Surf, 116, n/a-n/a, https://doi.org/10.1029/2009JF001632, 2011.

NIU, L., LOHMANN, G., HINCK, S., GOWAN, E. J., and KREBS-KANZOW, U.: The sensitivity of Northern Hemisphere ice sheets to atmospheric forcing during the last glacial cycle using PMIP3 models, Journal of Glaciology, 65, 645–661, https://doi.org/10.1017/jog.2019.42, 2019.

NorthGRIPMembers, Andersen, K. K., Azuma, N., Barnola, J.-M., Bigler, M., Biscaye, P. E., Caillon, N., Chappellaz, J., Clausen, H. B., Dahl-Jensen, D., Fischer, H., Flückiger, J., Fritzsche, D., Fujii, Y., Goto-Azuma, K., Grønvold, K., Gundestrup, N. S., Hansson, M., Huber, C., Hvidberg, C. S., Johnsen, S. J., Jonsell, U., Jouzel, J., Kipfstuhl, S., Landais, A., Leuenberger, M., Lorrain, R., Masson-Delmotte, V., Miller, H., Motoyama, H., Narita, H., Popp, T., Rasmussen, S. O., Raynaud, D., Rothlisberger, R., Ruth, U., Samyn, D., Schwander, J., Shoji, H., Siggaard-Andersen, M.-L., Steffensen, J.-P. P., Stocker, T., Sveinbjörnsdóttir, A. E., Svensson, A., Takata, M., Tison, J.-L., Thorsteinsson, T., Watanabe, O., Wilhelms, F., White, J. W. C., and Siggard-Andersen, M.-L.: High-resolution record of Northern Hemisphere climate extending into the last interglacial period., Nature, 431, 147–151, https://doi.org/10.1038/nature02805, 2004.

Ó Cofaigh, C., Dowdeswell, J. A., Jennings, A. E., Hogan, K. A., Kilfeather, A., Hiemstra, J. F., Noormets, R., Evans, J., McCarthy, D. J., Andrews, J. T., Lloyd, J. M., and Moros, M.: An extensive and dynamic ice sheet on the west greenland shelf during the last glacial cycle, Geology, 41, 219–222, https://doi.org/10.1130/G33759.1, ~~2013a~~2013.

Ó Cofaigh, C., Lloyd, J. M., Callard, S. ~~Dowdeswell, J. A., Jennings, A. E., Hogan~~L., Gebhardt, C., Streuff, K. T., Dorschel, B., Smith~~A., Kilfeather, A., Hiemstra~~, J. A., Lane, T. ~~F., Noormets,~~P., Jamieson, S. S. R., ~~Evans, J., McCarthy~~Kanzow, T., and Roberts, D. ~~J., Andrews, J. T., Lloyd, J. M., and Moros, M.: An extensive and dynamic ice sheet on the west greenland shelf~~H.: Shelf-edge glaciation offshore of northeast Greenland during the last glacial ~~cycle, Geology, 41, 219–222~~maximum and timing of initial ice-sheet retreat, Quat Sci Rev, 359, 109326, https://doi.org/10.~~1130/G33759.1, 2013b~~1016/j.quascirev.2025.109326, 2025.

Oerlemans, J., Anderson, B., Hubbard, A., Huybrechts, P., Jóhannesson, T., Knap, W. H., Schmeits, M., Stroeven, A. P., van de Wal, R. S. W., Wallinga, J., and Zuo, Z.: Modelling the response of glaciers to climate warming, Clim Dyn, 14, 267–274, https://doi.org/10.1007/s003820050222, 1998.

Osman, M. B., Tierney, J. E., Zhu, J., Tardif, R., Hakim, G. J., King, J., and Poulsen, C. J.: Globally resolved surface temperatures since the Last Glacial Maximum, Nature, 599, 239–244, https://doi.org/10.1038/s41586-021-03984-4, 2021.

Patterson, V. L., Gregoire, L. J., Ivanovic, R. F., Gandy, N., Owen, J., Smith, R. S., Pollard, O. G., Astfalck, L. C., and Valdes, P. J.: Contrasting the Penultimate Glacial Maximum and the Last Glacial Maximum (140 and 21 ka) using coupled climate–ice sheet modelling, Climate of the Past, 20, 2191–2218, https://doi.org/10.5194/cp-20-2191-2024, 2024.

Peltier, W. R., Argus, D. F., and Drummond, R.: Space geodesy constrains ice age terminal deglaciation: The global ICE-6G_C (VM5a) model, J Geophys Res Solid Earth, 120, 450–487, https://doi.org/10.1002/2014JB011176, 2015.

Pittard, M. L., Whitehouse, P. L., Bentley, M. J., and Small, D.: An ensemble of Antarctic deglacial simulations constrained by geological observations, Quat Sci Rev, 298, 107800, https://doi.org/10.1016/j.quascirev.2022.107800, 2022.

Plach, A., Nisancioglu, K. H., Langebroek, P. M., Born, A., and Le clec'h, S.: Eemian Greenland ice sheet simulated with a higher-order model shows strong sensitivity to surface mass balance forcing, Cryosphere, 13, 2133–2148, https://doi.org/10.5194/tc-13-2133-2019, 2019.

Pritchard, H. D., Ligtenberg, S. R. M., Fricker, H. A., Vaughan, D. G., van den Broeke, M. R., and Padman, L.: Antarctic ice-sheet loss driven by basal melting of ice shelves, Nature, 484, 502–505, https://doi.org/10.1038/nature10968, 2012.

Quiquet, A., Roche, D. M., Dumas, C., Bouttes, N., and Lhardy, F.: Climate and ice sheet evolutions from the last glacial maximum to the pre-industrial period with an ice-sheet–climate coupled model, Climate of the Past, 17, 2179–2199, https://doi.org/10.5194/cp-17-2179-2021, 2021.

Rasmussen, S. O., Abbott, P. M., Blunier, T., Bourne, A. J., Brook, E., Buchardt, S. L., Buizert, C., Chappellaz, J., Clausen, H. B., Cook, E., Dahl-Jensen, D., Davies, S. M., Guillevic, M., Kipfstuhl, S., Laepple, T., Seierstad, I. K., Severinghaus, J. P., Steffensen, J. P., Stowasser, C., Svensson, A., Vallelonga, P., Vinther, B. M., Wilhelms, F., and Winstrup, M.: A first chronology for the North Greenland Eemian Ice Drilling (NEEM) ice core, Climate of the Past, 9, 2713–2730, https://doi.org/10.5194/cp-9-2713-2013, 2013.

Rasmussen, S. O., Dahl-Jensen, D., Fischer, H., Fuhrer, K., Hansen, S. B., Hansson, M., Hvidberg, C. S., Jonsell, U., Kipfstuhl, S., Ruth, U., Schwander, J., Siggaard-Andersen, M.-L., Sinnl, G., Steffensen, J. P., Svensson, A. M., and Vinther, B. M.: Ice-core data used for the construction of the Greenland Ice-Core Chronology 2005 and 2021 (GICC05 and GICC21), Earth Syst Sci Data, 15, 3351–3364, https://doi.org/10.5194/essd-15-3351-2023, 2023.

Rieckh, T., Born, A., Robinson, A., Law, R., and Gülle, G.: Design and performance of ELSA v2.0: an isochronal model for ice-sheet layer tracing, Geosci Model Dev, 17, 6987–7000, https://doi.org/10.5194/gmd-17-6987-2024, 2024.

Rinterknecht, V., Jomelli, V., Brunstein, D., Favier, V., Masson-Delmotte, V., Bourlès, D., Leanni, L., and Schläppy, R.: Unstable ice stream in Greenland during the Younger Dryas cold event, Geology, 42, 759–762, https://doi.org/10.1130/G35929.1, 2014.

Ritz, C.: EISMINT Intercomparison Experiment: Comparison of existing Greenland models., Laboratoire de Glaciologie et de Géophysique de l'Environnement, Saint Martin d'Hères, France, 1997.

Roberts, D. H., Lane, T. P., Jones, R. S., Bentley, M. J., Darvill, C. M., Rodes, A., Smith, J. A., Jamieson, S. S. R., Rea, B. R., Fabel, D., Gheorghiu, D., Davidson, A., Cofaigh, C. Ó., Lloyd, J. M., Callard, S. L., and Humbert, A.: The deglacial history of 79N glacier and the Northeast Greenland Ice Stream, Quat Sci Rev, 336, 108770, https://doi.org/10.1016/j.quascirev.2024.108770, ~~2024a~~2024.

~~Roberts, D. H., Lane, T. P., Jones, R. S., Bentley, M. J., Darvill, C. M., Rodes, A., Smith, J. A., Jamieson, S. S. R., Rea, B. R., Fabel, D., Gheorghiu, D., Davidson, A., Cofaigh, C. Ó., Lloyd, J. M., Callard, S. L., and Humbert, A.: The deglacial history of 79N glacier and the Northeast Greenland Ice Stream, Quat Sci Rev, 336, 108770, https://doi.org/10.1016/j.quascirev.2024.108770, 2024b.~~

Rogozhina, I., Martinec, Z., Hagedoorn, J. M., Thomas, M., and Fleming, K.: On the long-term memory of the Greenland ice sheet, J Geophys Res Earth Surf, 116, 1–16, https://doi.org/10.1029/2010JF001787, 2011.

Rovere, A., Stocchi, P., and Vacchi, M.: Eustatic and Relative Sea Level Changes, Curr Clim Change Rep, 2, 221–231, https://doi.org/10.1007/s40641-016-0045-7, 2016.

Sbarra, C. M., Briner, J. P., Graham, B. L., Poinar, K., Thomas, E. K., and Young, N. E.: Evidence for a more extensive Greenland Ice Sheet in southwestern Greenland during the Last Glacial Maximum, Geosphere, 18, 1316–1329, https://doi.org/10.1130/GES02432.1, 2022a.

Sbarra, C. M., Briner, J. P., Graham, B. L., Poinar, K., Thomas, E. K., and Young, N. E.: Evidence for a more extensive Greenland Ice Sheet in southwestern Greenland during the Last Glacial Maximum, Geosphere, 18, 1316–1329, https://doi.org/10.1130/GES02432.1, 2022b.

Seguinot, J. and Rogozhina, I.: Daily temperature variability predetermined by thermal conditions over ice-sheet surfaces, Journal of Glaciology, 60, 603–605, https://doi.org/10.3189/2014JoG14J036, 2014.

Seroussi, H., Nowicki, S., Simon, E., Abe-Ouchi, A., Albrecht, T., Brondex, J., Cornford, S., Dumas, C., Gillet-Chaulet, F., Goelzer, H., Golledge, N. R., Gregory, J. M., Greve, R., Hoffman, M. J., Humbert, A., Huybrechts, P., Kleiner, T., Larour, E., Leguy, G., Lipscomb, W. H., Lowry, D., Mengel, M., Morlighem, M., Pattyn, F., Payne, A. J., Pollard, D., Price, S. F., Quiquet, A., Reerink, T. J., Reese, R., Rodehacke, C. B., Schlegel, N. J., Shepherd, A., Sun, S., Sutter, J., Van Breedam, J., Van De Wal, R. S. W., Winkelmann, R., and Zhang, T.: InitMIP-Antarctica: An ice sheet model initialization experiment of ISMIP6, Cryosphere, 13, 1441–1471, https://doi.org/10.5194/tc-13-1441-2019, 2019.

Simonsen, S. B., Barletta, V. R., Colgan, W. T., and Sørensen, L. S.: Greenland Ice Sheet Mass Balance (1992–2020) From Calibrated Radar Altimetry, Geophys Res Lett, 48, 1–10, https://doi.org/10.1029/2020GL091216, 2021.

Simpson, M. J. R., Milne, G. A., Huybrechts, P., and Long, A. J.: Calibrating a glaciological model of the Greenland ice sheet from the Last Glacial Maximum to present-day using field observations of relative sea level and ice extent, Quat Sci Rev, 28, 1631–1657, https://doi.org/10.1016/j.quascirev.2009.03.004, 2009.

Sinclair, G., Carlson, A. E., Mix, A. C., Lecavalier, B. S., Milne, G., Mathias, A., Buizert, C., and DeConto, R.: Diachronous retreat of the Greenland ice sheet during the last deglaciation, Quat Sci Rev, 145, 243–258, https://doi.org/10.1016/j.quascirev.2016.05.040, 2016.

Sinet, S., von der Heydt, A. S., and Dijkstra, H. A.: AMOC Stabilization Under the Interaction With Tipping Polar Ice Sheets, Geophys Res Lett, 50, https://doi.org/10.1029/2022GL100305, 2023.

Smith-Johnsen, S., de Fleurian, B., Schlegel, N., Seroussi, H., and Nisancioglu, K.: Exceptionally high heat flux needed to sustain the Northeast Greenland Ice Stream, Cryosphere, 14, 841–854, https://doi.org/10.5194/tc-14-841-2020, 2020.

Søndergaard, A. S., Larsen, N. K., Steinemann, O., Olsen, J., Funder, S., Egholm, D. L., and Kjær, K. H.: Glacial history of Inglefield Land, north Greenland from combined in situ 10Be and 14C exposure dating, Climate of the Past, 16, 1999–2015, https://doi.org/10.5194/cp-16-1999-2020, 2020.

Stein, M.: Large Sample Properties of Simulations Using Latin Hypercube Sampling, Technometrics, 29, 143–151, https://doi.org/10.1080/00401706.1987.10488205, 1987.

Swift, D. A., Persano, C., Stuart, F. M., Gallagher, K., and Whitham, A.: A reassessment of the role of ice sheet glaciation in the long-term evolution of the East Greenland fjord region, Geomorphology, 97, 109–125, https://doi.org/10.1016/j.geomorph.2007.02.048, 2008.

Tabone, I., Blasco, J., Robinson, A., Alvarez-Solas, J., and Montoya, M.: The sensitivity of the Greenland Ice Sheet to glacial–interglacial oceanic forcing, Climate of the Past, 14, 455–472, https://doi.org/10.5194/cp-14-455-2018, 2018.

Tabone, I., Robinson, A., Montoya, M., and Alvarez-Solas, J.: Holocene thinning in central Greenland controlled by the Northeast Greenland Ice Stream, Nat Commun, 15, 6434, https://doi.org/10.1038/s41467-024-50772-5, 2024.

Tadono, T., Ishida, H., Oda, F., Naito, S., Minakawa, K., and Iwamoto, H.: Precise Global DEM Generation by ALOS PRISM, ISPRS Annals of the Photogrammetry, Remote Sensing and Spatial Information Sciences, II–4, 71–76, https://doi.org/10.5194/isprsannals-II-4-71-2014, 2014.

Tarasov, L., Dyke, A. S., Neal, R. M., and Peltier, W. R.: A data-calibrated distribution of deglacial chronologies for the North American ice complex from glaciological modeling, Earth Planet Sci Lett, 315–316, 30–40, https://doi.org/10.1016/j.epsl.2011.09.010, 2012.

The IMBIE Team: Mass balance of the Greenland Ice Sheet from 1992 to 2018, Nature, 579, 233–239, https://doi.org/10.1038/s41586-019-1855-2, 2019.

Tierney, J. E., Zhu, J., King, J., Malevich, S. B., Hakim, G. J., and Poulsen, C. J.: Glacial cooling and climate sensitivity revisited, Nature, 584, 569–573, https://doi.org/10.1038/s41586-020-2617-x, 2020.

Tulaczyk, S., Kamb, W. B., and Engelhardt, H. F.: Basal mechanics of Ice Stream B, west Antarctica: 2. Undrained plastic bed model, J Geophys Res Solid Earth, 105, 483–494, https://doi.org/10.1029/1999JB900328, 2000.

van Kampenhout, L., Lenaerts, J. T. M., Lipscomb, W. H., Lhermitte, S., Noël, B., Vizcaíno, M., Sacks, W. J., and van den Broeke, M. R.: Present-Day Greenland Ice Sheet Climate and Surface Mass Balance in CESM2, J Geophys Res Earth Surf, 125, https://doi.org/10.1029/2019JF005318, 2020.

Vinther, B. M., Buchardt, S. L., Clausen, H. B., Dahl-Jensen, D., Johnsen, S. J., Fisher, D. A., Koerner, R. M., Raynaud, D., Lipenkov, V., Andersen, K. K., Blunier, T., Rasmussen, S. O., Steffensen, J. P., and Svensson, A. M.: Holocene thinning of the Greenland ice sheet, Nature, 461, 385–388, https://doi.org/10.1038/nature08355, 2009.

Winkelmann, R., Martin, M. A., Haseloff, M., Albrecht, T., Bueler, E., Khroulev, C., and Levermann, A.: The Potsdam Parallel Ice Sheet Model (PISM-PIK) – Part 1: Model description, Cryosphere, 5, 715–726, https://doi.org/10.5194/tc-5-715-2011, 2011.

Yan, Q., Zhang, Z., Gao, Y., Wang, H., and Johannessen, O. M.: Sensitivity of the modeled present-day Greenland Ice Sheet to climatic forcing and spin-up methods and its influence on future sea level projections, J Geophys Res Earth Surf, 118, 2174–2189, https://doi.org/10.1002/jgrf.20156, 2013.

Yang, H., Krebs-Kanzow, U., Kleiner, T., Sidorenko, D., Rodehacke, C. B., Shi, X., Gierz, P., Niu, L., Gowan, E. J., Hinck, S., Liu, X., Stap, L. B., and Lohmann, G.: Impact of paleoclimate on present and future evolution of the Greenland Ice Sheet, PLoS One, 17, 1–21, https://doi.org/10.1371/journal.pone.0259816, 2022.

Yu, L., Gao, Y., and Otterå, O. H.: The sensitivity of the Atlantic meridional overturning circulation to enhanced freshwater discharge along the entire, eastern and western coast of Greenland, Clim Dyn, 46, 1351–1369, https://doi.org/10.1007/s00382-015-2651-9, 2016.

Zhu, J., Liu, Z., Brady, E., Otto-Bliesner, B., Zhang, J., Noone, D., Tomas, R., Nusbaumer, J., Wong, T., Jahn, A., and Tabor, C.: Reduced ENSO variability at the LGM revealed by an isotope-enabled Earth system model, Geophys Res Lett, 44, 6984–6992, https://doi.org/10.1002/2017GL073406, 2017.

Zoet, L. K. and Iverson, N. R.: A slip law for glaciers on deformable beds, Science (1979), 368, 76–78, https://doi.org/10.1126/science.aaz1183, 2020.